

**PREPARATION AND CHARACTERIZATION OF  
BIODEGRADABLE STEREOCOMPLEX POLY  
(PROPYLENE GLYCOL)-*B*-POLYLACTIDE  
USING SOLUTION BLENDING METHOD**

**DUTCHANEE PHOLHARN**

**A dissertation submitted in partial fulfillment of the requirements for  
the degree of Doctor of Philosophy Program in Chemistry  
at Maharakham University**

**July 2017**

**All rights reserved by Maharakham University**



**PREPARATION AND CHARACTERIZATION OF  
BIODEGRADABLE STEREOCOMPLEX POLY  
(PROPYLENE GLYCOL)-*B*-POLYLACTIDE  
USING SOLUTION BLENDING METHOD**

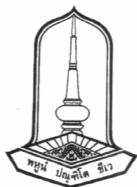
**DUTCHANEE PHOLHARN**

**A dissertation submitted in partial fulfillment of the requirements for  
the degree of Doctor of Philosophy Program in Chemistry  
at Maharakham University**

**July 2017**

**All rights reserved by Maharakham University**





The examining committee has unanimously approved this dissertation, submitted by Miss Dutchanee Pholharn, as a partial fulfillment of the requirements for the Doctor of Philosophy degree in Chemistry at Maharakham University.

Examining Committee

- ..... *Sittipong Amnuaypanich* ..... Chairman  
(Assoc. Prof. Sittipong Amnuaypanich, Ph.D.) (External expert)
- ..... *Yodthong Baimark* ..... Committee  
(Assoc. Prof. Yodthong Baimark, Ph.D.) (Advisor)
- ..... *Onanong Cheerarot* ..... Committee  
(Asst. Prof. Onanong Cheerarot, Ph.D.) (Co-advisor)
- ..... *Khongvit* ..... Committee  
(Khongvit Prasitnok, Ph.D.) (Faculty graduate committee)
- ..... *Kansiri Pakkethati* ..... Committee  
(Kansiri Pakkethati, Ph.D.) (Faculty graduate committee)

Maharakham University has granted approval to accept this dissertation as a partial fulfillment of the requirements for the Doctor of Philosophy degree in Chemistry.

..... *Wichian Magtoon* .....  
(Prof. Wichian Magtoon, Ph.D.)

..... *A* .....  
(Prof. Pradit Terdtoon, Ph.D.)

Dean of the Faculty of Science

Dean of Graduate School



## ACKNOWLEDGEMENTS

This dissertation was granted by Rajabhat Maha Sarakham University Fund for higher Education.

The dissertation would not have been accomplished if without the help from several people. First of all, I would like to express my sincere thanks and appreciation to my major advisor Assoc. Prof. Dr. Yodthong Baimark for his excellent supervision, inspiring guidance, encouragement and helpful discussion throughout this dissertation. Sincere gratefulness is also extended to my co-advisor Dr. Onanong Cheerarot, for her helpful suggestions and comments for completion of this dissertation. I would like to thank Dr. Khongvit Prasitnok, Dr. Kansiri Pakkethati and Assoc. Prof. Dr. Sittipong Amnuaypanich for their valuable suggestions and comments as committee members and dissertation examinees.

I was very fortunate to have many friends both within and outside the Faculty of Accountancy and Management during my doctoral life. I thank them all for their being very supportive.

Nevertheless, I would like to thank the Department of Chemistry, Faculty of Science, Mahasarakham University for partially support of chemicals, instruments and facilities, and the Faculty of Graduate Studies, Mahasarakham University for the guidance in preparing this dissertation. I would also like to thank Miss Yaowaluk Srisuwan and Mr. Supasin Pasee for their enthusiasm, insigeful help, many useful suggestion laboratory techniques, sharing extensive assistance in laboratory apparatus, Miss Nual-anong Narkong for Scanning Electron Microscope experiments, Assoc. Prof. Dr. Prasong Srihanarm and Asst. Prof. Dr. Rakrudee Sarnthima for their many helpful and useful suggestions.

Especially, I deeply indepted my parents and my family for their love, kindness, encouragement and financial support throughout my life.

Dutchanee Pholharn



ชื่อเรื่อง	การเตรียมและการศึกษาลักษณะเฉพาะของสเตอริโอคอมเพล็กซ์พอลิโพรพิลีนไกลคอล-บล็อก-พอลิแล็กไทด์ที่แตกสลายทางชีวภาพได้โดยวิธีการผสมแบบสารละลาย
ผู้วิจัย	นางสาวดรชรชนีย์ พลหาญ
ปริญญา	ปรัชญาดุษฎีบัณฑิต สาขาวิชา เคมี
อาจารย์ที่ปรึกษา	รองศาสตราจารย์ ดร.ยอดธง ไบมาก ผู้ช่วยศาสตราจารย์ ดร.อรอนงค์ ชีระโรจน์
มหาวิทยาลัย	มหาวิทยาลัยมหาสารคาม ปีที่พิมพ์ 2560

### บทคัดย่อ

การสังเคราะห์พอลิเมอร์ร่วมแบบบล็อกของพอลิโพรพิลีนไกลคอล (PPG) แอล-แล็กไทด์ (LL) และ ดี-แล็กไทด์ (DL) ทำโดยการเกิดพอลิเมอร์แบบเปิดวงวิธีบัลค์โดยมีสแตนนัสออกโทเอทเป็นตัวเร่งปฏิกิริยา มอนอเมอร์ทิลอีเทอร์ พอลิโพรพิลีนไกลคอล (mPPG) และ PPG ใช้เป็นตัวเริ่มปฏิกิริยาสำหรับสังเคราะห์พอลิเมอร์ร่วมแบบสองและสามบล็อก ตามลำดับ ได้มีการศึกษาลักษณะเฉพาะของพอลิเมอร์ร่วมแบบบล็อกโดยอาศัยเทคนิคการวิเคราะห์หลายวิธีร่วมกันคือ สมบัติออปติคอลโรเทชัน (เทคนิคการวัดโพลาริซ) องค์กรประกอบทางเคมี (โปรตอน-เอ็นเอ็มอาร์) วิธีหาน้ำหนักโมเลกุล (โปรตอน-เอ็นเอ็มอาร์ และ จีพีซี) และ วิธีทางความร้อน (ดีเอสซี) พบว่าองค์กรประกอบทางเคมีจากโปรตอน-เอ็นเอ็มอาร์มีค่าใกล้เคียงกับอัตราส่วนมอนอเมอร์ที่ใช้ น้ำหนักโมเลกุลเฉลี่ยโดยจำนวน ( $M_n$ ) ของบล็อกพอลิแล็กไทด์ (PL) ถูกควบคุมโดยอัตราส่วนของตัวเริ่มปฏิกิริยา/แล็กไทด์ จากผลดีเอสซีพบว่าอุณหภูมิเปลี่ยนสภาพคล้ายแก้ว ( $T_g$ ) อุณหภูมิหลอม ( $T_m$ ) และความร้อนการหลอม ( $\Delta H_m$ ) ของบล็อกพอลิแล็กไทด์เพิ่มขึ้นเมื่อความยาวบล็อกพอลิแล็กไทด์ยาวขึ้นและเมื่อความยาวบล็อกพอลิโพรพิลีนไกลคอลลดลง พิล์มสเตอริโอคอมเพล็กซ์พอลิแล็กไทด์เตรียมโดยวิธีการผสมสารละลายของพอลิเมอร์ร่วมแบบบล็อกของพอลิโพรพิลีนไกลคอล-บล็อก-พอลิแอล-แล็กไทด์ และ พอลิโพรพิลีนไกลคอล-บล็อก-พอลิดี-แล็กไทด์ ทำการศึกษาฟิล์มที่มีอัตราส่วนผสม 75/25 50/50 และ 25/75 โดยน้ำหนัก การเกิดผลึกแบบโฮโมและสเตอริโอคอมเพล็กซ์ของฟิล์มผสมวิเคราะห์ด้วยเทคนิคเอฟทีไออาร์ เอ็กซ์อาร์ดี และดีเอสซี พบว่าฟิล์มผสมที่มีอัตราส่วนผสม 75/25 และ 25/75 โดยน้ำหนักมีทั้งผลึกแบบโฮโมและสเตอริโอคอมเพล็กซ์ ขณะที่ฟิล์มผสมที่มีอัตราส่วนผสม 50/50 โดยน้ำหนักมีผลึกแบบสเตอริโอคอมเพล็กซ์เท่านั้น ระดับความเป็นผลึกแบบสเตอริโอคอมเพล็กซ์ ( $\chi_{sc}$ ) ของฟิล์มผสมที่มีอัตราส่วนผสม 50/50 โดยน้ำหนักมีค่าเพิ่มขึ้นเมื่อความยาวบล็อกพอลิแล็กไทด์เพิ่มขึ้นแต่มีค่าลดลงเมื่อความยาวบล็อกพอลิโพรพิลีนไกลคอลเพิ่มขึ้น จากผลเอซซีเอ็มไม่พบการแยกเฟสระหว่างเฟสพอลิโพรพิลีนไกลคอล และพอลิแล็กไทด์ สำหรับสมบัติเชิงกลของฟิล์มผสมขึ้นอยู่กับโครงสร้างของพอลิเมอร์ร่วมแบบบล็อกและความยาวบล็อก โดยโครงสร้างแบบสามบล็อกมีสมบัติการต้านแรงดึงดีกว่าแบบสองบล็อก ฟิล์มผสมที่มีอัตรา



ส่วนผสม 50/50 โดยน้ำหนักมีค่าความแข็งแรงและการยึดตัว ณ จุดขาดสูงสุด โดยค่าความแข็งแรง การยึดตัว และมอดูลัสของยังของฟิล์มผสมเพิ่มขึ้นเมื่อความยาวบล็อกพอลิแล็กไทด์เพิ่มขึ้น นอกจากนี้บล็อกพอลิโพรพิลีนไกลคอล ที่ยาวกว่าทำให้การยึดตัวของฟิล์มมากขึ้น แต่ลดความแข็งแรงและมอดูลัสของยัง

**คำสำคัญ:** พอลิเมอร์แตกสลายทางชีวภาพได้; พอลิแล็กไทด์; บล็อกโคพอลิเมอร์; พอลิแล็กไทด์แบบสเตอริโอคอมเพล็กซ์



**TITLE** Preparation and Characterization of Biodegradable Stereocomplex Poly(propylene glycol)-*b*-Polylactide Using Solution Blending Method

**AUTHOR** Miss Dutchanee Pholharn

**DEGREE** Doctor of Philosophy **MAJOR** Chemistry

**ADVISORS** Assoc. Prof. Yodthong Baimark, Ph.D.  
Asst. Prof. Onanong Cheerarot, Ph.D.

**UNIVERSITY** Mahasarakham University **YEAR** 2017

### ABSTRACT

Block copolymers of poly(propylene glycol) (PPG), L-lactide (LL) and D-lactide (DL) were synthesized via ring-opening polymerization in bulk using stannous octoate as a catalyst. PPG monobutyl ether (mPPG) and PPG were used as initiators for synthesis diblock and triblock copolymers, respectively. The block copolymers were characterized by a combination of analytical techniques: optical rotation property (polarimetry), chemical composition ( $^1\text{H-NMR}$ ), molecular weight methods ( $^1\text{H-NMR}$  and GPC) and thermal analysis method (DSC). The copolymer compositions obtained from  $^1\text{H-NMR}$  were nearly values with the feed monomer ratio. The number-average molecular weights ( $M_n$ ) of the polylactide (PL) blocks were controlled by the initiator/lactide ratio. From the DSC results, glass transition temperature ( $T_g$ ), melting temperature ( $T_m$ ) and heat of melting ( $\Delta H_m$ ) of the PL blocks increased as the PL block length increased and the PPG block length decreased. Stereocomplex PL films were prepared by solution blending of PPG-*b*-PLL and PPG-*b*-PDL block copolymers before solvent evaporation. The films with blend ratios of 75/25, 50/50 and 25/75 wt% were investigated. The homo- and stereocomplex crystallites of the blend films were clearly demonstrated by FTIR, XRD and DSC. The 75/25 and 25/75 (w/w) blend films exhibited both homo- and stereocomplex crystalline characters. The 50/50 (w/w) blend films consisted of only stereocomplex crystallites for all the block copolymer types. Stereocomplex crystallinities ( $\chi_{sc}$ ) values of 50/50 (w/w) blend films increased with the PL block length but decreased as the PPG block length was increased. From SEM, phase separation between PPG and PL phases was not observed. Mechanical properties of the blend films strongly depended upon the block copolymer structures and block lengths. The triblock structure showed better tensile properties than the diblock structure. The 50/50 (w/w) blend films exhibited the highest stress and elongation at break. Strength, extensible and Young's modulus of the blend films increased as the PL block length increased. The longer PPG block also improved film extensible but reduced film strength and Young's modulus.



**Key words:** Biodegradable; polymer; Polylactide; Block copolymer; Stereocomplex polylactide





## CONTENTS

	PAGE
ACKNOWLEDGMENTS.....	I
ABSTRACT (in Thai).....	II
ABSTRACT (in English).....	IV
LIST OF TABLES.....	IX
LIST OF FIGURES.....	X
LIST OF ABBREVIATIONS.....	XV
CHAPTER 1 INTRODUCTION.....	1
1.1 Background and significance of research.....	1
1.2 Research objectives.....	2
1.3 Scopes of research.....	3
1.4 Expected results .....	3
1.5 Definition of terms.....	3
CHAPTER 2 LITERATURE REVIEW.....	5
2.1 Biodegradable polymers.....	5
2.1.1 Definitions of biodegradable polymers.....	5
2.1.2 Examples for biodegradable polymers.....	6
2.1.2.1 Polyethers.....	6
2.1.2.2 Polyesters.....	6
2.1.2.3 Polyurethane.....	7
2.1.3 Mechanisms of polymer degradation and erosion.....	8
2.2 Polylactide.....	9
2.2.1 Production of polylactide.....	9
2.2.2 Optical structures of polylactide.....	12
2.2.3 Physical properties of polylactide.....	13
2.2.3.1 Rheology of polylactide.....	15
2.2.3.2 Crystallinity of polylactide.....	17
2.2.4 Degradation of polylactide.....	19
2.2.4.1 Hydrolysis.....	19
2.2.4.2 Enzymatic degradation.....	20



	PAGE
2.2.5 Applications and performance.....	20
2.2.5.1 polylactide advantages.....	22
2.2.5.2 polylactide limitations.....	22
2.2.6 Modification properties of polylactide.....	23
2.2.6.1 Stereocomplexation .....	23
2.2.6.2 Polycondensation copolymerization.....	25
2.2.6.3 Ring-opening copolymerization.....	25
2.2.6.4 Blending with plasticizers.....	26
CHAPTER 3 METHODOLOGY.....	29
3.1 Chemicals and instruments.....	29
3.1.1 Chemicals.....	29
3.1.2 Instruments.....	30
3.2 Preparation of lactide monomers.....	30
3.3 Synthesis of diblock copolymers.....	31
3.4 Synthesis of triblock copolymers.....	33
3.5 Characterization of diblock and triblock copolymers.....	34
3.5.1 Polarimetry.....	34
3.5.2 <sup>1</sup> H-NMR spectroscopy.....	35
3.5.3 Gel Permeation Chromatography.....	35
3.5.4 Differential Scanning Calorimetry.....	35
3.6 Preparation of stereocomplex polylactide films.....	36
3.7 Characterization of stereocomplex polylactide films.....	36
3.7.1 Fourier Transform Infrared spectroscopy.....	36
3.7.2 X-ray Diffractometer.....	37
3.7.3 Differential Scanning Calorimetry.....	37
3.7.4 Scanning Electron Microscopy.....	37
3.7.5 Tensile testing.....	37
CHAPTER 4 RESULTS AND DISCUSSIONS.....	38
4.1 Characterization of block copolymers.....	38
4.1.1 Optical rotation property.....	38
4.1.2 Chemical compositions.....	39



	PAGE
4.1.3 Molecular weight characteristics.....	46
4.1.4 Thermal transition properties of block copolymers.....	53
4.2 Characterization of stereocomplex polylactide films.....	58
4.2.1 Crystalline structure .....	58
4.2.2 Thermal transition properties.....	65
4.2.3 Film morphology.....	79
4.2.4 Mechanical properties.....	82
CHAPTER 5 CONCLUSIONS.....	87
5.1 Synthesis and characterization of block copolymers.....	87
5.2 Preparation and characterization of stereocomplex block copolymer films.....	88
REFERENCES.....	90
BIOGRAPHY.....	97



## LIST OF TABLES

	PAGE
Table 2.1 Properties of extrusion/thermoforming and injection molding grades of Nature Works PL.....	14
Table 3.1 Chemical used in this research.....	29
Table 3.2 Instruments used in this research.....	30
Table 3.3 Codes and theoretical molecular weights of diblock copolymers....	32
Table 3.4 Codes and theoretical molecular weights of triblock copolymers.....	34
Table 4.1 Specific optical rotations of block copolymers.....	39
Table 4.2 Chemical compositions of diblock and triblock copolymers calculated from <sup>1</sup> H-NMR spectra.....	46
Table 4.3 Molecular weight characteristics of diblock copolymers.....	52
Table 4.4 Molecular weight characteristics of triblock copolymers.....	53
Table 4.5 DSC results of block copolymers obtained from the 1 <sup>st</sup> heating scan curves.....	56
Table 4.6 DSC results of block copolymers obtained from the 2 <sup>nd</sup> heating scan curves.....	58
Table 4.7 The weight fraction of PL ( $w_{PL}$ ) of block copolymer blend films obtained from calculation with mole ratio of PG:PL.....	69
Table 4.8 DSC results of block copolymer blend films obtained from the 1 <sup>st</sup> heating scan curves.....	71
Table 4.9 DSC results of block copolymer blend films obtained from the 2 <sup>nd</sup> heating scan curves.....	78



## LIST OF FIGURES

	PAGE
Figure 2.1 Schematic representations of surface erosion and bulk erosion.....	8
Figure 2.2 Lactic acid optical monomers.....	10
Figure 2.3 Synthesis methods for high molecular weight PL.....	11
Figure 2.4 Coordination-insertion chain growth mechanism of lactide to PL....	12
Figure 2.5 Chemical structures of PLL and PDL.....	13
Figure 2.6 Melt rheology of $M_w$ 213,000 (relative to polystyrene) 13.0%D PL shifted to 180°C.....	16
Figure 2.7 Morphology of PL by optical microscopy and AFM; (a) molecular formula of PL, (b) picture of the central region of a spherulite by optical microscopy, (c) copy of an AFM picture of a section of the spherulite shown in (b) and (d) schematic drawing of the lamellae within a spherulite.....	18
Figure 2.8 Articles produced from PL; (a) injection stretch-blow molded bottles, (b) films, (c) extrusion-thermoformed containers, (d) fiberfill products and (e) Carpet and coverings.....	21
Figure 2.9 Synthesis and molecular structures of PLL [(a) and (b)], PDL [(c) and (d)] and stereo-block isotactic PL [(e) and (f)].....	24
Figure 3.1 Synthesis of lactides.....	31
Figure 3.2 Polymerization reactions of mPPG- <i>b</i> -PL diblock copolymers.....	32
Figure 3.3 Polymerization reactions of PL- <i>b</i> -PPG- <i>b</i> -PL triblock copolymers...	33
Figure 4.1 <sup>1</sup> H-NMR spectrum of 2.5K- <i>b</i> -L20K.....	41
Figure 4.2 <sup>1</sup> H-NMR spectrum of 2.5K- <i>b</i> -D20K .....	41
Figure 4.3 <sup>1</sup> H-NMR spectrum of 2.5K- <i>b</i> -L40K.....	42
Figure 4.4 <sup>1</sup> H-NMR spectrum of 2.5K- <i>b</i> -D40K.....	42
Figure 4.5 <sup>1</sup> H-NMR spectrum of L20K- <i>b</i> -2K- <i>b</i> -L20K.....	43
Figure 4.6 <sup>1</sup> H-NMR spectrum of D20K- <i>b</i> -2K- <i>b</i> -D20K.....	43
Figure 4.7 <sup>1</sup> H-NMR spectrum of L40K- <i>b</i> -2K- <i>b</i> -L40K.....	44
Figure 4.8 <sup>1</sup> H-NMR spectrum of D40K- <i>b</i> -2K- <i>b</i> -D40K.....	44
Figure 4.9 <sup>1</sup> H-NMR spectrum of L20K- <i>b</i> -4K- <i>b</i> -L20K.....	45



	PAGE
Figure 4.10 <sup>1</sup> H-NMR spectrum of D20K- <i>b</i> -4K- <i>b</i> -D20K.....	45
Figure 4.11 GPC curve of 2.5K- <i>b</i> -L20K.....	47
Figure 4.12 GPC curve of 2.5K- <i>b</i> -D20K.....	48
Figure 4.13 GPC curve of 2.5K- <i>b</i> -L40K.....	48
Figure 4.14 GPC curve of 2.5K- <i>b</i> -D40K.....	49
Figure 4.15 GPC curve of L20K- <i>b</i> -2K- <i>b</i> -L20K.....	49
Figure 4.16 GPC curve of D20K- <i>b</i> -2K- <i>b</i> -D20K.....	50
Figure 4.17 GPC curve of L40K- <i>b</i> -2K- <i>b</i> -L40K.....	50
Figure 4.18 GPC curve of D40K- <i>b</i> -2K- <i>b</i> -D40K.....	51
Figure 4.19 GPC curve of L20K- <i>b</i> -4K- <i>b</i> -L20K.....	51
Figure 4.20 GPC curve of D20K- <i>b</i> -4K- <i>b</i> -D20K.....	52
Figure 4.21 First heating scan DSC thermograms of (a) 2.5K- <i>b</i> -L20K, (b) 2.5K- <i>b</i> -L40K, (c) L20K- <i>b</i> -2K- <i>b</i> -L20K, (d) L40K- <i>b</i> -2K- <i>b</i> -L40K and (e) L20K- <i>b</i> -4K- <i>b</i> - L20K.....	55
Figure 4.22 First heating scan DSC thermograms of (a) 2.5K- <i>b</i> -D20K, (b) 2.5K- <i>b</i> -D40K, (c) D20K- <i>b</i> -2K- <i>b</i> -D20K, (d) D40K- <i>b</i> -2K- <i>b</i> -D40K and (e) D20K- <i>b</i> -4K- <i>b</i> - D20K.....	55
Figure 4.23 Second heating scan DSC thermograms of (a) 2.5K- <i>b</i> -L20K, (b) 2.5K- <i>b</i> -L40K, (c) L20K- <i>b</i> -2K- <i>b</i> -L20K, (d) L40K- <i>b</i> -2K- <i>b</i> -L40K and (e) L20K- <i>b</i> -4K- <i>b</i> -L20K.....	57
Figure 4.24 Second heating scan DSC thermograms of (a) 2.5K- <i>b</i> -D20K, (b) 2.5K- <i>b</i> -D40K, (c) D20K- <i>b</i> -2K- <i>b</i> -D20K, (d) D40K- <i>b</i> -2K- <i>b</i> -D40K and (e) D20K- <i>b</i> -4K- <i>b</i> -D20K.....	57
Figure 4.25 FTIR spectra of mPPG- <i>b</i> -PL films prepared with 2.5K- <i>b</i> - L20K/2.5K- <i>b</i> -D20K blend ratios of (a) 100/0, (b) 75/25, (c) 50/50, (d) 25/75 and (e) 0/100 (w/w).....	59
Figure 4.26 FTIR spectra of mPPG- <i>b</i> -PL films prepared with 2.5K- <i>b</i> - L40K/2.5K- <i>b</i> -D40K blend ratios of (a) 100/0, (b) 75/25, (c) 50/50, (d) 25/75 and (e) 0/100 (w/w).....	60



	PAGE
Figure 4.27 FTIR spectra of PL- <i>b</i> -PPG- <i>b</i> -PL films prepared with L20K- <i>b</i> -2K- <i>b</i> -L20K/ D20K- <i>b</i> -2K- <i>b</i> -D20K blend ratios of (a) 100/0, (b) 75/25, (c) 50/50, (d) 25/75 and (e) 0/100 (w/w).....	60
Figure 4.28 FTIR spectra of PL- <i>b</i> -PPG- <i>b</i> -PL films prepared with L40K- <i>b</i> -2K- <i>b</i> -L40K/ D40K- <i>b</i> -2K- <i>b</i> -D40K blend ratios of (a) 100/0, (b) 75/25, (c) 50/50, (d) 25/75 and (e) 0/100 (w/w).....	61
Figure 4.29 FTIR spectra of PL- <i>b</i> -PPG- <i>b</i> -PL films prepared with L20K- <i>b</i> -4K- <i>b</i> -L20K/ D20K- <i>b</i> -4K- <i>b</i> -D20K blend ratios of (a) 100/0, (b) 75/25, (c) 50/50, (d) 25/75 and (e) 0/100 (w/w).....	61
Figure 4.30 XRD patterns of mPPG- <i>b</i> -PL films prepared with 2.5K- <i>b</i> -L20K/2.5K- <i>b</i> -D20K blend ratios of (a) 100/0, (b) 75/25, (c) 50/50, (d) 25/75 and (e) 0/100 (w/w).....	62
Figure 4.31 XRD patterns of mPPG- <i>b</i> -PL films prepared with 2.5K- <i>b</i> -L40K/2.5K- <i>b</i> -D40K blend ratios of (a) 100/0, (b) 75/25, (c) 50/50, (d) 25/75 and (e) 0/100 (w/w).....	63
Figure 4.32 XRD patterns of PL- <i>b</i> -PPG- <i>b</i> -PL films prepared with L20K- <i>b</i> -2K- <i>b</i> -L20K/ D20K- <i>b</i> -2K- <i>b</i> -D20K blend ratios of (a) 100/0, (b) 75/25, (c) 50/50, (d) 25/75 and (e) 0/100 (w/w).....	63
Figure 4.33 XRD patterns of PL- <i>b</i> -PPG- <i>b</i> -PL films prepared with L40K- <i>b</i> -2K- <i>b</i> -L40K/ D40K- <i>b</i> -2K- <i>b</i> -D40K blend ratios of (a) 100/0, (b) 75/25, (c) 50/50, (d) 25/75 and (e) 0/100 (w/w).....	64
Figure 4.34 XRD patterns of PL- <i>b</i> -PPG- <i>b</i> -PL films prepared with L20K- <i>b</i> -4K- <i>b</i> -L20K/ D20K- <i>b</i> -4K- <i>b</i> -D20K blend ratios of (a) 100/0, (b) 75/25, (c) 50/50, (d) 25/75 and (e) 0/100 (w/w).....	64
Figure 4.35 First heating scan DSC thermograms of mPPG- <i>b</i> -PL films prepared with 2.5K- <i>b</i> -L20K/2.5K- <i>b</i> -D20K blend ratios of (a) 100/0, (b) 75/25, (c) 50/50, (d) 25/75 and (e) 0/100 (w/w).....	67
Figure 4.36 First heating scan DSC thermograms of mPPG- <i>b</i> -PL films prepared with 2.5K- <i>b</i> -L40K/2.5K- <i>b</i> -D40K blend ratios of (a) 100/0, (b) 75/25, (c) 50/50, (d) 25/75 and (e) 0/100 (w/w).....	67



	PAGE
Figure 4.37 First heating scan DSC thermograms of PL- <i>b</i> -PPG- <i>b</i> -PL films prepared with L20K- <i>b</i> -2K- <i>b</i> -L20K/ D20K- <i>b</i> -2K- <i>b</i> -D20K blend ratios of (a) 100/0, (b) 75/25, (c) 50/50, (d) 25/75 and (e) 0/100 (w/w).....	68
Figure 4.38 First heating scan DSC thermograms of PL- <i>b</i> -PPG- <i>b</i> -PL films prepared with L40K- <i>b</i> -2K- <i>b</i> -L40K/ D40K- <i>b</i> -2K- <i>b</i> -D40K blend ratios of (a) 100/0, (b) 75/25, (c) 50/50, (d) 25/75 and (e) 0/100 (w/w).....	68
Figure 4.39 First heating scan DSC thermograms of PL- <i>b</i> -PPG- <i>b</i> -PL films prepared with L20K- <i>b</i> -4K- <i>b</i> -L20K/ D20K- <i>b</i> -4K- <i>b</i> -D20K blend ratios of (a) 100/0, (b) 75/25, (c) 50/50, (d) 25/75 and (e) 0/100 (w/w).....	69
Figure 4.40 $\chi_{hc}$ (left row) and $\chi_{sc}$ (right row) of mPPG- <i>b</i> -PL blend films.....	72
Figure 4.41 $\chi_{hc}$ (left row) and $\chi_{sc}$ (right row) of PL- <i>b</i> -PPG-PL blend films.....	73
Figure 4.42 Second heating scan DSC thermograms of mPPG- <i>b</i> -PL films prepared with 2.5K- <i>b</i> -L20K/2.5K- <i>b</i> -D20K blend ratios of (a) 100/0, (b) 75/25, (c) 50/50, (d) 25/75 and (e) 0/100 (w/w).....	75
Figure 4.43 Second heating scan DSC thermograms of mPPG- <i>b</i> -PL films prepared with 2.5K- <i>b</i> -L40K/2.5K- <i>b</i> -D40K blend ratios of (a) 100/0, (b) 75/25, (c) 50/50, (d) 25/75 and (e) 0/100 (w/w).....	75
Figure 4.44 Second heating scan DSC thermograms of PL- <i>b</i> -PPG- <i>b</i> -PL films prepared with L20K- <i>b</i> -2K- <i>b</i> -L20K/ D20K- <i>b</i> -2K- <i>b</i> -D20K blend ratios of (a) 100/0, (b) 75/25, (c) 50/50, (d) 25/75 and (e) 0/100 (w/w).....	76
Figure 4.45 Second heating scan DSC thermograms of PL- <i>b</i> -PPG- <i>b</i> -PL films prepared with L40K- <i>b</i> -2K- <i>b</i> -L40K/ D40K- <i>b</i> -2K- <i>b</i> -D40K blend ratios of (a) 100/0, (b) 75/25, (c) 50/50, (d) 25/75 and (e) 0/100 (w/w).....	76





Figure 4.46 Second heating scan DSC thermograms of PL- <i>b</i> -PPG- <i>b</i> -PL films prepared with L20K- <i>b</i> -4K- <i>b</i> -L20K/ D20K- <i>b</i> -4K- <i>b</i> -D20K blend ratios of (a) 100/0, (b) 75/25, (c) 50/50, (d) 25/75 and (e) 0/100 (w/w).....	77
Figure 4.47 SEM images of cross-section of 2.5K- <i>b</i> -L20K/2.5K- <i>b</i> -D20K (left row) and 2.5K- <i>b</i> -L40K/2.5K- <i>b</i> -D40K (right row) blend films.....	80
Figure 4.48 SEM images of cross-section of L20K- <i>b</i> -2K- <i>b</i> -L20K/ D20K- <i>b</i> -2K- <i>b</i> -D20K (left row), L40K- <i>b</i> -2K- <i>b</i> -L40K/ D40K- <i>b</i> -2K- <i>b</i> -D40K (middle row) and L20K- <i>b</i> -4K- <i>b</i> -L20K/ D20K- <i>b</i> -4K- <i>b</i> -D20K (right row) blend films.....	81
Figure 4.49 Tensile curves of diblock copolymer films prepared with 2.5K- <i>b</i> -L40K/ 2.5K- <i>b</i> -D40K blend ratios of (□) 100/0, (◇) 75/25, (▲) 50/50, (◆) 25/75 and (■) 0/100 (w/w).....	83
Figure 4.50 Tensile curves of triblock copolymer films prepared with L20K- <i>b</i> -2K- <i>b</i> -L20K/D20K- <i>b</i> -2K- <i>b</i> -D20K blend ratios of (□) 100/0, (◇) 75/25, (▲) 50/50, (◆) 25/75 and (■) 0/100 (w/w).....	83
Figure 4.51 Tensile curves of triblock copolymer films prepared with L40K- <i>b</i> -2K- <i>b</i> -L40K/D40K- <i>b</i> -2K- <i>b</i> -D40K blend ratios of (□) 100/0, (◇) 75/25, (▲) 50/50, (◆) 25/75 and (■) 0/100 (w/w).....	84
Figure 4.52 Tensile curves of triblock copolymer films prepared with L20K- <i>b</i> -4K- <i>b</i> -L20K/D20K- <i>b</i> -4K- <i>b</i> -D20K blend ratios of (□) 100/0, (◇) 75/25, (▲) 50/50, (◆) 25/75 and (■) 0/100 (w/w).....	84
Figure 4.53 Stress at break of diblock and triblock copolymer films.....	85
Figure 4.54 Elongation at break of diblock and triblock copolymer films.....	85
Figure 4.55 Young's modulus of diblock and triblock copolymer films.....	86



### LIST OF ABBREVIATIONS

HDT	Heat distortion temperature
DSC	Differential scanning calorimetry
DL	D-lactide
FTIR	Fourier transform infrared spectroscopy
GPC	Gel permeation chromatography
<sup>1</sup> H-NMR	Proton nuclear magnetic resonance
LCR	Linear crystal growth rate
LL	L-lactide
M <sub>n</sub>	Number average molecular weight
MW	Molecular weight
M <sub>w</sub>	Weight average molecular weight
MWD	Molecular weight distribution
mPPG- <i>b</i> -PL	Diblock copolymers of poly(propylene glycol) monobutyl ether- <i>b</i> - polylactide
OP	Optical purity
PCL	Poly(ε-caprolactone)
PDI	Polydispersity index
PDL	Poly(D-lactide)
PET	Poly(ethylene terephthalate)
PEG	Poly(ethylene glycol)
PHA	Polyhydroxyalkanoate
PL	Polylactide
PLL	Poly(L-lactide)
PPDO	Poly(p-dioxanone)
PPG	Poly(propylene glycol)
PS	Polystyrene
PU	Polyurethane
PL- <i>b</i> -PPG- <i>b</i> -PL	Triblock copolymers of polylactide- <i>b</i> -poly(propylene glycol)- <i>b</i> - polylactide
RI	Refractive index



ROC	Ring-opening copolymerization
ROP	Ring-opening polymerization
SEM	Scanning electron microscopy
scPL	Stereocomplex polylactide
TC	Triethyl citrate
$T_c$	Temperature of crystallization
$T_g$	Glass transition temperature
TGA	Thermogravimetric analysis
$T_m$	Melting temperature
$T_{m, hc}$	Melting temperature of homo block copolymers
$T_{m, sc}$	Melting temperature of stereocomplex
$T_{c, hc}$	Cold crystallization temperature of homo crystallite
$T_{c, sc}$	Cold crystallization temperature of stereocomplex crystallite
$[\alpha]_{25}$	Specific optical rotation
$\alpha$	The optical rotation of lactide unit (deg.)
$\chi_{hc}$	Degree of crystallinity of homo crystallites
$\chi_{sc}$	Degree of crystallinity of stereocomplex crystallites
$\Delta H_{hc}$	Melting enthalpy of homo crystallites
$\Delta H_{hc}^\circ$	Melting enthalpy for 100% homo crystallites of PL
$\Delta H_{sc}$	Melting enthalpy of stereocomplex crystallites of PL
$\Delta H_{sc}^\circ$	Melting enthalpy for 100% stereocomplex crystallites of PL
$\Delta H_{c, hc}$	Enthalpy of homo crystallization
$\Delta H_{c, sc}$	Enthalpy of stereocomplex crystallization



## CHAPTER 1

### INTRODUCTION

#### 1.1 Background and significance of research

Synthetic plastics have been one of the most highly valued materials because of their extremely versatility and low cost. Most of the commodity plastics such as poly(propylene) (PP), poly(vinyl chloride) (PVC), poly(carbonate) (PC), poly(styrene) (PS), poly(ethylene) (PE) *etc.* are made from fossil resources; petroleum and its derivative components. In addition, plastic derived from the fossil resources are largely non-biodegradable (Pilla, 2011). Nowadays, the disposal of plastic wastes has become a serious problem in all over the world. The way for solving this problem is development of biodegradable polymers which can be degraded by microorganism actions or by simple hydrolytically (Niar, *et al.*, 2007) and finally obtained carbon dioxide, water and other harmless compounds after damping in nature (Quynh *et al.*, 2013). Among those biodegradable polymers, poly(lactic acid) or poly(lactide) (PL) has been gaining much attention by both academic and industrial fields because the PL can be easily produced from renewable resources in huge scale. In addition, PL shows a good biocompatibility, no toxic, high strength and high modulus (Quynh *et al.*, 2013; Garlotta, 2001). However, there are limitations for utilization of PL, such as low toughness, low heat resistant and high production costs (Liu *et al.*, 2014). Addition of plasticizers and nucleating agents could enhance the toughness and heat resistant of PL, respectively, but it is hard to improve both properties simultaneously.

Stereocomplexation of PL would be the importance procedure to improve heat resistance of PL products. This may be due to the stereocomplex PL had higher melting point and crystallinity than the PL. The scPL can be prepared by solution and melt blending of enantiomeric poly(L-lactide) (PLL) and poly(D-lactide) (PDL) (Ikada *et al.* 1987). It has been found that the stereocomplex is stabilized by van der Waals between opposite configuration of PLL and PDL chains, resulting in faster crystallization and higher heat resistant of PL was much enhanced (Brizzolara *et al.*, 1996).



Glass transition temperature ( $T_g$ ) of PL is usually in the range 50-60°C (Garlotta, 2001). Amorphous PL at below  $T_g$  is rigid, brittle and low flexibility. Poly(3-methyl-1,4-dioxan-2-one), poly(ethylene oxide), citrate esters, triacetine, poly(ethylene glycol)s and poly(propylene glycol) (PPG) were found to be efficient plasticizers for PL. In the plasticized PL, the  $T_g$  is shifted to lower temperature and have transition from brittle to ductile behavior. Recent studies, the PPG demonstrated an increase in the efficiency of plasticization for PL resulting from increased miscibility with PL and more efficiently reduced the  $T_g$  (Kuliski, 2006). However, blends of PL with PPG affect to phase separation at a slight PPG content. Phase separate occurrence of PPG lead to increase stiffness and decrease an elongation of the plasticized PL. Somehow, the phase separation of PPG quite still undergoes when used at much content. To solve the phase separation problem of plasticizer, this research aims at synthesizing mPPG-*b*-PL diblock copolymers and PL-*b*-PPG-*b*-PL triblock copolymers and expects that this will solve the problem of phase separation. The scPLs studied in this research include the mPPG-*b*-PLL/mPPG-*b*-PDL and PLL-*b*-PPG-*b*-PLL/PDL-*b*-PPG-*b*-PDL blends at different blend ratios and molecular weights of each block.

## 1.2 Research objectives

The objectives of this research are as following:

1.2.1 To synthesize and characterize mPPG-*b*-PLL and mPPG-*b*-PDL diblock copolymers.

1.2.2 To synthesize and characterize PLL-*b*-PPG-*b*-PLL and PDL-*b*-PPG-*b*-PDL triblock copolymers.

1.2.3 To prepare and characterize stereocomplex PL films from mPPG-*b*-PLL /mPPG-*b*-PDL blending.

1.2.4 To prepare and characterize stereocomplex PL films from PLL-*b*-PPG-*b*-PLL/PDL-*b*-PPG-*b*-PDL blending.



### 1.3 Scopes of research

1.3.1 The diblock copolymers of mPPG-*b*-PLL and mPPG-*b*-PDL with mPPG block length of 2,500 g/mol and PL block lengths of 20,000 and 40,000 g/mol were synthesized and characterized.

1.3.2 The triblock copolymers of PLL-*b*-PPG-*b*-PLL and PDL-*b*-PPG-*b*-PDL with PPG block lengths of 2,000 and 4,000 g/mol and PL block lengths of 20,000 and 40,000 g/mol were synthesized and characterized.

1.3.3 The PL blend films of PLL-*b*-PPG-*b*-PLL/PDL-*b*-PPG-*b*-PDL and mPPG-*b*-PLL/mPPG-*b*-PDL blends with blend ratios of 100/0, 75/25, 50/50, 25/75 and 0/100 wt % were prepared and characterized.

### 1.4 Expected results

To obtain novel stereocomplex PL films with controllable stereocomplex crystallinity and mechanical properties, which have potential use in high performance bioplastic applications.

### 1.5 Definition of terms

1.5.1 Biodegradable polymers are polymers that break down and lose their initial integrity by microorganism action or by simple hydrolysis.

1.5.2 Block copolymers comprise two or more homopolymer subunits linked by covalent bonds. The union of the homopolymer subunits may require an intermediate non-repeating subunit, known as a junction block. Block copolymers with two or three distinct blocks are called diblock copolymers and triblock copolymers, respectively.

1.5.3 Copolymer is a polymer derived from two (or more) monomeric species, as opposed to a homopolymer where only one monomer is used.

1.5.4 Elongation at break is defined as the length at breaking point expressed as a percentage of its original length (i.e. length at rest) e.g. if a rubber reaches twice its length before breaking its elongation is 100%.



1.5.5 Flexibility is a measure of a material's ability to flex or bend.

1.5.6 Plasticizer is an additive that increases the plasticity or fluidity of a material.

1.5.7 Polymerization is a process of reacting monomer molecules together in a chemical reaction to form polymer chains or three-dimensional networks.

1.5.8 Polymer blend is a member of a class of materials analogous to metal alloys, in which at least two polymers are blended together to create a new material with different physical properties.

1.5.9 Stereocomplexation of poly(lactide)s are the interaction between enantiomeric poly(lactide) chains including poly(L-lactide) and poly(D-lactide) which have different tacticities or configurations, a stereo selective association of the former polymer pair takeplace.

1.5.10 Strain is the displacement (also a vector quantity) per unit length and is also a vector quantity.

1.5.11 Stress is a force (a vector property) divided by the cross sectional area.

1.5.12 Young's modulus is a measure of the stiffness of an elastic isotropic material and is a quantity used to characterize materials.



## CHAPTER 2

### LITERATURE REVIEW

#### 2.1 Biodegradable polymers

##### 2.1.1 Definitions of biodegradable polymers

According to ASTM D996-04, biodegradable is defined as capable of undergoing decomposition into carbon dioxide, methane, water, inorganic compounds, or biomass in which the predominant mechanism is enzymatic action of microorganisms (Lafranche *et al.*, 2005). Biodegradable polymers are a material in which at least one steps in the degradation process is through metabolism in the presence of naturally occurring organisms. Under appropriate conditions of moisture, temperature and oxygen availability, biodegradation leads to fragmentation or disintegration of the plastics with no toxic or environmentally harmful residue (Kumar *et al.*, 2007). Some of the important properties of a biodegradable biomaterial can be summarized as follows: (Lloyd, 2002)

- 1) The material should not evoke a sustained inflammatory or toxic response upon implantation in the body.
- 2) The material should have acceptable shelf life.
- 3) The degradation time of the material should match the healing or regeneration process.
- 4) The material should have appropriate mechanical properties for the indicated application and the variation in mechanical properties with degradation should be compatible with the healing or regeneration process.
- 5) The degradation products should be non-toxic, and able to get metabolized and cleared from the body.
- 6) The material should have appropriate permeability and processibility for the intended application.





## 2.1.2 Types of biodegradable polymers

Biodegradable polymers mean both synthetic polymers and biologically derived polymers in which have been extensively investigate. In this topic would focus on the synthetic biodegradable polymers, there are many as follow: (Premraj *et al.*, 2004).

### 2.1.2.1 Polyethers

Poly(ethylene glycol)s (PEGs), poly(propylene glycol)s (PPGs) and poly(tetramethylene glycol)s come under the class of polyethers and are used in pharmaceuticals, cosmetics, lubricants, inks, and surfactants. *Flavobacterium* sp. and *Pseudomonas* sp. together associate and mineralize PEGs completely under aerobic conditions. During degradation, the PEG molecules are reduced by one glycol unit at a time after each oxidation cycle. *Pelobacter venetianus* was found to degrade PEG and ethylene glycol under anaerobic conditions.

### 2.1.2.2 Polyesters

Polyesters are polymers in which component monomers are bonded via ester linkages. Many kinds of esters occur in nature and the esterase enzymes that degrade them are ubiquitous in living organisms. Ester linkages are generally easy to hydrolyze and hence a number of synthetic polyesters are biodegradable. Therefore, bacterial polyesters (polyhydroxy alkanoates) have been used to make biodegradable plastics. Hydrolytic cleavage of the ester bond in the low molecular weight polyester by the lipase of *Pseudomonas* species has been reported.

#### 1) Polyhydroxyalkanoates

Polyhydroxyalkanoates (PHAs) is naturally occurring polyesters that accumulates in bacterial cells as a carbon and energy storage compound. PBH and copolymers containing polyhydroxyalkanoate, PHA (for example 3-hydroxyvalerate) are being used for the manufacture of biodegradable plastics. The PHA depolymerases are serine hydrolases usually having single substrate-binding domain. The presence of two substrate-biding domains enlarges substrate specificity or enhances adsorption of the enzyme.

#### 2) Polycaprolactone

Polycaprolactone (PCL) is a synthetic polyester that can be degraded by microorganisms and enzymes like lipases and esterases. Cutinases, which are



obtained from fungal phytopathogens, degrade cutin (the structural polymer of the plant cuticle) and act as PCL depolymerases. The biodegradability of PCL in the form of blend sheets (for example in polycarbonate-polycaprolactone blend sheets) is much reduced because the packed form of the PCL in the blend sheets protects it from enzymatic digestion. However, the enzymatic degradation can be promoted by means of surface etching by oxygen plasma treatments.

### 3) poly(*p*-dioxanone)

Poly(*p*-dioxanone) (PDO) is known as a polyether-ester and has good tensile strength and flexibility. It is used for bioabsorbable sutures in clinical applications. PPDO is found to be degraded by strains that belong to the  $\alpha$  and  $\beta$  subdivision of the class *Proteobacteria* and the class *Actinobacteria*. Degradation leads to the formation of monomeric acids.

#### 2.1.2.3 Polyurethane

Polyurethane (PU) produced by the diisocyanate polyaddition process is the characteristic chain link of urethane bond. PU degradation proceeded in a selective manner, with the amorphous regions being degraded prior to the crystalline regions. Also, PU's with long repeating units and hydrolytic groups would be less likely to pack into high crystalline regions as normal polyurethane, and these polymers were more accessible to biodegradation.

Among those biodegradable polymers, poly(lactic acid) (PLA) is an aliphatic polyester, has been attention by industrial sections because it can be easily produce, no toxicity and high mechanical performance. Furthermore, the detail of PLA as describe in the topic 2.2.

**2.1.3 Mechanisms of polymer degradation and erosion** (Lakshmi *et al.*, 2007; Chhaya *et al.*, 2011)

The difference between polymer “degradation” and “erosion” is not clear in many cases. Biodegradable polymers undergo hydrolytic bond cleavage to form water soluble degradation products that can dissolve in an aqueous environment, resulting in polymer erosion. In this context, degradation is a chemical phenomenon and erosion encompasses physical phenomena, such as dissolution and diffusion. Polymer degradation is the key route of erosion.



Polymer erosion is so far more complex than degradation, because it depends on many other processes, such as degradation, swelling, dissolution and diffusion of oligomers and monomers, and morphological changes. The erosion of a polymer matrix can proceed through two alternative physical mechanisms: (a) surface erosion and (b) bulk erosion as shown in Figure 2.1. For ideal surface erosion, erosion rate is constant and proportional to external surface area.

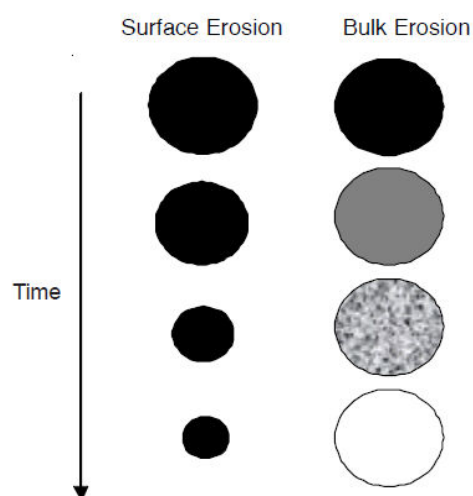


**Figure 2.1** Schematic representations of surface erosion and bulk erosion. (Chhaya *et al.*, 2011).

Hydrolytically degradable polymers are polymers that have hydrolytically labile chemical bonds in their back bone. The functional groups susceptible to hydrolysis include esters, ortho-esters, anhydrides, carbonates, amides, urethanes, ureas, etc. Two general routes are used to develop hydrolytically sensitive polymers for biomedical applications. They are step (condensation) polymerization and addition (chain) polymerization including ring-opening polymerization (ROP). Step process is used to prepare a variety of hydrolytically sensitive polymer classes, such as polyanhydrides, poly(ortho-esters) and polyurethanes. The ROP is an extensively investigated polymerization route to develop hydrolytically sensitive polymers, including the poly( $\alpha$ -esters) and polyphosphazenes. Radical polymerization mostly results in the formation of non-degradable polymers; however, recent studies have demonstrated the feasibility of developing synthetic degradable polymers or cross-



linked gels by radical polymerization processes. In addition, several polymers enveloped by microbial bioprocess are gaining significant interest as biodegradable polymers. The following sections discuss some of the most promising hydrolytically sensitive synthetic polymers developed and their biomedical applications.

## 2.2 Polylactide

### 2.2.1 Production of polylactide

Lactic acid (2-hydroxypropionic acid) is the basic monomer for synthesis of polylactide (PL). In addition it is used as acidulate in food, as a unit of biodegradable polymer, and is converted to esters and used as green solvent for metal cleaning, paints and coatings (Henton *et al.*, 2005). Its chemical structure present an asymmetric carbon atom and exists as two optically active configurations there are L-isomer that produced in humans and other mammals, whereas both D- and L- enantiomers are produced in bacterial systems, the chemical structure of L- and D-lactic acid as shown in Figure 2.2. The L-lactic acid rotates the plane of polarized light clockwise and the D-lactic acid rotates it counterclockwise. In order that a sugar or starch obtaining from plant source such as corn, wheat or rice are converted into lactic acid by either bacterial fermentation or petrochemical route. The organisms that predominantly yield the L-isomer are *Lactobacilli amylophilus*, *L. bavaricus*, *L. casei*, *L. maltaromicus*, and *L. salivarius*. Strains such as *L. delbrueckii*, *L. jensenii*, or *L. acidophilus* yield the D-isomer or mixture of both (Garlotta, 2001).

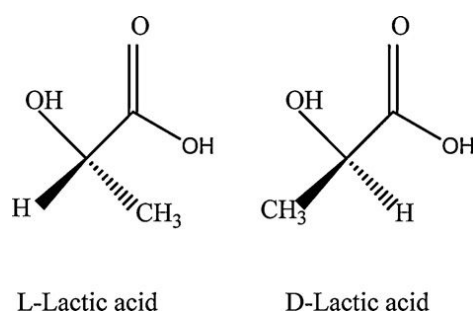


**Figure 2.2** Lactic acid optical monomers (Rahul, 2010).



The synthesis of lactic acid into PL can follow three different routes of polymerization, as shown in Figure 2.3. Lactic acid is condensation polymerized to obtain a low molecular weight poly(lactic acid) (PLA) which is brittle and unusable for any applications. The molecular weight of this condensation polymer is low due to difficulties of removing trace amounts of water in the late stages of polymerization. The second route of producing PLA is to collect, purify to yield high weight average molecular weight ( $M_w \sim 100,000$ ) PLA. Mitsui Toatsu Chemicals recently commercialized a process wherein lactic acid and catalyst are azeotropically dehydrated in a refluxing, high-boiling, aprotic solvent under reduced pressures to obtain PLA with weight-average molecular weights greater than 300,000. And the last route starts with lactic acid, followed by a continuous condensation reaction of aqueous lactic acid to produce low molecular weight PLA prepolymer. Then, the low molecular weight oligomers are converted into a mixture of lactide stereoisomers using a catalyst to enhance the rate and selectivity of the intramolecular cyclization reaction. The molten lactide mixture is then purified by vacuum distillation. Finally, polylactide (PL) with high molecular weight is produced using an organotin-catalyzed, ring-opening lactide polymerization in the melt, completely eliminating the use of costly and environmentally unfriendly solvents (Garlotta, 2001; Henton *et al.*, 2005).



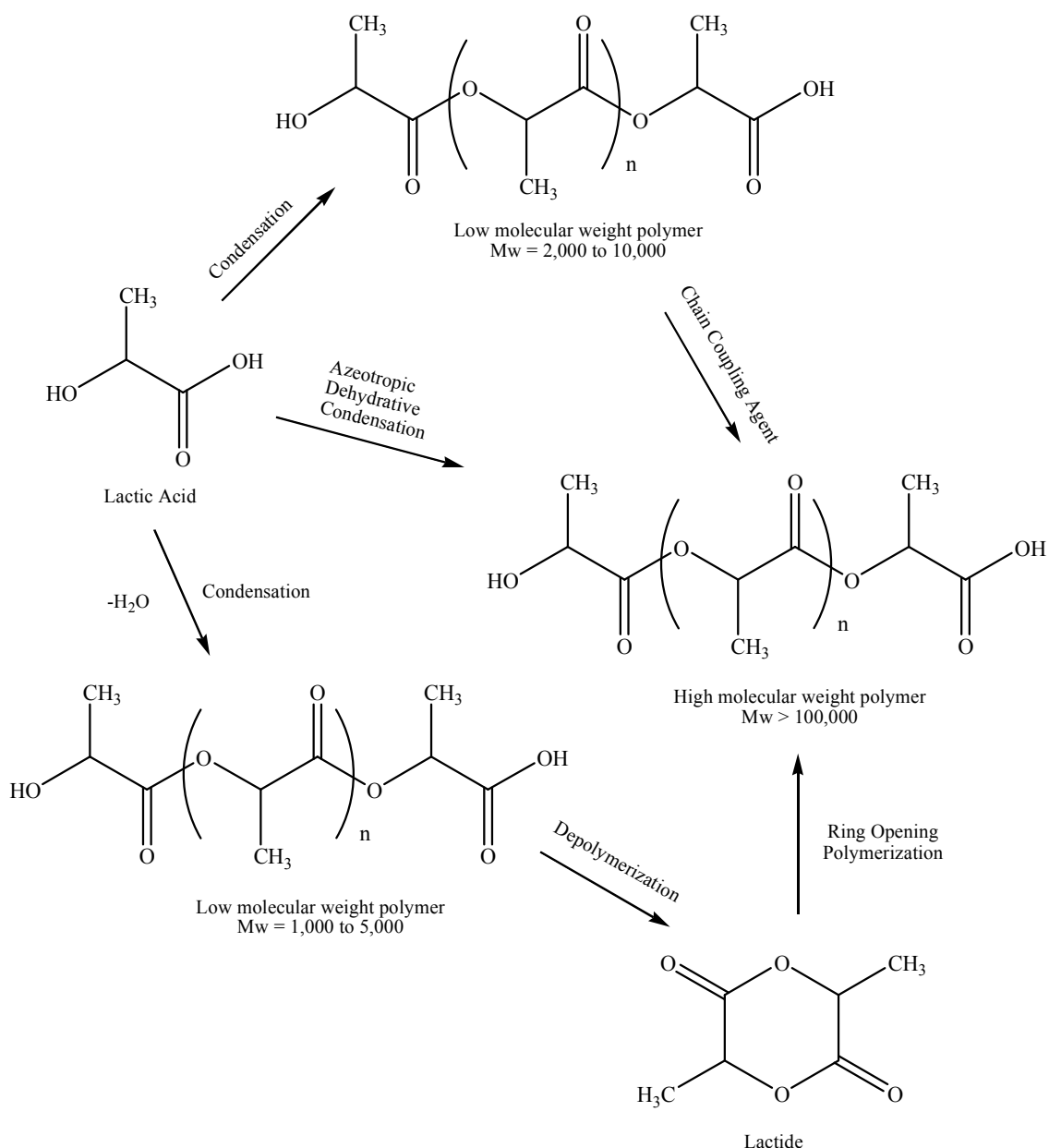


**Figure 2.3** Synthesis methods for high molecular weight PL (Garlotta, 2001).

Many catalyst systems have been evaluated for the polymerization of lactide including complexes of aluminum, zinc, tin, and lanthanides. Even strong bases such as metal alkoxides have been used with some success. Tin compounds, especially tin(II) bis-2-ethylhexanoic acid (tin octoate), are preferred for the bulk polymerization of lactide due to their solubility in molten lactide, high catalytic activity, and low rate of racemization of the polymer. Conversions of more than 90% and less than 1% racemization can be obtained while providing polymer with high molecular weight. The polymerization of lactide using tin octoate is generally thought to occur via a coordination-insertion



mechanism with ring opening of the lactide to add two lactyl units (a single lactide unit) to the growing end of the polymer chain shown schematically in Figure 2.4. The tin catalyst facilitates the polymerization, but hydroxyl or other nucleophilic species are the actual initiators. There is generally several hundred parts per million of hydroxyl impurities in the lactide from water, lactic acid, and linear dimers and trimers. High molecular weight polymer, good reaction rate, and low levels of racemization are obtained with tin octoate catalyzed polymerization of lactide. Typical conditions for polymerization are 180-210°C, tin octoate concentrations of 100–1000 ppm, and 2-5 h to reach 95% conversion. The polymerization is first order in both catalyst and lactide. Frequently hydroxyl-containing initiators such as 1-octanol are used to both control molecular weight and accelerate the reaction (Henton *et al.*, 2005).

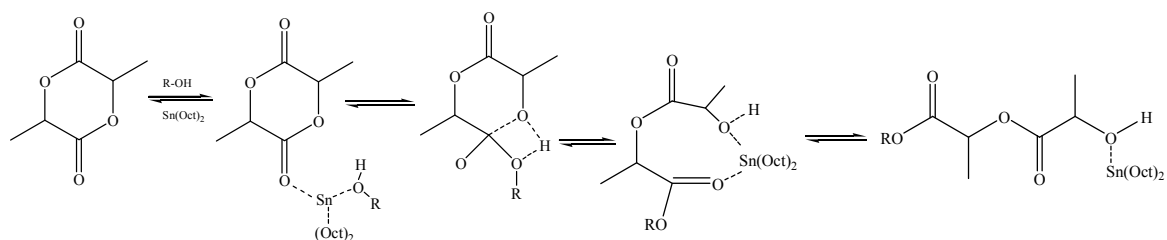


**Figure 2.4** Coordination-insertion chain growth mechanism of lactide to PL (Henton *et al.*, 2005)

### 2.2.2 Optical structures of polylactide

There are two optical arrangements for lactic acid monomer such as L-lactic acid and D-lactic acid, and three optical arrangements for lactide monomer are L-lactide, D-lactide and *meso*-lactide, therefore, the variety of primary structures available for PL. The notable primary structure of PL is that of the isotactic homopolymer poly(L-lactide) (PLL) or its opposite enantiomer poly(D-lactide) (PDL) where all of the monomers in the chain are of the same optical composition (Henton *et al.*, 2005). Figure 2.5 show the chemical structure of PLL and PDL which synthesis from various monomers. Both of PL has the same melting temperature at about 175°C (Fan *et al.*, 2004). A greater amount of research has been done on PLL due to the fact that the commercial production of lactic acid has been predominantly L-lactic acid.



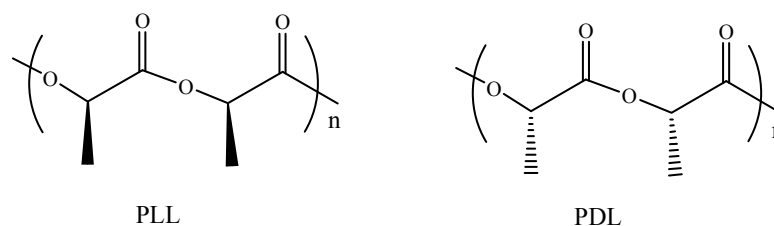


**Figure 2.5** Chemical structures of PLL and PDL (Tsuji, 2005).

### 2.2.3 Physical properties of polylactide

The physical characteristics of high molecular weight PL are dependent on its transition temperatures for common qualities such as density, heat capacity, and mechanical and rheological properties. In the solid state, PL can be either amorphous or semi-crystalline, depending on the stereochemistry and thermal history. For amorphous PL, the glass transition temperature ( $T_g$ ) impose the upper use temperature for most commercial applications. For semi-crystalline PL, both the  $T_g$ , about  $58^\circ\text{C}$  and melting point ( $T_m$ ),  $130\text{-}230^\circ\text{C}$  (depending on structure) are important for determining the use temperatures across various applications. Both of these transitions,  $T_g$  and  $T_m$ , are strongly affected by overall optical composition, primary structure, thermal history, and molecular weight. Above  $T_g$  amorphous PL transition from glassy to rubbery and will behave as a viscous fluid upon further heating. Below  $T_g$ , PL behaves as a glass with the ability to creep until cooled to its  $\beta$  transition temperature of approximately  $45^\circ\text{C}$ . Below this temperature PL will only behave as a brittle polymer (Henton *et al.*, 2005).

PL has good mechanical and thermal properties similar to poly(ethylene terephthalate) (PET) or polystyrene (PS) depending on the considered properties. However, properties of PL are highly related to the ratio between two meso-forms (D and L). PLL has higher crystallinity, which can lead to higher melting temperature and brittleness. Furthermore, PL can be plasticized using poly(ethylene glycol) (PEG), triethyl citrate (TC), and partial fatty acid ester. PL has moderate barrier properties (water vapor permeability and oxygen permeability) as compared to those of polystyrene (PS). However, high density, high polarity, poor heat resistance and brittleness limit its use (Pilla, 2011).

Typical properties of Nature Works PL from Cargill Dow LLC for injection molding and extrusion applications are given in Table 2.1. Each grade is optimized for both processing and end use performance in its intended application.





**Table 2.1** Properties of extrusion/thermoforming and injection molding grades of Nature Works PL.

	PL Polymer 2000D <sup>a</sup>	ASTM Method	PL Polymer 3010D <sup>b</sup>	ASTM Method
<b>Physical property</b>				
Specific gravity (g/cc)	1.25	D792	1.21	D792
Melt index, g/10min (190°C/2.16 kg)	4-8	D1238	10-30	D1238
Clarity	Transparent		Transparent	
<b>Mechanical Properties</b>				
Tensile strength at break, psi (MPa)	7,700 (53)	D882	7,000 (48)	D638
Tensile yield strength, psi (MPa)	8,700 (60)	D882		
Tensile modulus, Kpsi (GPa)	500 (3.5)	D882		
Tensile elongation (%)	6.0	D882	2.5	D638
Notched izod impact, Ft-lb/in (J/m)	0.24 (0.33)	D256	0.3 (0.16)	D256
Flexural strength, psi (MPa)			12,000 (83)	D790
Flexural modulus, Kpsi (GPa)			555 (3.8)	D790

<sup>a</sup> 2000D is a product of Cargill Dow LLC designed as an extrusion/thermoforming grade; properties typical of extruded sheet.

<sup>b</sup> 3010D is a product of Cargill Dow LLC designed as an injection molding grade; properties typical of injection molded tensile bars.

### 2.2.3.1 Rheology of polylactide

Rheological properties are useful in evaluating thermoplastics for their performance during processing operations. The literature reports a wide variety of processes and products using PL, spanning from high orientation processes such as fiber



spinning and oriented films to lower orientation processes such as thermoforming and foams. The time scales of these processes are very different. Considerations for material flow characteristics, orientation, and crystallization must be made to gauge and predict the resulting properties of the products made from these processes. Intrinsic factors affecting the flow characteristics of PL are molecular weight distribution, degree and type of branching, optical composition, optical block length distributions, and melt stability.

### 1) Melt Rheology of Linear polylactide

PL, like many thermoplastics, is a pseudoplastic, non-Newtonian fluid. Above the melting point, PL behaves as a classic flexible-chain polymer across all optical compositions. PL's zero shear viscosity and shear thinning behavior have been measured by a variety of groups. However, complicated by the array of optical copolymers studied, the difficulty associated with measuring the absolute molecular weight of PL, and the issues of melt stability, the interpretation of PL's rheology has not always been consistent.

The most comprehensive studies of linear PLs in the melt were performed by Dorgan *et al.* (2000) who showed that zero shear viscosity ( $\eta_0$ ) scales very close to the usual 3.4 power with  $M_w$ , and that PL obeys the Cox-Merz rule well into the shear thinning region when in the linear viscoelastic range. The plateau modulus for PLL is about 1 MPa, which corresponds to a critical molecular weight of about 9000 g/mol. Previous reports by Cooper-White and MacKay 51 measured the rheological properties of PLL with molecular weights ranging from 2,000 to 360,000 and reported a dependence of zero shear viscosity ( $\eta_0$ ) on chain length to the 4.0 power. However, only a very small number of samples were used to build the 4.0 power relationship. Dorgan also showed that PL exhibits strain hardening during extension in the melt, a characteristic necessary for fiber spinning. The complex viscosity for PL with  $M_w$  213,000 (relative to polystyrene) and 13.0% D was measured at many temperatures and shear rates. The shifted data shown in Figure 2.6 depict rheological behavior across six orders of magnitude in shear for 180°C.



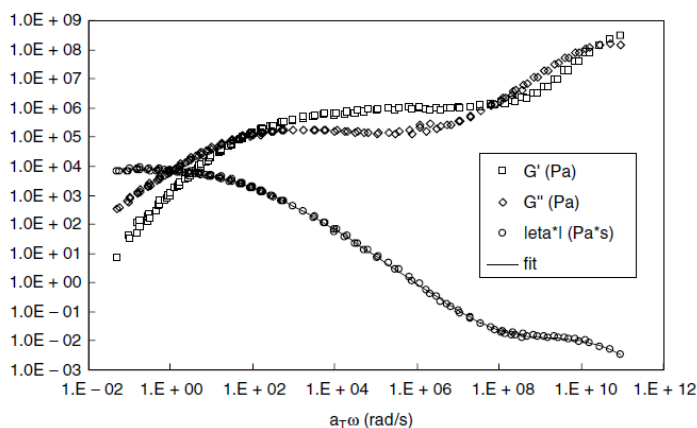


**Figure 2.6** Melt rheology of  $M_w$  213,000 (relative to polystyrene) 13.0%D PL shifted to  $180^\circ\text{C}$  (Henton *et al.*, 2005).

## 2) Melt stability

The melt stability of polylactide have been reported by Witzke *et al.* (1997) Dorgan *et al.* (2000) Ramkumar and Bhattacharya (1998) and Feng and Hanna (1999). Reactions leading to poor melt stability include chain scission due to hydrolysis, chain scission due to thermal instability. Hydrolysis can be reduced or essentially eliminated with conventional drying operations where water is removed prior to melting. Recommended drying conditions are available for commercial PL. When PL is exposed to a humid environment following drying, moisture is quickly absorbed into the polymer up to its equilibrium level of swelling. Kinetics for melt hydrolysis depends on water concentration, acid or base catalysis, and polymerization catalyst concentration. The proton in the CH group of the main chain of PL is labile. It has been suggested that the proximity of this labile proton to the ester group affects the thermal sensitivity of the polymer (Ramkumar *et al.*, 1998). The proton may be abstracted resulting in the breakdown of the molecular chain. In practical extrusion processes, thermal stability becomes important at temperatures greater than  $250^\circ\text{C}$ . Using PL polymerized with tin octoate catalyst, Cicero *et al.* (2002) showed that the melt stability of PL can be improved by the addition of small amounts of tris(nonylphenyl)phosphite (TNPP), likely due to balancing chain extension with degradation reactions. Adding TNPP during rheological testing greatly stabilized the polymer and lengthened the time available for testing. The thermodynamic equilibrium between polylactide and lactide



monomer varies with temperature and is about 4.3% lactide at 210°C (Witzke, 1997). Since lactide imparts undesirable characteristics during processing, such as fuming, it is desirable to depress the lactide formation kinetics and stabilize the polymer. Gruber et al. (Gruber *et al.*, 1999) showed that lactide formation could be substantially reduced under normal processing by complexing the catalyst with additives, resulting in a melt-stable PL polymer.

### 2.2.3.2 Crystallinity of polylactide

#### 1) Morphology

The morphology of PL crystals is influenced by composition and thermal history. Abe *et al.* (2001) showed that PLL crystals grown at different temperatures go through three regime changes associated with nucleation and crystal growth rates. For PLL crystallized isothermally from the melt, spherulitic morphology is observed at crystallization temperatures below 145°C (regime II). During isothermal growth, the radius of the spherulites increases linearly with time, and the slope of the curve is the lineal crystal growth rate (LCR). At higher temperatures, a smaller number of spherulites are formed due to a decrease in the nucleation density. This leads to larger spherulites with increasing crystallization temperature. Crystallizing PLL at temperatures greater than 150°C (regime I) results in hexagonal lamellar stacking crystal morphology. Spherulites have been shown to contain stacked lamellar morphology, with the long axis of the lamellar crystal running parallel to the spherulite radius. The lamellar thickness of PL varies with the temperature of crystallization ( $T_c$ ), crystallization time ( $t_c$ ), optical purity (OP), and molecular weight. Figure 2.7 shows the crystal imaging using AFM and polarized light microscopy.



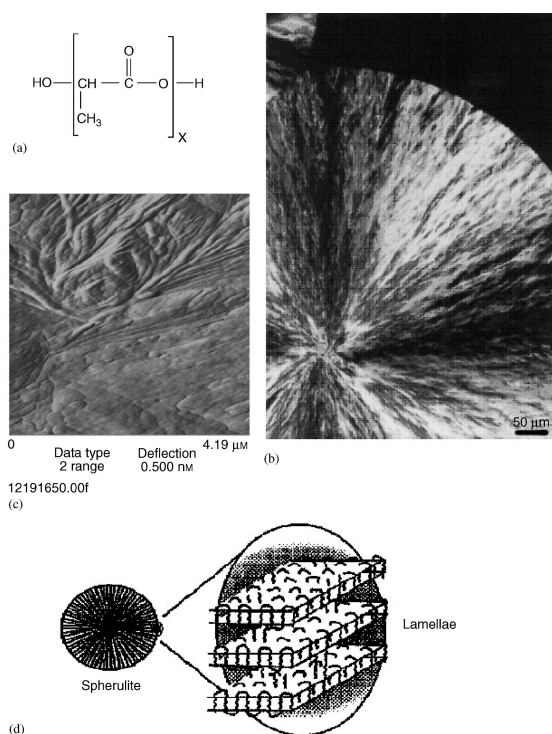


**Figure 2.7** Morphology of PL by optical microscopy and AFM; (a) molecular formula of PL, (b) picture of the central region of a spherulite by optical microscopy, (c) copy of an AFM picture of a section of the spherulite shown in (b) and (d) schematic drawing of the lamellae within a spherulite (Henton *et al.*, 2005).

## 2) Degree of crystallinity

Most commonly, an enthalpy of fusion of 93 J/g is used for a 100% crystalline PLL or PDL homopolymers (i.e.  $\Delta H_m^0 = 93 \text{ J/g}$ ) (Fischer *et al.*, 1973) having infinite crystal thickness, and Equation (2.1) is used to calculate percent crystallinity from DSC scans.

$$\text{Crystallinity (\%)} = \frac{\Delta H_m - \Delta H_c}{93} \times 100 \quad \dots\dots\dots(2.1)$$

where  $\Delta H_m$  is the measured heat of fusion and  $\Delta H_c$  is the heat of crystallization. This value of 93 J/g is used throughout the PL literature. However, since  $T_m^0$  decreases with decreasing OP, it is expected that using a constant value for  $\Delta H_m^0$  across all optical compositions will introduce error. No reference was found that systematically calculated  $\Delta H_m^0$  for homopolymers of reduced OP. It is well known that for PL of

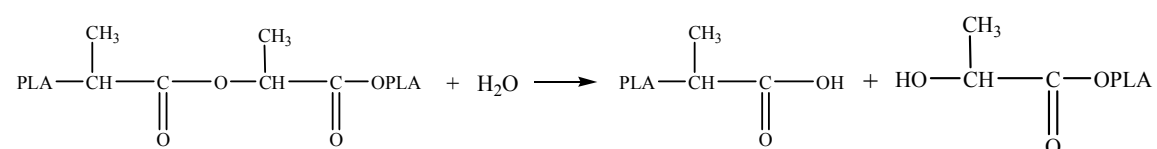
essentially random optical copolymers of predominantly L-lactide, with small amounts of D- and *meso*lactides, the attainable percentage of crystallinity ( $x_c$ ) decreases with decreasing optical purity (OP) and crystallization is essentially nonexistent about when OP less than 0.78.

### 2.2.4 Degradation of polylactide

Under conditions of high temperature and high humidity, as in active compost, for example, PL will degrade quickly and disintegrate within weeks to months. The primary mechanism of degradation is hydrolysis, followed by bacterial attack on the fragmented residues. The environmental degradation of PL occurs by a two-step process (Lunt *et al.*, 1998). During the initial phases of degradation, the high molecular weight polyester chains hydrolyze to lower molecular weight oligomers. The rate of hydrolysis is accelerated by acids or bases and is dependent on moisture content and temperature. Article dimensions, crystallinity, and blends will affect the rate of degradation. PL products rapidly degrade in both aerobic and anaerobic composting conditions. But under typical use conditions, PL is very stable and will retain its molecular weight and physical properties for years. This is typified by its growing use in clothing and durable applications. High molecular weight PL is also naturally resistant to supporting bacterial and fungal growth, which allows it to be safely used for applications such as food packaging and sanitation.

#### 2.2.4.1 Hydrolysis

Degradation of PL is primarily due to hydrolysis of the ester linkages, which occurs more or less randomly along the backbone of the polymer. It requires the presence of water according to the following reaction:



Four key features mark the hydrolytic degradation of PLA:

1) The  $pK_a$  of PL's carboxylic acid end group and its oligomers is unusually low ( $\sim 3$ ) compared to most carboxylic acid groups (4.5-5). PL's carboxylic acid end groups catalyze the ester hydrolysis, which generally leads to a faster rate of degradation as the polymer degrades (autocatalysis).

2) Two reaction mechanisms apparently occur. The first is a random chain scission and the second a chain-end hydrolysis. The chain end scission is about 10 times faster than the random scission reaction at low pH values but is negligible at neutral and basic pH values. The number of ester groups along the chain is much greater than that of the chain ends and is statistically much more important.

3) The crystalline regions hydrolyze much more slowly than the amorphous regions.

4) The rate of hydrolysis is much greater above the glass transition temperature ( $T_g$ ) than below.

#### 2.2.4.2 Enzymatic degradation

Several enzymes have been shown to catalyze PL hydrolysis. Enzymatic hydrolysis of PLL with varied crystal morphologies was studied using proteinase K by Tsuji *et al.* (2000; 2001). It was concluded that the enzymatic degradation proceeded via mainly a surface erosion mechanism. Amorphous regions hydrolyzed more readily than crystalline regions. The enzymatic hydrolysis rate ( $R_{EH}$ ) was modeled using the equation (2.2)

$$R_{EH} (\mu\text{g}/(\text{mm}^2 \cdot \text{h})) = 0.36(1-x_c) \dots\dots\dots(2.2)$$

where  $x_c$  is the fraction of crystalline PLL. Tie chains degraded more readily than folds or restricted amorphous chains.

#### 2.2.5 Applications and performance

Since PL is an environmentally friendly polymer that can be designed to controllably biodegrade, it is ideally suited for many applications in the environment where recovery of the product is not practical, such as agricultural mulch films and bags. Composting of post-consumer PL items is also a viable solution for many PL



products. However, the large growth seen for PL in many applications does not depend upon the biodegradability of the material.

Injection molding of heat-resistant products requires rapid crystallization rates that can be achieved by PL, typically containing less than 1% D-isomer and often with the addition of nucleating agents (Kolstad, 1996). These compositions allow high levels of crystallinity to develop during the fast cooling cycle in the mold. Extrusion-thermoforming is optimized at a D-isomer content that does not allow crystallization to occur during the melt processing steps, with 4–8% D-content being the effective range. Branching can be introduced by a variety of methods (Tasaka *et al.*, 2002; Lehermeier *et al.*, 2001) thus enhancing melt strength during fabrication and opening up new application opportunities in the areas of foams and extrusion coating. Examples of a number of articles fabricated from PL are shown in Figure 2.8. In short, the rheological characteristics and physical properties of PL can be tailored for use in a variety of processes and applications.

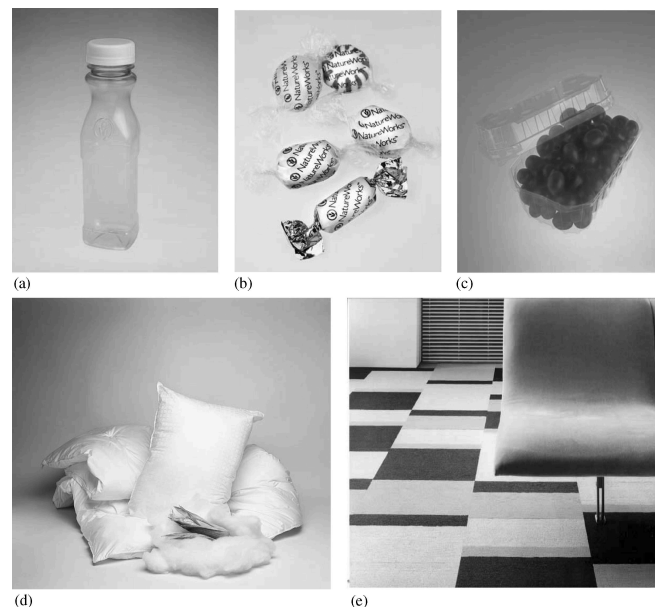


**Figure 2.8** Articles produced from PL; (a) injection stretch-blow molded bottles, (b) films, (c) extrusion-thermoformed containers, (d) fiberfill products and (e) Carpet and coverings (Henton *et al.*, 2005).





### 2.2.5.1 Polylactide advantages (Rahul, 2010)

#### 1) Eco-friendly

Apart from being derived from renewable resources (e.g., corn, wheat, or rice), PL is biodegradable, recyclable, and compostable. Its production also consumes carbon dioxide. These sustainability and eco-friendly characteristics make PL an attractive biopolymer.

#### 2) Biocompatibility

The most attractive aspect of PL, especially with respect to biomedical applications, is its biocompatibility. A biocompatible material should not produce toxic or carcinogenic effects in local tissues. Also, the degradation products should not interfere with tissue healing. PL hydrolyzes to its constituent-hydroxy acid when implanted in living organisms, including the human body. Moreover, PL degradation products are non-toxic (at a lower composition) making it a natural choice for biomedical applications. The Food and Drug Administration (FDA) has also approved PLA for direct contacting with biological fluids.

#### 3) Processibility

PL has better thermal processibility compared to other biopolymers such as poly(hydroxy alkanates) (PHAs), poly(ethylene glycol) (PEG), poly( $\epsilon$ -caprolactone) (PCL), etc. It can be processed by injection molding, film extrusion, blow molding, thermoforming, fiber spinning, and film forming, with PL resins for these methods commercialized by NatureWorks LLC.

#### 4) Energy savings

PL requires 25–55% less energy to produce than petroleum-based polymers and estimations show that this can be further reduced to less than 10% in the future. Lower energy use makes PL production potentially advantageous with respect to cost as well.

### 2.2.5.2 Polylactide limitations

#### 1) Poor toughness

PL is a very brittle material with less than 10% elongation at break. Although its tensile strength and elastic modulus are comparable to poly(ethylene terephthalate) (PET), the poor toughness limits its use in the applications that need plastic deformation at higher stress levels (e.g., screws and fracture fixation plates).



## 2) Slow degradation rate

PL degrades through the hydrolysis of backbone ester groups and the degradation rate depends on the PL crystallinity, molecular weight, molecular weight distribution, morphology, water diffusion rate into the polymer, and the stereoisomeric content. The degradation rate is often considered to be an important selection criterion for biomedical applications. The slow degradation rate leads to a long in vivo life time, which could be up to years in some cases. There have been reports of a second surgery almost 3 years after implantation to remove a PLA-based implant. The slow degradation rate is a serious problem with respect to disposal of consumer commodities as well.

## 3) Hydrophobicity

PL is relatively hydrophobic, with a static water contact angle of approximately 80°C. This results in low cell affinity, and can elicit an inflammatory response from the living host upon direct contact with biological fluids.

## 4) Lack of reactive side-chain groups

PL is chemically inert with no reactive side-chain groups making its surface and bulk modifications a challenging task.

## 2.2.6 Modification properties of polylactide

### 2.2.6.1 Stereocomplexation

Although the  $T_m$  of isotactic PL (e.g., PLL) is about 170°C and its  $T_g$  is about 60°C, its crystallization is very slow and almost no crystallization proceeds under fast cooling such as practical processing. This results in the lower heat deformation temperature (HDT) of PL. Therefore, modification of thermal resistance is essential to the practical applications of PL.

When the interaction between polymers having different tacticities or on figurations prevails over that one between polymers with the same tacticity or configuration, a stereoselective association of the former polymer pair takes place. Such association is described as stereocomplexation or stereocomplex formation (Tsuji, 2005). In 1987, Ikada *et al.* (1987) reported that equimolar PLL and PDL can crystallize in a stereocomplex polylactide (scPL), occur in solution, in a solid (bulk) state from the melt, during polymerization, or during hydrolytic degradation, as long as L-lactide (or L-lactyl) unit sequences and D-lactide (or D-lactyl) unit sequences coexist in a system (Tsuji *et al.*, 2000). In other words, PL stereocomplexation can take place both in



enantiomeric PL-based polymer blends and in nonblended stereoblock PL. The synthetic procedures and structures of PLL, PDL, and scPL are given in Figure 2.9.  $T_m$  of PL sc crystallites (210-240°C) is around 50°C higher than that of its homocrystallites (hc). Because two enantiomeric chains pack tightly through the stronger van der Waals forces of the stereocomplex crystallites (Brizzolara *et al.*, 1996; Okihara *et al.*, 1991) the scPL has many unique properties such as high mechanical strength, modulus, and toughness (Tsuji, 1999; Rodriguez *et al.*, 2014), good thermomechanical properties (Hirata, 2008), good resistance to solvent, low thermal and hydrolytic degradation rates (Fundador *et al.* 2010).

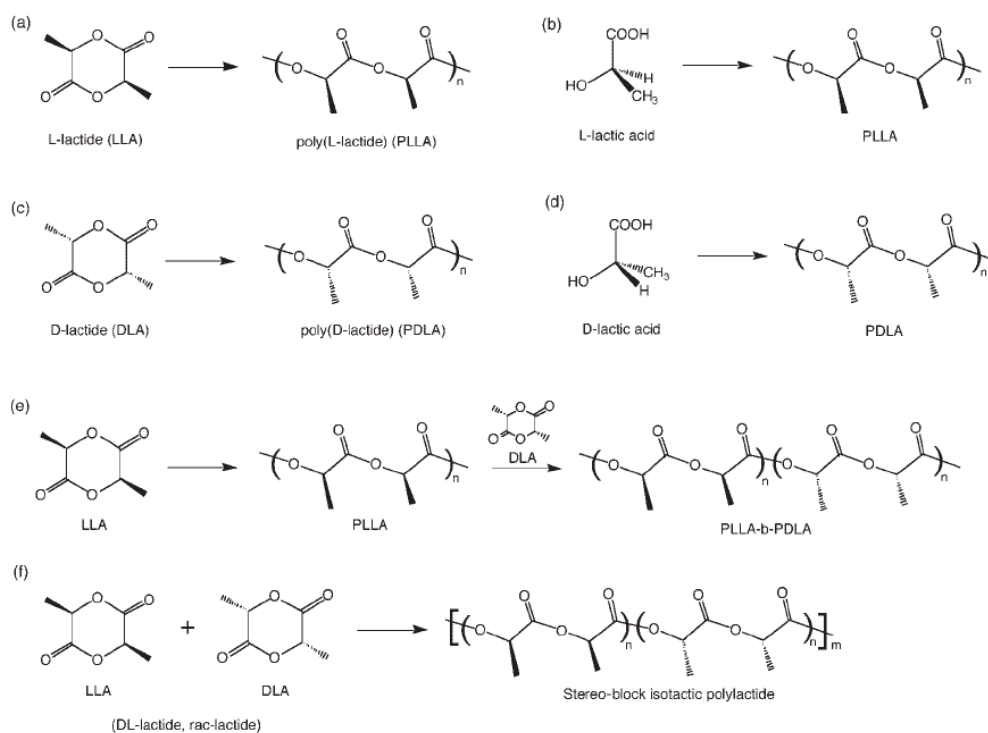


**Figure 2.9** Synthesis and molecular structures of PLL [(a) and (b)], PDL [(c) and (d)], and stereo-block isotactic PL [(e) and (f)] (Tsuji, 2005).

### 2.2.6.2 Polycondensation copolymerization

Acid and hydroxyl groups present in the lactic acid make it feasible to copolymerize through polycondensation. Fukuzaki *et al.* (1990) copolymerized L-lactic acid and  $\epsilon$ -caprolactone without any catalyst to produce low molecular weight ( $M_w \sim 6.8\text{--}8.8$  kDa) copolymers for biomedical applications. These copolymers showed excellent *in vitro* (enzymatic) and *in vivo* degradation properties. L-lactic acid and  $\epsilon$ -



caprolactone condensation copolymerization, using stannous octoate as a catalyst, was followed by crosslinking through reaction with diisocyanate to form biodegradable thermoplastic elastomers. L-lactic acid has also been polycondensed with D,L-mandelic acid and other  $\alpha$ -hydroxy acids such as D,L- $\alpha$ -hydroxybutyric acid, D,L- $\alpha$ -hydroxyisovaleric acid and D,L- $\alpha$ -hydroxyisocaproic acid (Fukuzaki *et al.*, 1989)

### 2.2.6.3 Ring-opening copolymerization

Grijpma and Pennings (1994) copolymerized L-lactide with D-lactide, glycolide,  $\epsilon$ -caprolactone, and trimethylene carbonate using an ROC approach involving a stannous octoate  $[\text{Sn}(\text{Oct})_2]$  catalyst. This copolymerization strategy resulted in controlled degradation, thermal, and mechanical properties. Glycolide, l-lactide, and  $\epsilon$ -caprolactone were copolymerized using a similar ROC approach and resulting copolymers (PGLC) were found to present an amorphous structure over a wide range of compositions with a variable *in vitro* degradation rate. PGLC (10/10/80 molar ratio) was found to have the slowest degradation rate. The degradation rates of three other compositions investigated were in the order of PGLC63/27/10 > PGLC45/45/10 > PGLC27/63/10 initially, but insignificant differences were observed at later stages. The amorphous structure is typically more favored in applications demanding higher toughness and degradation rate. In another example, poly(D,L-lactide)-*co*-poly( $\epsilon$ -caprolactone) elastic properties were modified by chemically crosslinking the copolymer network. The %elongation at break varied between  $50 \pm 10\%$  and  $350 \pm 40\%$  for the composition range investigated. The elastic network formation was confirmed by the absence of a flow region in DMA analyses, increase in the glass transition temperature in DSC, and the full recovery of the sample dimensions after tensile testing. Haynes *et al.* (2007) copolymerized lactide with another commercially available biodegradable and renewably derived thermoplastic polyester, polyhydroxyalkanoate (PHA).

### 2.2.6.4 Blending with plasticizers

PL is a glassy polymer that has poor elongation at break (<10%) (Rasal *et al.*, 2008). Different biodegradable as well as non-biodegradable plasticizers have been used to lower the glass transition temperature, increase ductility, and improve processibility. Lactide is a natural choice to plasticize PL. Lactide plasticized PL showed a significant increase in elongation at break but underwent stiffening with time



due to low molecular weight lactide migration toward the surface. Oligomeric plasticizers that would not tend to migrate toward the surface due to their relatively higher molecular weight have also been utilized.

Martin and Avérous (2001) used glycerol, citrate ester, PEG, PEG monolaurate, and oligomeric lactic acid to plasticize PL and found that oligomeric lactic acid and low molecular weight PEG (Mw 400 g/mol) gave the best results while glycerol was found to be the least efficient plasticizer. Citrate esters (molecular weight 276-402 g/mol) derived from naturally occurring citric acid were found to be miscible with PL at all compositions. For these blends with citrate esters, elongation at break was significantly improved accompanied with considerable loss of tensile yield strength.

Ljungberg and Wesslén (2002) plasticized PL using triacetine and tributyl citrate, successfully lowering  $T_g$  to  $\sim 10^\circ\text{C}$  at 25 wt%, after which phase separation occurred. Triacetine- or tributyl-citrate-plasticized PL films underwent crystallization, and plasticizer molecules migrated toward the surface with storage time due to their low molecular weight. To overcome the aging problem, tributyl citrate oligomers were synthesized by trans-esterification of tributyl citrate and diethylene glycol. However, these oligomeric tributyl citrate plasticizers also underwent phase separation with storage time.

Baiardo *et al.* (2003) used acetyl tri-*n*-butyl citrate and PEGs with different molecular weights (Mw  $\sim 0.4$ – $10$  kDa) to plasticize PL. Acetyl tri-*n*-butyl citrate miscibility limit was found to be 50 wt% while PEG miscibility decreased with increasing molecular weight. These researchers also observed a significant increase in elongation at break at the expense of strength and tensile modulus. Apart from plasticizer molecular weight and polarity, the effect of plasticizer end groups might significantly affect PL bulk properties and has been investigated. PL was plasticized with PEGs (MW  $\sim 0.4$ – $0.75$  Kg/mol) having hydroxyl and ether end groups. The thermal and mechanical properties were significantly dependent on PEG composition, while the PEG end groups had very little effect. Lai *et al.* (2004) found that the PEG end groups (hydroxy and methyl) influenced the miscibility and crystallization behavior when added to PL.

Pillin *et al.* (2006) also reported PEG as the most efficient for  $T_g$  reduction when compared with poly(1,3-butanediol), dibutyl sebacate, and acetyl



glycerol monolaurate. Poly(propylene glycol) (PPG) was recently used to plasticize PL since it does not crystallize, has a low  $T_g$ , and is miscible with PL. PPG successfully plasticized PL and influenced the crystallization behavior less than PEG did. High molecular weight PEG ( $M_n \sim 2$  Kg/mol)/PL blends cast from chloroform solution (40 wt% PEG) were found to be very ductile. Melt processed PL/PEG blends (PEG  $M_n \sim 2$  Kg/mol) were found to be miscible, showed improved ductility, and reduced tensile strength for concentrations up to 50 wt% PEG. However, above 50 wt% PEG, blend crystallinity was found to increase significantly and resulted in an increased modulus and decreased ductility.

Much less is known about the plasticizing effect of PEG on semicrystalline PL. In studies devoted to the mechanical properties of plasticized PL, its crystallization was rather a side effect that occurred at relatively high plasticizer content, where PEG separation in the amorphous phase was also observed (Sheth *et al.*, 1997). Piorkowska *et al.* (2006) blended PL with a new plasticizer poly(propylene glycol) (PPG) is described. PL was plasticized with PPG with nominal Mw of 425 g/mol and 1000 g/mol and crystallized. The plasticization decreased  $T_g$ , which was reflected in a lower yield stress and improved elongation at break. The crystallization in the blends was accompanied by a phase separation facilitated by an increase of plasticizer concentration in the amorphous phase and by annealing of blends at crystallization temperature.

Adding impact modifiers (flexible polymers) or nucleating agents into PL resin could increase the toughness or HDT of PL separately. But it is hard to increase the toughness and HDT simultaneously, because a higher crystallinity always means low ductility, in general. Liu *et al.* (2014) synthesized poly(D-lactide)-*b*-poly(ethylene glycol)-*b*-poly(D-lactide) (PDL-*b*-PEG-*b*-PDL) and added into PLL matrix by solution casting method. The heat resistance of these blends could be improved when the amount of copolymer exceeded 30 wt%, because the high melting point stereocomplex was preferentially formed at that addition amount, whenever from solutions or from melt. Both the tensile strength and elongation at break of the blends were enhanced when 30wt% copolymer was added, which were partly caused by the synergistic effects of stereocomplexation between enantiomeric PLs and plasticization of PEG blocks. The blends showed higher thermal stability than neat PLL at



temperature above 370°C. These results showed that the toughness and heat resistance of PLL were improved, which made the application of PL probable.

Han *et al.* (2016) was prepared enantiomeric blends in equal mass of high molecular weight poly(lactic acid)/poly(ethylene glycol) (PEG) triblock copolymers in order to enhanced stereocomplexation and thermomechanical properties. They found that the synergistic effects of stereocomplexation and plasticization of flexible PEG midblocks offer the PLLA-PEG-PLLA/PDLA-PEG-PDLA blended materials better mechanical and thermomechanical properties than PLL/PDL blend. The enantiomeric blends exhibit higher tensile strength, larger elongation-at-break, and better thermal resistance than the corresponding PLL-PEG-PLL copolymers.

Pakkethati and Baimark (2017) was plasticized the stereocomplex polylactide (scPL) with poly(propylene glycol) (PPG). The poly(*L*-lactide) (PLL), poly(*D*-lactide) (PDL) and PPG were completely blended in chloroform before film casting to prepare scPL/PPG blend films. The PLL/PDL ratio was fixed at 50/50 (w/w). The stereocomplex crystallinities of the scPL films increased as the PPG blend ratio increased, the PPG molecular weight decreased and the PDL molecular weight decreased. The PPG blending significantly decreased the  $T_g$  and film transparency, and improved the elongation at break of the scPL films. The results indicated that the PPG blending had an effect on the stereocomplexation and it improved the flexibility of the scPL films.



## CHAPTER 3

### METHODOLOGY

#### 3.1 Chemicals and instruments

##### 3.1.1 Chemicals

The chemicals used in this research were listed in Table 3.1.

**Table 3.1** Chemicals used in this research.

Chemicals	Usage	Grade	Supplier
L-lactic acid (LLA)	Monomer precursor	88%	Purac (Thailand)
D-lactic acid (DLA)	Monomer Precursor	90%	Haihang Industry Co., Ltd. (China)
Poly(propylene glycol) monobutyl ether (mPPG)	Initiator	Mw 2,500 g/mol	Acros Organics
Poly(propylene glycol) (PPG)	Initiator	Mw 2,000 g/mol	Acros Organics
Poly(propylene glycol) (PPG)	Initiator	Mw 4,000 g/mol	Acros Organics
Tin(II) 2-ethylhexanoate (Sn(Oct) <sub>2</sub> )	Catalyst	95%	Sigma
Chloroform	Solvent	AR grade	Carlo Erba
Toluene	Solvent	AR grade	Carlo Erba
<i>n</i> -Hexane	Non-solvent	Commercial grade <sup>a</sup>	-
Ethyl acetate	Solvent	Commercial grade <sup>a</sup>	-

<sup>a</sup> fractional distillation before use.





### 3.1.2 Instruments

The main items of equipments used in this research were listed in Table 3.2.

**Table 3.2** Instruments used in this research.

Instrument	Model	Company
Fourier transform infrared spectrometer (FTIR)	Spectrum 2000	Perkin-Elmer
Polarimeter	ADP220	Bellingham and Stanley
<sup>1</sup> H-Nuclear magnetic resonance spectrometer ( <sup>1</sup> H-NMR)	DPX 300	Bruker Advanced
Gel permeation chromatograph (GPC)	e2695	Waters
Differential scanning calorimeter (DSC)	Pyris Daimond	Perkin-Elmer
X-ray diffractometer (XRD)	D8 Advance	Bruker Advanced
Universal mechanical testing machine	LRX+	Lloyds

### 3.2 Preparation of lactide monomers

The L-lactide (LL) and D-lactide (DL) monomers were synthesized from L-lactic acid and D-lactic acid, respectively, by direct polycondensation followed with thermal decomposition. In the first step, the lactic acid (5,000 g) was dehydrated to generate low molecular weight poly(lactic acid) (PLA) by direct polycondensation reaction at 190°C under atmospheric pressure for 3 h. After that, the reaction temperature and pressure were reduced to 170°C and -25 inch of Hg, respectively, for 2 h to remove residue water by-product. In the second step, 5 g of Sn(Oct)<sub>2</sub> was added. The reaction temperature was increased to 240°C under reduced pressure (-28 inch of Hg). The crude lactide was then obtained by distillation. The reaction of lactide synthesis is illustrated in Figure 3.1. The crude lactide was purified by re-crystallization 4 times. Ethyl acetate was used as a solvent. The purified lactide was dried at 55°C in a vacuum oven for 48 h before polymerization.



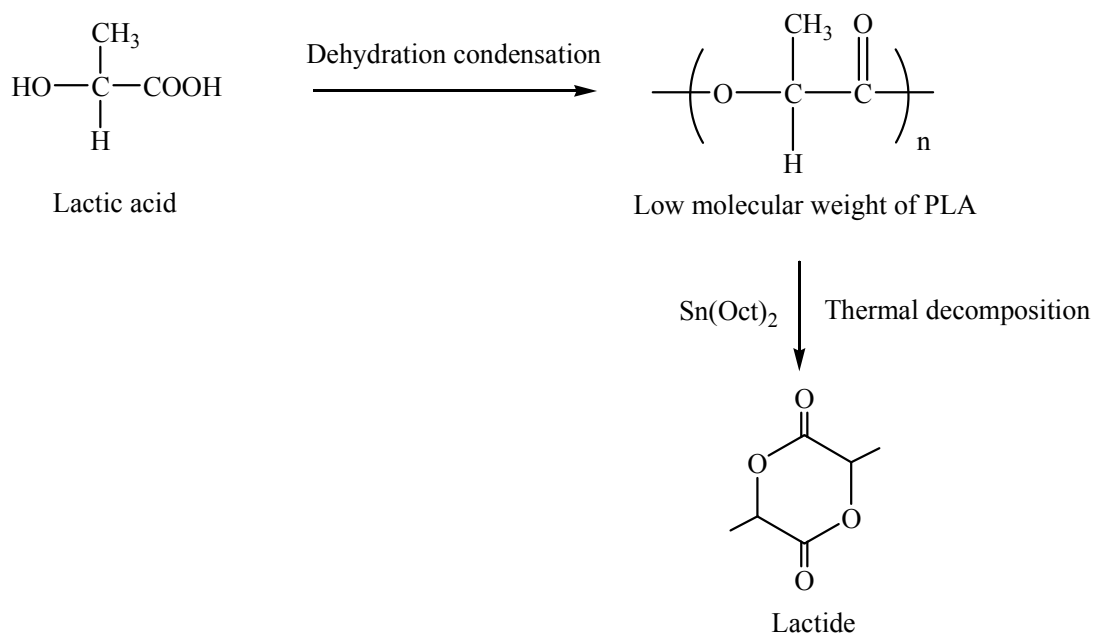


**Figure 3.1** Synthesis of lactides.

### 3.3 Synthesis of diblock copolymers

The diblock copolymers of poly(propylene glycol) monobutyl ether-*b*-polylactide (mPPG-*b*-PL) including of mPPG-*b*-poly(L-lactide) (mPPG-*b*-PLL) and mPPG-*b*-poly(D-lactide) (mPPG-*b*-PDL) were synthesized via a ring-opening polymerization of LL and DL monomers, respectively in bulk at 165°C under nitrogen atmosphere for 4 h. The 0.01 mol% Sn(Oct)<sub>2</sub> and mPPG (MW of 2,500 g/mol) were used as a catalyst and an initiator, respectively. The resulted diblock copolymers were purified by being dissolving in chloroform before precipitating in cool *n*-hexane. The purified copolymers were dried at 45°C in a vacuum oven overnight. The polymerization reaction of diblock copolymers is illustrated in Figure 3.2. Block lengths of PL were synthesized to be 20,000 and 40,000 g/mol. The expected molecular weights and codes of the synthesized diblock copolymers are shown in Table 3.3.



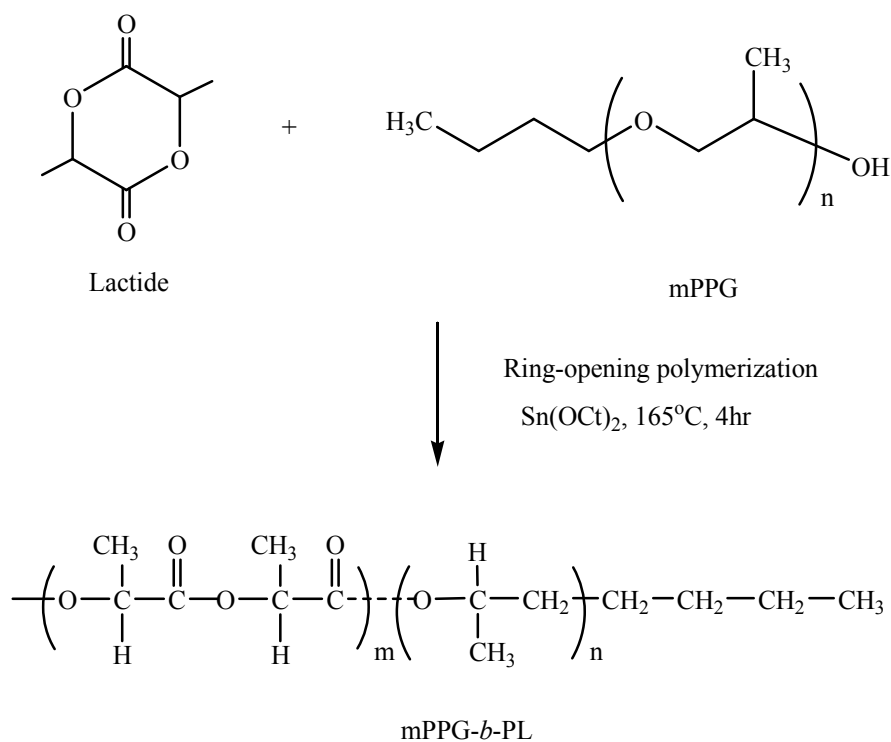


**Figure 3.2** Polymerization reaction of mPPG-*b*-PL diblock copolymers.

**Table 3.3** Codes and theoretical molecular weights of diblock copolymers.

Diblock copolymer	Molecular weight (g/mol)
	mPPG : PL
<b>mPPG-<i>b</i>-PLL</b>	
2.5K- <i>b</i> -L20K	2,500 : 20,000
2.5K- <i>b</i> -L40K	2,500 : 40,000
<b>mPPG-<i>b</i>-PDL</b>	
2.5K- <i>b</i> -D20K	2,500 : 20,000
2.5K- <i>b</i> -D40K	2,500 : 40,000



### 3.4 Synthesis of triblock copolymers

The triblock copolymers of polylactide-*b*-poly(propylene glycol)-*b*-polylactide (PL-*b*-PPG-*b*-PL) including of poly(L-lactide)-*b*-PPG-*b*-poly(L-lactide) (PLL-*b*-PPG-*b*-PLL) and poly(D-lactide)-*b*-PPG-*b*-poly(D-lactide) (PDL-*b*-PPG-*b*-PDL) were synthesized via a ring-opening polymerization of LL and DL monomers, respectively in bulk at 165°C under nitrogen atmosphere for 4 h. The 0.01 mol% Sn(Oct)<sub>2</sub> and PPG (Mw of 2,000 and 4,000 g/mol) were used as a catalyst and an initiator, respectively. The received triblock copolymers were purified by being dissolved in chloroform before precipitating in cool *n*-hexane. The purified copolymers were dried at 45°C in a vacuum oven overnight. The polymerization reaction of triblock copolymers is illustrated in Figure 3.3. Block lengths of the PL were synthesized to be 20,000 and 40,000 g/mol for each PPG type. The expected molecular weights and codes of the synthesized triblock copolymers are presented in Table 3.4.

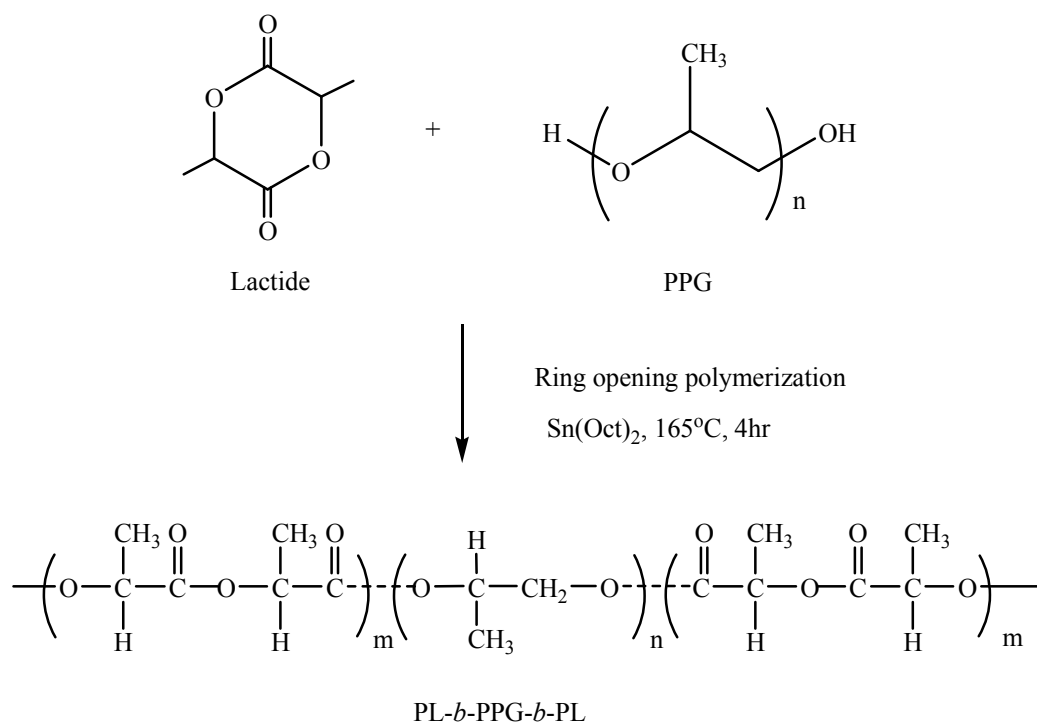


**Figure 3.3** Polymerization reaction of PL-*b*-PPG-*b*-PL triblock copolymers.



**Table 3.4** Codes and theoretical molecular weights of triblock copolymers.

Triblock copolymer	Molecular weight (g/mol) PL : PPG : PL
<b>PLL-<i>b</i>-PPG-<i>b</i>-PLL</b>	
L20K- <i>b</i> -2K- <i>b</i> -L20K	20,000 : 2,000 : 20,000
L40K- <i>b</i> -2K- <i>b</i> -L40K	40,000 : 2,000 : 40,000
L20K- <i>b</i> -4K- <i>b</i> -L20K	20,000 : 4,000 : 20,000
<b>PDL-<i>b</i>-PPG-<i>b</i>-PDL</b>	
D20K- <i>b</i> -2K- <i>b</i> -D20K	20,000 : 2,000 : 20,000
D40K- <i>b</i> -2K- <i>b</i> -D40K	40,000 : 2,000 : 40,000
D20K- <i>b</i> -4K- <i>b</i> -D20K	20,000 : 4,000 : 20,000

### 3.5 Characterization of diblock and triblock copolymers

The obtained diblock and triblock copolymers were characterized by the following of instrument methods:

#### 3.5.1 Polarimetry

The specific optical rotation of the copolymers was investigated at 25 °C using a Bellingham and Stanley Polarimeter ADP220 at a wavelength of 589 nm with 1.0 dm sample tube length. Chloroform was used as a solvent at a concentration of approximately 1.0 g/dL. The specific optical rotation of lactyl ( $[\alpha]_{25}$ ) was calculated by the following equation:

$$[\alpha]_{25} = \alpha / (l \cdot c) \quad \dots\dots\dots(3.1)$$

where  $\alpha$  is the optical rotation of lactide unit (deg.),  $l$  is a sample tube length (1.0 dm) and  $c$  is the sample concentration (g/cm<sup>3</sup>).

### 3.5.2 <sup>1</sup>H-NMR spectroscopy

Chemical composition of the block copolymers was determined by Proton Nuclear Magnetic Resonance spectrometry (<sup>1</sup>H-NMR) using a Bruker Advanced DPX 300 MHz <sup>1</sup>H-NMR spectrometer. CDCl<sub>3</sub> was used as a solvent at room temperature, and tetramethylsilane was used as the internal standard. The number-average molecular weights (M<sub>n</sub>) of block copolymers were also calculated based on copolymer composition and molecular weight of the initiator.

### 3.5.3 Gel Permeation Chromatography

The number average molecular weight (M<sub>n</sub>) and polydispersity index (PDI) of block copolymers were measured by Gel Permeation Chromatography (GPC) using a Waters e2695 separations module equipped with PL gel 10 μm mixed B 2 columns operating at 40°C and employing a refractive index (RI) detector. Tetrahydrofuran was used as the solvent at a flow rate of 1.0 mL/min.

### 3.5.4 Differential Scanning Calorimetry

Temperature transition and crystallinity of the diblock and triblock copolymers were characterized by non-isothermal Differential Scanning Calorimetry (DSC) using a Perkin-Elmer Pyris Daimond DSC under nitrogen flow. For first heating scan, approximate 3-5 mg of the sample was placed in a sealed aluminum pan and heated it from 0°C to 250°C at 10 °C/min. Melting temperature (T<sub>m</sub>) was determined from the first scan peak at maximum of the endotherm peak. After the first heating scan, the sample was rapid cooled to 0°C and heated again to 250°C for the second heating scan. T<sub>g</sub> was determined from the second heating scan. Degree of crystallinity of homo crystallites (χ<sub>hc</sub>) and stereocomplex crystallites (χ<sub>sc</sub>) were calculated from the 1<sup>st</sup> heating data by equations (3.2) and (3.3), respectively.

$$\chi_{hc} (\%) = \frac{\Delta H_{hc}}{w_{PL} \times \Delta H_{hc}^{\circ}} \times 100 \dots \dots \dots (3.2)$$

$$\chi_{sc} (\%) = \frac{\Delta H_{sc}}{w_{PL} \times \Delta H_{sc}^{\circ}} \times 100 \dots \dots \dots (3.3)$$

where ΔH<sub>hc</sub> is the melting enthalpy of homo-crystallites, ΔH<sub>hc</sub><sup>o</sup> is the melting enthalpy for 100% homo-crystallites of PL, 93J/g, ΔH<sub>sc</sub> is the melting enthalpy of stereocomplex crystallites of PL and ΔH<sub>sc</sub><sup>o</sup> is the melting enthalpy for 100% stereocomplex crystallinity



of PL, 142 J/g (Tsuji, 2005). The  $w_{PL}$  was a weight fraction of PL including PLL and PDL that determined from  $^1\text{H-NMR}$ .

### 3.6 Preparation of stereocomplex poly lactide films

Stereocomplex poly lactide (scPL) films of mPPG-*b*-PLL/mPPG-*b*-PDL and PLL-*b*-PPG-*b*-PLL/PDL-*b*-PPG-*b*-PDL blends were prepared by solution blending before film casting. Chloroform was used as a blending solvent. Each polymer sample was completely dissolved in chloroform (1g/dL) before blending. The 60ml of blend solution was vigorously stirred for 20 min before film casting. The film was dried at 40°C in an air oven for 24 h before drying at 45°C in a vacuum oven overnight. The polymer blends with blending ratios of 75/25, 50/50 and 25/75 wt % were prepared as following:

2.5K-*b*-L20K / 2.5K-*b*-D20K blend films

2.5K-*b*-L40K / 2.5K-*b*-D40K blend films

L20K-*b*-2K-*b*-L20K / D20K-*b*-2K-*b*-D20K blend films

L40K-*b*-2K-*b*-L40K / D40K-*b*-2K-*b*-D40K blend films

L20K-*b*-4K-*b*-L20K / D20K-*b*-4K-*b*-D20K blend films

The neat polymer films of diblock and triblock copolymers were also prepared as the same method for comparison.

### 3.7 Characterization of stereocomplex poly lactide films

The obtained scPL films were characterized by the following of instrument methods:

#### 3.7.1 Fourier Transform Infrared spectroscopy

The crystalline structure of scPL films were studied by Fourier Transform Infrared spectroscopy (FTIR) using a Perkin-Elmer Spectrum 2000 FTIR spectrometer with air as the reference. The resolution of 4  $\text{cm}^{-1}$  and 32 scans were used in this research project.



### 3.7.2 X-ray Diffractometer

To confirm the scPL crystal structure of the scPL films, X-ray diffraction (XRD) spectra was recorded on a BrukerD8 Advanced Bio Spin AG (Karlsruhe, Germany). The range of  $2\theta$  from  $5^\circ$  to  $30^\circ$  in the reflection mode was scanned at 3 degree/min under a voltage of 40 kV and a current of 40 mA using Cu  $K\alpha$  radiation ( $\lambda=0.15418$  nm).

### 3.7.3 Differential Scanning Calorimetry

Temperature transition and crystallinity of scPL films were characterized by non-isothermal Differential Scanning Calorimetry (DSC) using a Perkin-Elmer Pyris Diamond DSC. Approximately 2-5 mg of the sample was placed in a sealed aluminum pan and heated from 0-250°C at the rate 10°C/min under nitrogen flow.

### 3.7.4 Scanning Electron Microscopy

Morphology of film samples was determined by Scanning Electron Microscopy (SEM). Prior to examination the samples were sputter-coated with gold for enhancing surface conductivity. The scanning electron microscope operated at 10 kV.

### 3.7.5 Tensile testing

Tensile properties including stress at break, elongation at break and initial Young's modulus, of the film samples were determined at 25 °C and 65% relative humidity with a Lloyds LRX+ universal mechanical testing machine. The film samples (10 × 100 mm) were tested with a gauge length of 25 mm and a crosshead speed of 10 mm/min. The mechanical properties were determined from the average of five measurements for each sample.





## CHAPTER 4

### RESULTS AND DISCUSSIONS

#### 4.1 Characterization of block copolymers

The diblock copolymers of poly(propylene glycol) monobutyl ether-*b*-polylactide (mPPG-*b*-PL) including mPPG-*b*-PLL and mPPG-*b*-PDL and the triblock copolymers of polylactide-*b*-poly(propylene glycol)-*b*-polylactide (PL-*b*-PPG-*b*-PL) including of PLL-*b*-PPG-*b*-PLL and PDL-*b*-PPG-*b*-PDL were synthesized via a ring-opening polymerization of LL and DL monomers in bulk. The optical rotation property, chemical composition, molecular weight and thermal transition properties were investigated by polarimeter, <sup>1</sup>H-NMR, GPC and DSC techniques, respectively. The results are demonstrated following:

##### 4.1.1 Optical rotation property

Specific optical rotation ( $[\alpha]_{25}$ ) is a property of a chiral chemical compound. It is defined as the change in orientation of monochromatic plane-polarized light, per unit distance-concentration product, as the light passes through a sample of a compound in solution. Compounds which rotate light clockwise are said to be *dextrorotary* (D-form), and correspond with positive specific rotation values, while compounds which rotate light counterclockwise are said to be *levorotary* (L-form), and correspond with negative values. If a compound is able to rotate plane-polarized light, it is said to be “optically active”. With a known concentration of a sample, polarimeter may also be applied to determine the specific optical rotation when characterizing a new substance. Therefore, to distinguishing the optical isomer of synthesized L- and D-block copolymers, this technique is applied.

The  $[\alpha]_{25}$  are summarized in Table 4.1, which indicates that the PLL-*b*-PPG-*b*-PLL and PDL-*b*-PPG-*b*-PDL contained predominantly the L-form and D-form, identified by presenting the negative and positive specific rotation values, respectively. Tsuji and Ikada (1992) have been reported that the  $[\alpha]_{25}$  of PLL and PDL were -156 and +156 deg.cm<sup>3</sup>/dm.g, respectively. The  $[\alpha]_{25}$  value of both diblock and triblock copolymers were lower than the PLL and PDL. This may be due to the PPG blocks were attached



the PL end-blocks. It should be noted that the  $[\alpha]_{25}$  increased with the PL end-block length.

**Table 4.1** Specific optical rotations of block copolymers.

Block copolymer	c (g/cm <sup>3</sup> )	$\alpha$ (deg.)	$[\alpha]_{25}$ (deg.cm <sup>3</sup> /dm.g)
2.5K-L20K	0.02012	-5.35	-132.95
2.5K-L40K	0.02007	-5.53	-137.77
L20K-2K-L20K	0.02039	-5.57	-136.59
L40K-2K-L40K	0.02047	-5.81	-141.92
L20K-4K-L20K	0.02045	-5.47	-133.74
2.5K-D20K	0.02004	5.35	133.48
2.5K-D40K	0.02016	5.44	134.92
D20K-2K-D20K	0.02031	5.58	137.37
D40K-2K-D40K	0.02002	5.67	141.61
D20K-4K-D20K	0.02049	5.46	133.24

#### 4.1.2 Chemical compositions

End-group analysis by NMR offers an easy alternative method using an instrument commonly found in many analytical labs. In addition, NMR analysis can also be used to accurately determine monomer ratios for various copolymers. In this research the chemical compositions of mPPG-*b*-PL and PL-*b*-PPG-*b*-PL were determined from the <sup>1</sup>H-NMR spectra as shown in Figures 4.1-4.10. The chemical shift ( $\delta$ ) at ~1.56 ppm (peak b) and ~5.20 ppm (peak a) corresponding to methyl protons (CH<sub>3</sub>) and methine protons (CH) in L-lactide (LL) or D-lactide (DL) repeating units, respectively (Kaitian *et al.*, 1996). For propylene glycol (PG) unit presented the chemical shift at ~1.1 ppm (peak d), ~3.3 ppm (peak c) and ~3.5 ppm (peak e) corresponding to CH<sub>3</sub>, CH and CH<sub>2</sub> protons of the PG units, respectively (Ho and Young, 2006). Mole ratios of PG:PL were calculated from integral peak areas of CH<sub>3</sub> protons (peak d) of PG units and CH protons (peak a) of LL or DL units. The calculated mole ratios of all samples are shown in Table 4.2.



The calculation of mole ratios of PG:PL is shown following (Izunobi *et al.*, 2011; Paulsen and Frasco, 2016):

$$\begin{array}{lcl}
 \text{PG unit} & : & \text{LL unit (or DL unit)} \\
 \frac{\text{Integrals peak area (peak d)}}{3\text{H of methyl groups}} & : & \frac{\text{Integrals peak area (peak a)}}{2\text{H of methine groups}} \\
 \text{Integral per proton (X)} & : & \text{Integral per proton (Y)} \\
 \frac{\text{Integral per proton (X)}}{\text{sum of intergral per proton (X+Y)}} \times 100 & : & \frac{\text{Integral per proton (Y)}}{\text{sum of intergral per proton (X+Y)}} \times 100 \\
 \text{Mole\% of PG unit} & : & \text{Mole\% of LL (or DL) unit}
 \end{array}$$

The calculation example for 2.5K-b-L40K from Figure 4.3 is illustrated as following:

$$\begin{array}{lcl}
 \text{PG unit} & : & \text{LL unit} \\
 \frac{\text{Integrals peak area (peak d)}}{3\text{H of methyl groups}} & : & \frac{\text{Integrals peak area (peak a)}}{2\text{H of methine groups}} \\
 \frac{2.00}{3} = 0.67 & : & \frac{10.13}{2} = 5.065 \\
 \frac{0.67}{5.735} \times 100 & : & \frac{5.065}{5.735} \times 100
 \end{array}$$

$$\text{Mole\% of PG unit} = 12\% \quad : \quad \text{Mole\% of PL unit} = 88\%$$

The calculated PG:LL of the 2.5K-b-L40K was 12:88 mol%.

The copolymer compositions of the triblock copolymers were calculated by the same method. For each copolymer, when compare the mole ratios of PG:LL and PG:DL between feed quantity and calculated values, it is obvious that their ratios are nearly values. This result indicates that the synthesized reaction was taken to near quantitative conversion. Further, can be implies that the copolymerization process was nearly completed.



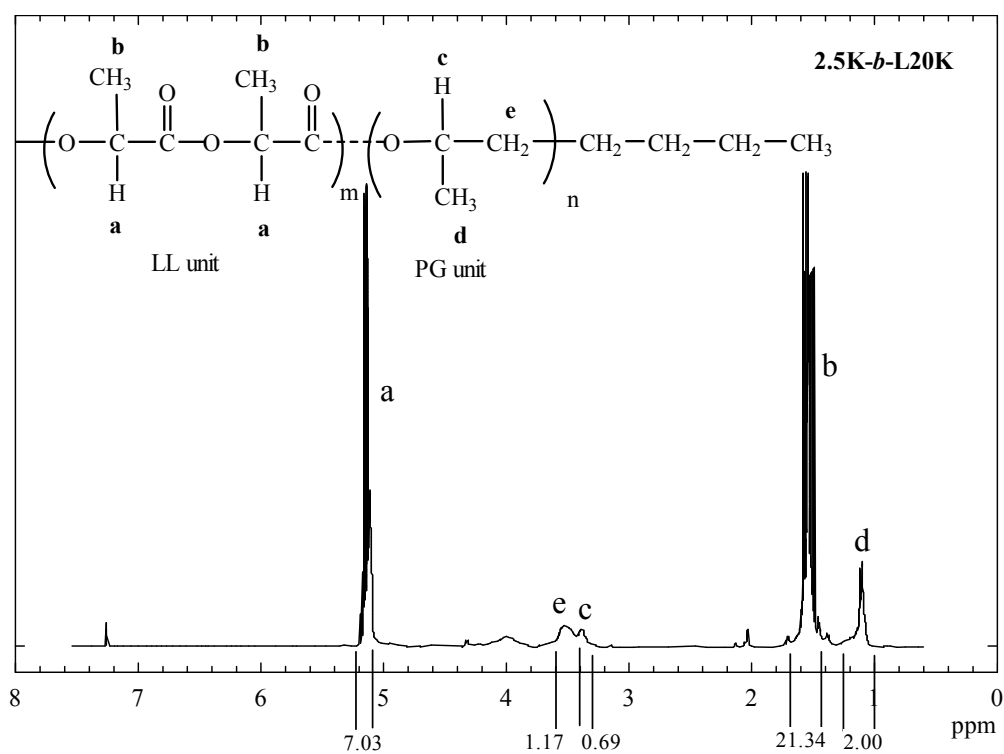


**Figure 4.1**  $^1\text{H}$ -NMR spectrum of 2.5K-*b*-L20K (peak assignment as shown).

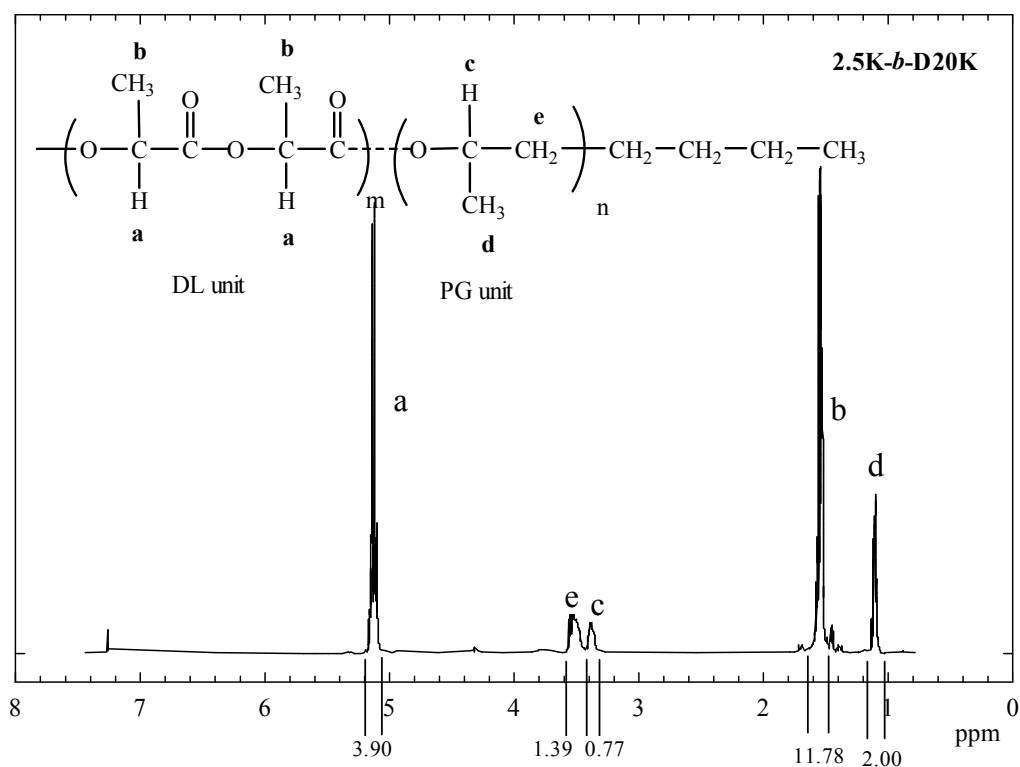


**Figure 4.2**  $^1\text{H}$ -NMR spectrum of 2.5K-*b*-D20K (peak assignment as shown).



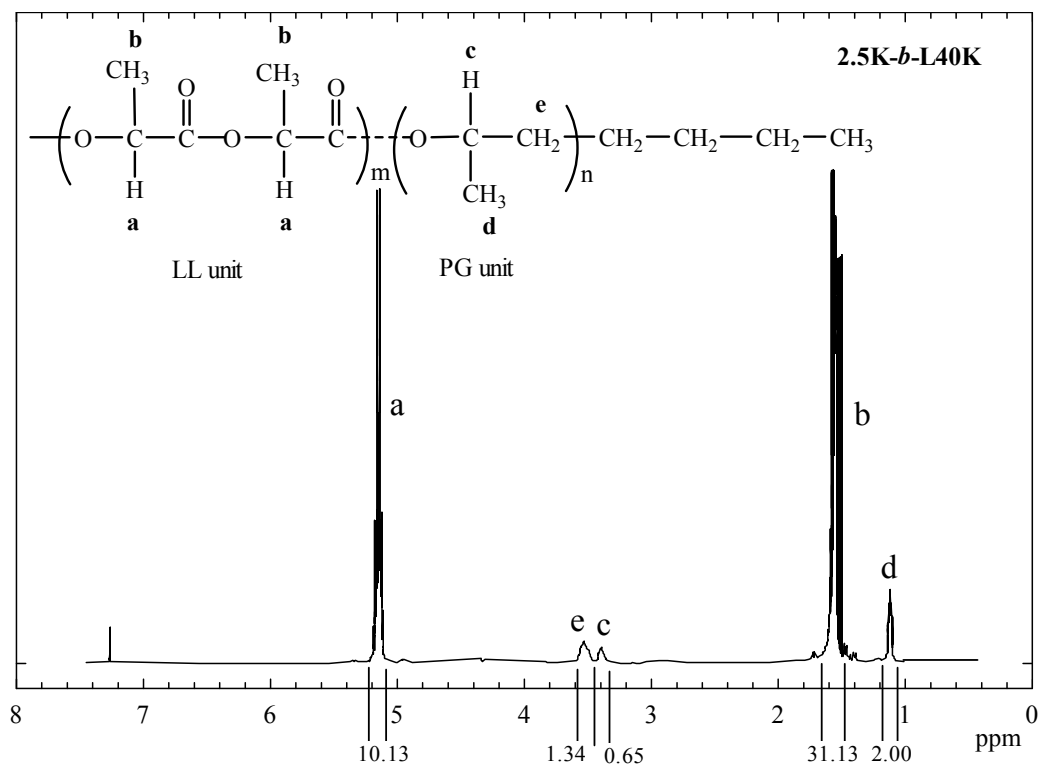


**Figure 4.3**  $^1\text{H}$ -NMR spectrum of 2.5K-*b*-L40K (peak assignment as shown).

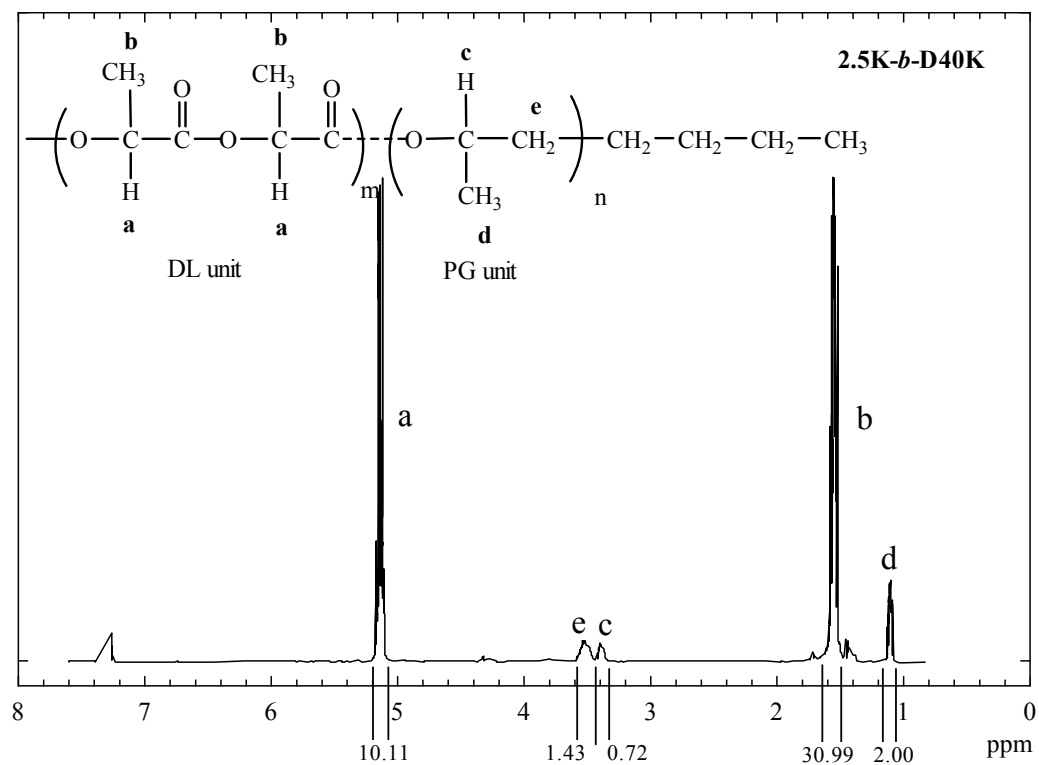


**Figure 4.4**  $^1\text{H}$ -NMR spectrum of 2.5K-*b*-D40K (peak assignment as shown).



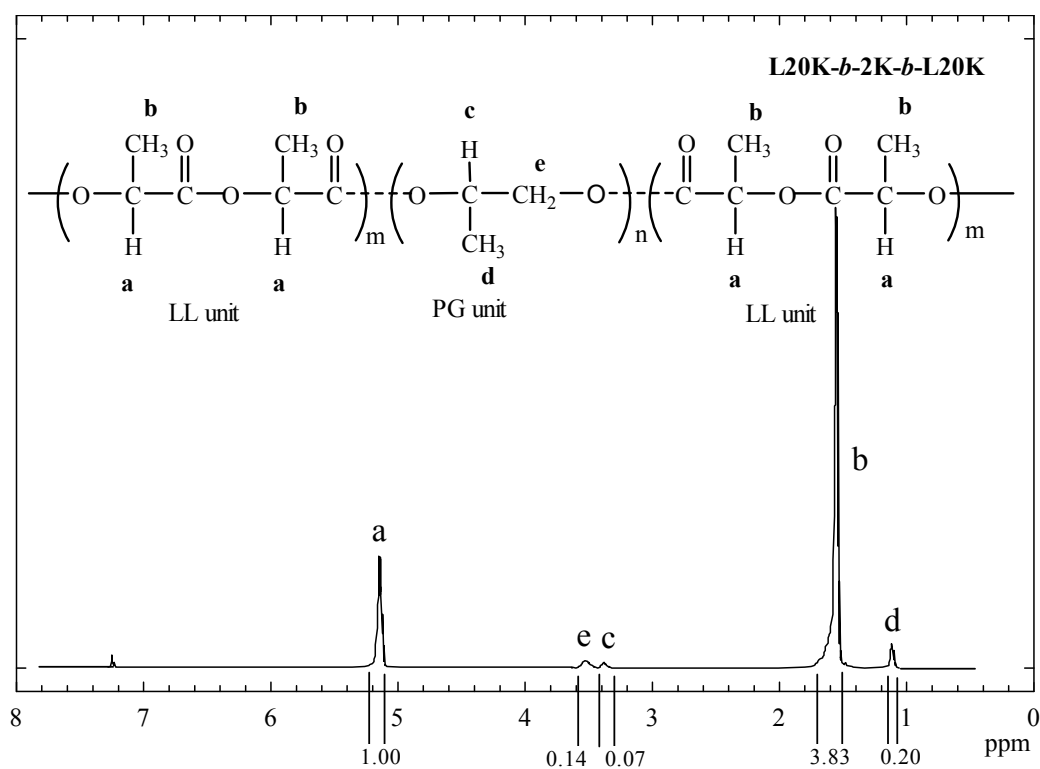


**Figure 4.5**  $^1\text{H}$ -NMR spectrum of L20K-*b*-2K-*b*-L20K (peak assignment as shown).

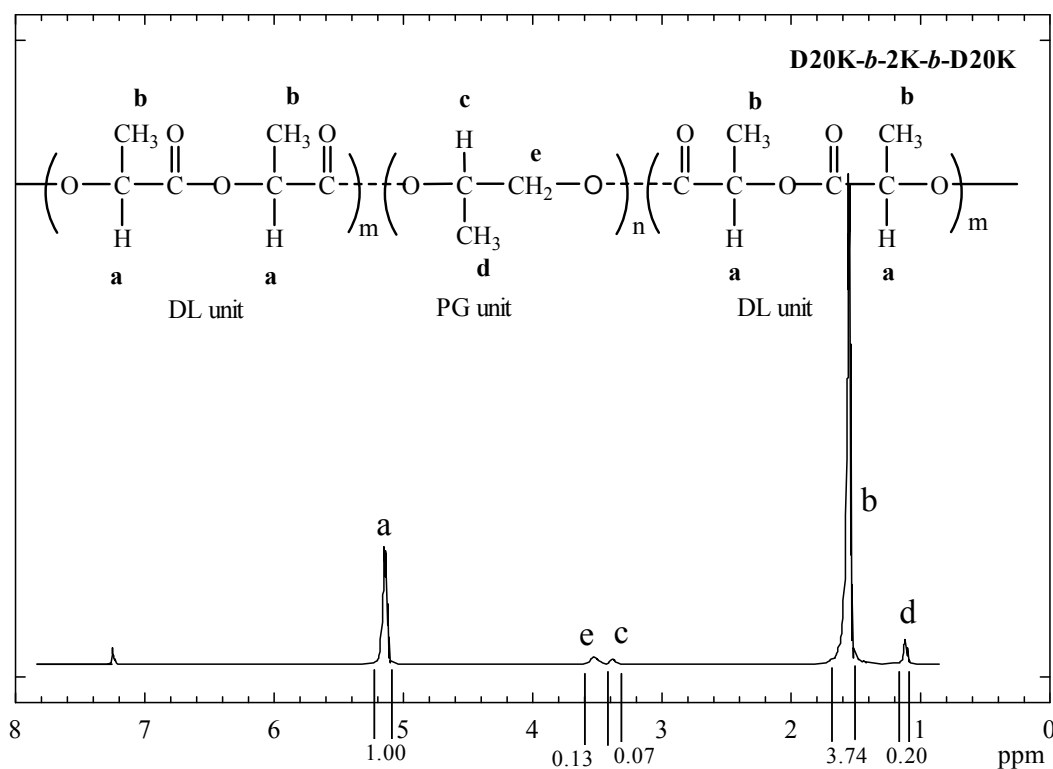


**Figure 4.6**  $^1\text{H}$ -NMR spectrum of D20K-*b*-2K-*b*-D20K (peak assignment as shown).



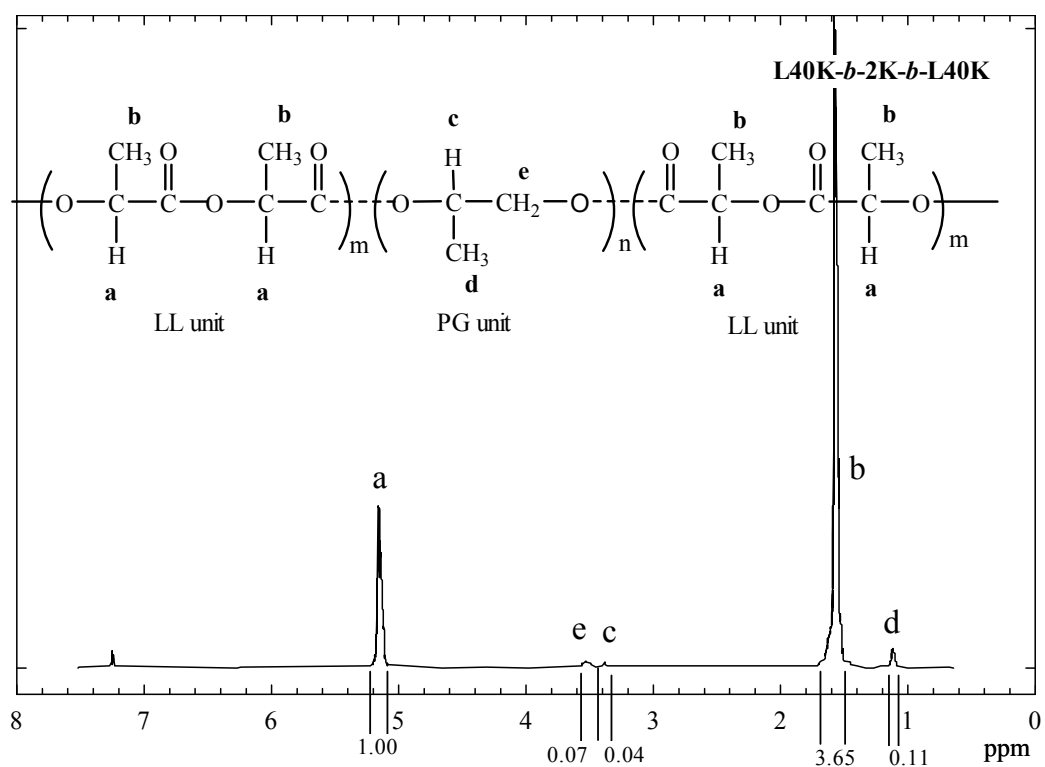


**Figure 4.7**  $^1\text{H}$ -NMR spectrum of L40K-*b*-2K-*b*-L40K (peak assignment as shown).

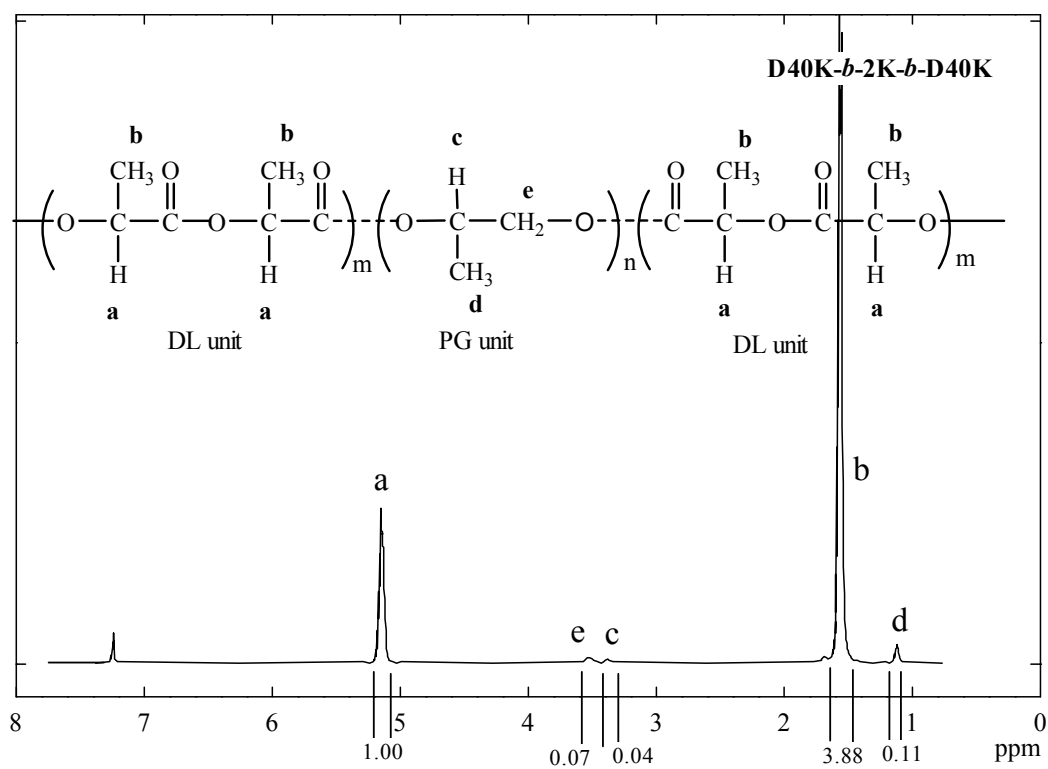


**Figure 4.8**  $^1\text{H}$ -NMR spectrum of D40K-*b*-2K-*b*-D40K (peak assignment as shown).



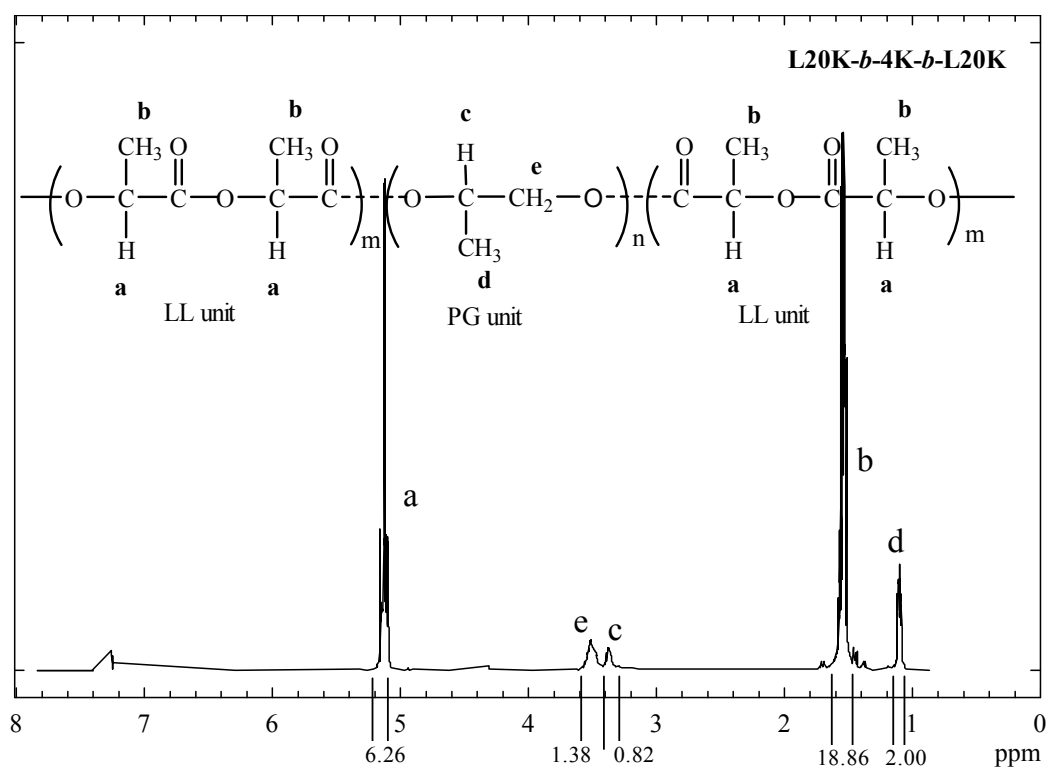


**Figure 4.9**  $^1\text{H}$ -NMR spectrum of L20K-*b*-4K-*b*-L20K (peak assignment as shown).

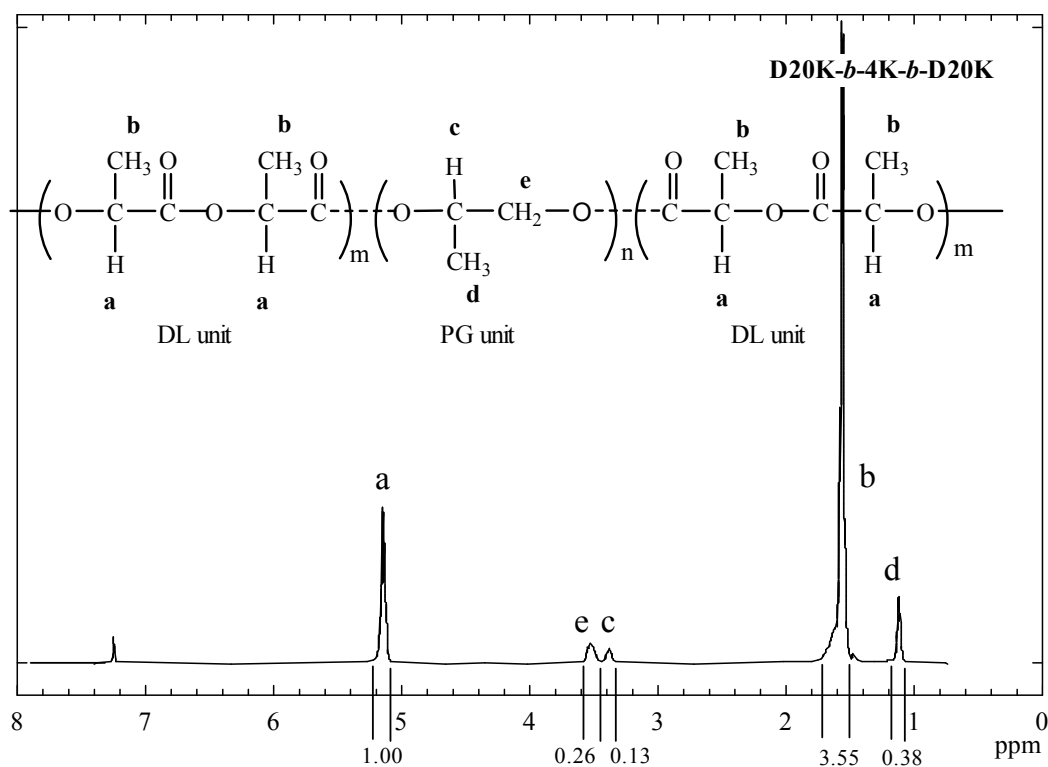


**Figure 4.10**  $^1\text{H}$ -NMR spectrum of D20K-*b*-4K-*b*-D20K (peak assignment as shown).





**Table 4.2** Chemical compositions of diblock and triblock copolymers calculated from  $^1\text{H-NMR}$  spectra.

Block Copolymers	Copolymer composition (mol %)			
	Feed ratio (mol %)		$^1\text{H-NMR}$ (mol %)	
	PG	LL or DL	PG	LL or DL
<b>mPPG-<i>b</i>-PLL</b>				
2.5K- <i>b</i> -L20K	22	78	16	84
2.5K- <i>b</i> -L40K	13	87	12	88
<b>mPPG-<i>b</i>-PDL</b>				
2.5K- <i>b</i> -D20K	22	78	26	74
2.5K- <i>b</i> -D40K	13	87	12	88
<b>PLL-<i>b</i>-PPG-<i>b</i>-PLL</b>				
L20K- <i>b</i> -2K- <i>b</i> -L20K	11	89	12	88
L40K- <i>b</i> -2K- <i>b</i> -L40K	6	94	7	93
L20K- <i>b</i> -4K- <i>b</i> -L20K	11	89	18	82
<b>PDL-<i>b</i>-PPG-<i>b</i>-PDL</b>				
D20K- <i>b</i> -2K- <i>b</i> -D20K	11	89	12	88
D40K- <i>b</i> -2K- <i>b</i> -D40K	6	94	7	93
D20K- <i>b</i> -4K- <i>b</i> -D20K	11	89	21	79

#### 4.1.3 Molecular weight characteristics

The number-average molecular weights ( $M_n$ ) of polymers were determined from  $^1\text{H-NMR}$  based on PG:LL and PG:DL ratios, and PG molecular weight (Paulsen and Frasco, 2016). The  $M_n$  of block copolymers which calculated from copolymer composition and molecular weight of PPG were summarized in Tables 4.3 and 4.4 for the diblock and triblock copolymers, respectively. The example of molecular weight calculation was as following (Izunobi *et al.*, 2011; Paulsen and Frasco, 2016):

For the 2.5K-*b*-L40K, the PG/LL ratio was 12/88 mol% (from Table 4.2). The PG repeating units of the 2.5K PPG was  $(2,500 \text{ g/mol})/(58 \text{ g/mol}) = 43$  units (58 g/mol is molecular weight of each PG repeating unit). The  $M_n$  of 2.5K-*b*-L40K was calculated as below.



Repeating unit of LL units on PLL blocks =  $\frac{88\% \times 43\%}{12\%} = 315$  units

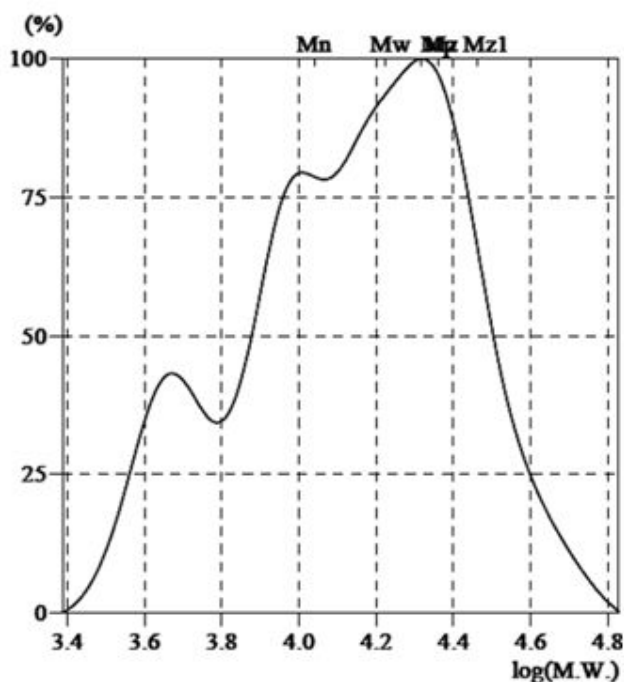
Therefore,  $M_n$  of PLL blocks = (315 units)  $\times$  (144.14 g/mol) = 45,404 g/mol (144.14 g/mol = molecular weight of each LL repeating unit)

Thus, the  $M_n$  of 2.5K-*b*-L40K = 2,500 + 45,404 = 47,904 g/mol

The  $M_n$  values of block copolymers in Tables 4.3 and 4.4 calculated from  $^1\text{H-NMR}$  spectra in accordance with the theoretical  $M_n$ . This indicates that the block copolymers with controllable molecular weights were successfully synthesized by adjusting the PPG/lactide ratio.

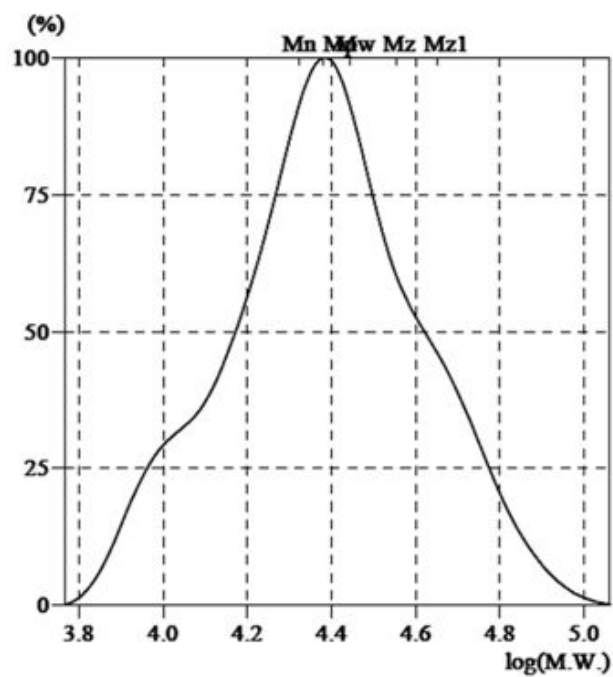
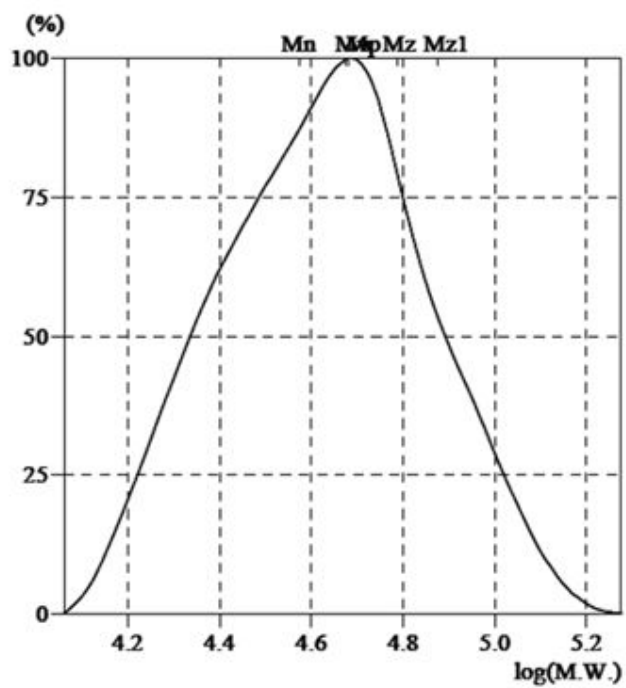
The molecular weight characteristics of the block copolymers were also determined from GPC curves as shown in Figures 4.11-4.20. They were uni-modal curves excepted the 2.5K-*b*-L20K. The  $M_n$  and PDI values obtained from the GPC curves were also summarized in Tables 4.3 and 4.4 for the diblock and triblock copolymers, respectively. The  $M_n$  from GPC were also nearly with the theoretical  $M_n$ . The PDI values were lower than the 2.0 suggested their molecular weight distributions were narrow.

**2.5K-*b*-L20K**



**Figure 4.11** GPC curve of 2.5K-*b*-L20K.



2.5K-*b*-D20KFigure 4.12 GPC curve of 2.5K-*b*-D20K.2.5K-*b*-L40KFigure 4.13 GPC curve of 2.5K-*b*-L40K.

2.5K-b-D40K

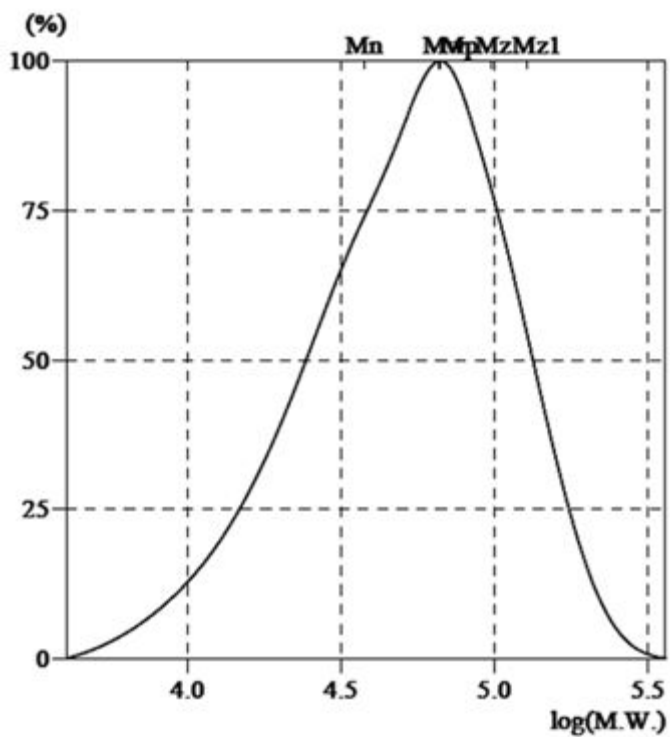


Figure 4.14 GPC curve of 2.5K-b-D40K.

L20K-b-2K-b-L20K

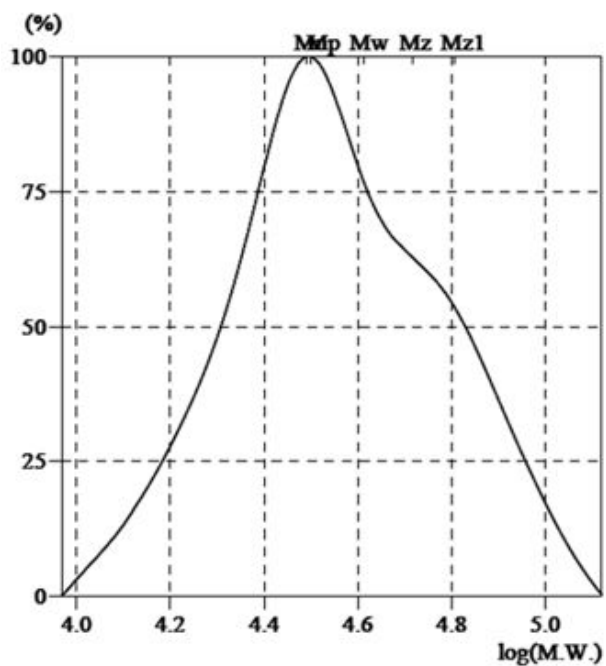
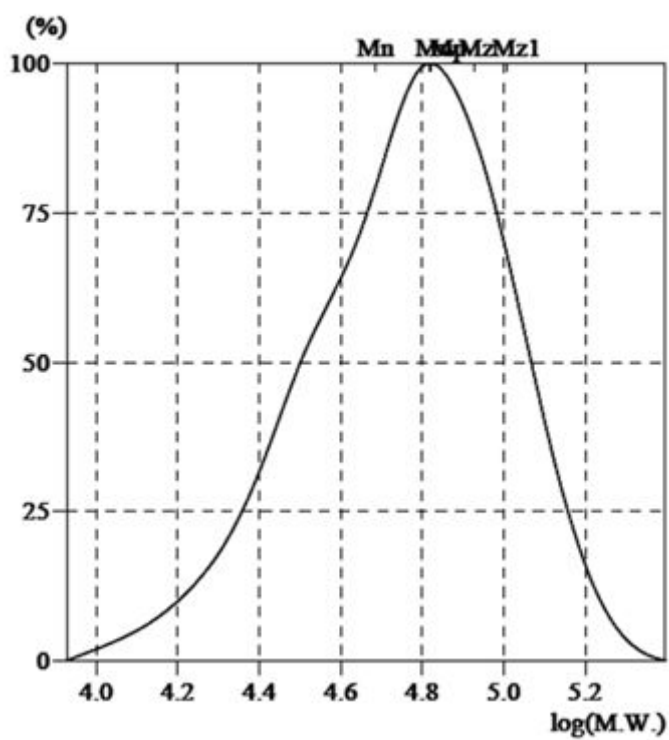
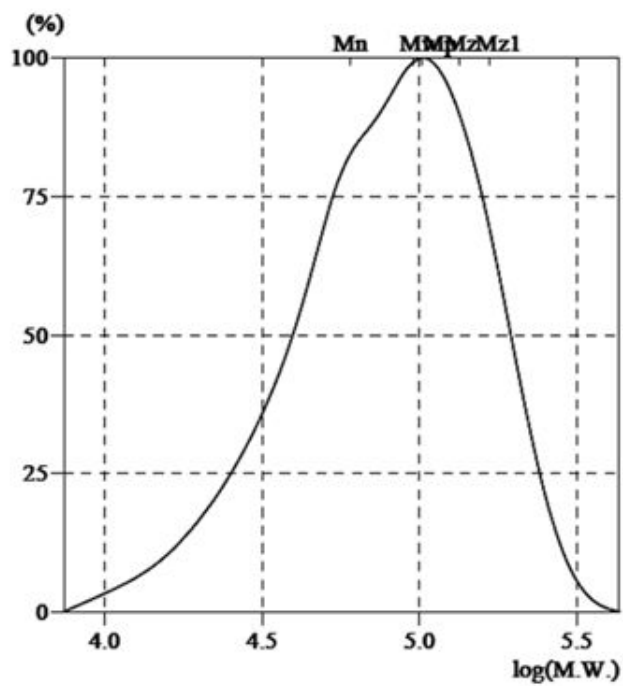


Figure 4.15 GPC curve of L20K-b-2K-b-L20K.



D20K-*b*-2K-*b*-D20KFigure 4.16 GPC curve of D20K-*b*-2K-*b*-D20K.L40K-*b*-2K-*b*-L40KFigure 4.17 GPC curve of L40K-*b*-2K-*b*-L40K.

D40K-*b*-2K-*b*-D40K

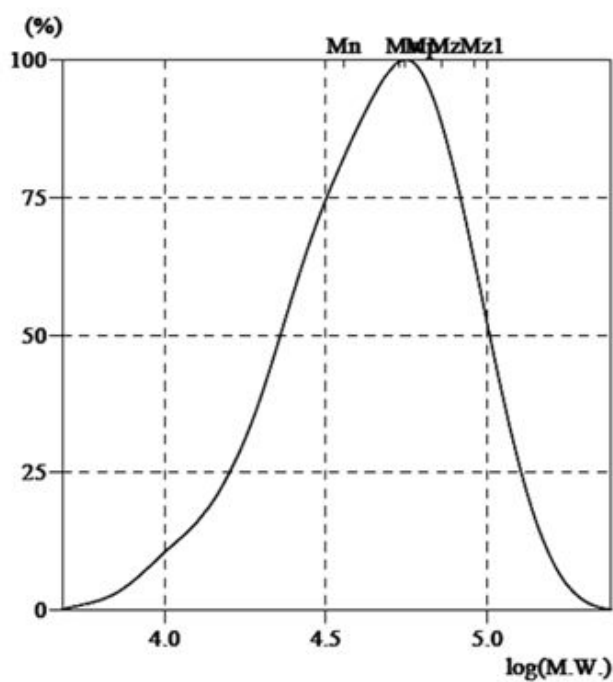


Figure 4.18 GPC curve of D40K-*b*-2K-*b*-D40K.

L20K-*b*-4K-*b*-L20K

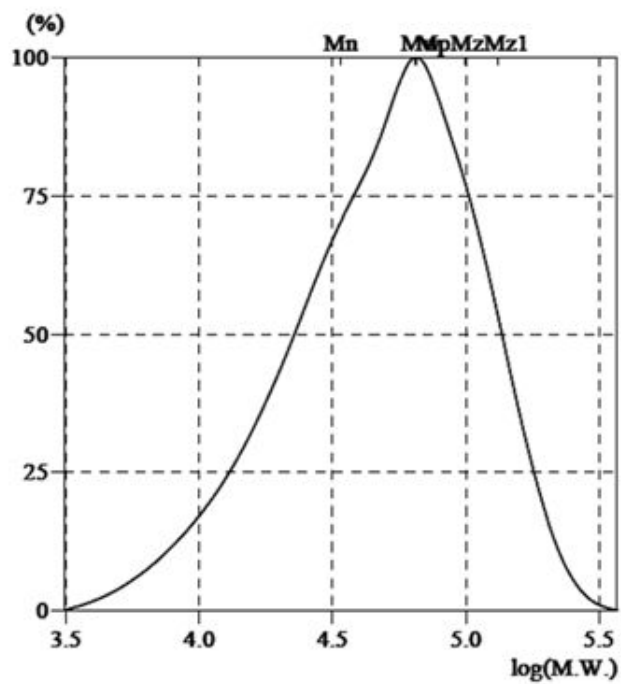
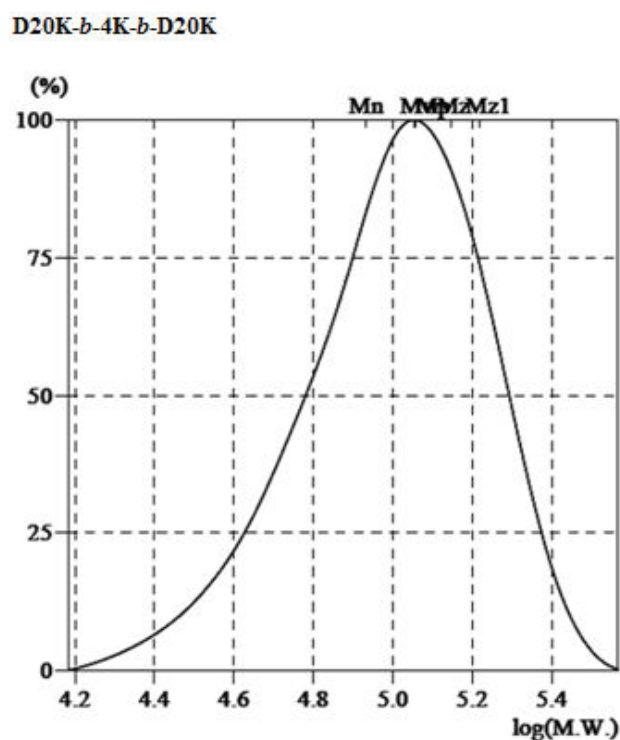


Figure 4.19 GPC curve of L20K-*b*-4K-*b*-L20K.





**Figure 4.20** GPC curve of D20K-*b*-4K-*b*-D20K.

**Table 4.3** Molecular weight characteristics of diblock copolymers.

Diblock copolymer	Theoretical $M_n^a$ (g/mol) mPPG : PL	$M_n^b$ (g/mol)	MW (g/mol) from GPC	
			$M_n^c$ (g/mol)	PDI <sup>c</sup>
<b>mPPG-<i>b</i>-PLL</b>				
2.5K- <i>b</i> -L20K	2,500 : 20,000	35,100	19,700	1.52
2.5K- <i>b</i> -L40K	2,500 : 40,000	47,900	37,400	1.29
<b>mPPG-<i>b</i>-PDL</b>				
2.5K- <i>b</i> -D20K	2,500 : 20,000	20,100	21,100	1.31
2.5K- <i>b</i> -D40K	2,500 : 40,000	47,900	37,700	1.74

<sup>a</sup> calculated from PPG/lactide feed ratio.

<sup>b</sup> calculated from <sup>1</sup>H-NMR.

<sup>c</sup> obtained from GPC.



**Table 4.4** Molecular weight characteristics of triblock copolymers.

Triblock copolymer	Theoretical $M_n^a$ (g/mol) PL:PPG:PL	$M_n^b$ (g/mol)	MW (g/mol) from GPC	
			$M_n^c$	PDI <sup>c</sup>
<b>PLL-<i>b</i>-PPG-<i>b</i>-PLL</b>				
L20K- <i>b</i> -2K- <i>b</i> -L20K	20,000 : 2,000 : 20,000	38,500	31,700	1.29
L40K- <i>b</i> -2K- <i>b</i> -L40K	40,000 : 2,000 : 40,000	68,000	60,300	1.59
L20K- <i>b</i> -4K- <i>b</i> -L20K	20,000 : 4,000 : 20,000	49,300	33,900	1.89
<b>PDL-<i>b</i>-PPG-<i>b</i>-PDL</b>				
D20K- <i>b</i> -2K- <i>b</i> -D20K	20,000 : 2,000 : 20,000	38,500	48,500	1.36
D40K- <i>b</i> -2K- <i>b</i> -D40K	40,000 : 2,000 : 40,000	68,000	85,800	1.32
D20K- <i>b</i> -4K- <i>b</i> -D20K	20,000 : 4,000 : 20,000	41,500	35,900	1.49

<sup>a</sup> calculated from PPG/lactide feed ratio.

<sup>b</sup> calculated from <sup>1</sup>H-NMR.

<sup>c</sup> obtained from GPC.

#### 4.1.4 Thermal transition properties of block copolymers

Differential Scanning Calorimetry (DSC) uses to detect the glass transition temperature ( $T_g$ ) of polymer, as an endothermic shift from the baseline is observed at the  $T_g$  in the clue of crystallizable polymers. A transition results from an increase in heat capacity due to the increase molecular motions in the polymers. The melting temperature ( $T_m$ ) of a polymer corresponds to a change from the solid to liquid state; this transition gives rise to an endothermic peak in the DSC curve. The width of the melting peak provides the heat of fusion that can be calculated to the degree of crystallinity of the polymer. For crystallizable polymers, its specific transition is observed between the  $T_g$  and  $T_m$  values. This is known as the cold crystallization temperature ( $T_c$ ).

In this work the  $T_m$  of PL block copolymers and the stereocomplexes and their degree of crystallinity ( $\chi_h$  and  $\chi_{sc}$ ) were determined from the 1<sup>st</sup> heating scan of DSC process. While the  $T_g$  and  $T_c$  were observed during the 2<sup>nd</sup> heating scan running. The thermal transition results of block copolymers by DSC illustrate following:





The 1<sup>st</sup> heating scan DSC thermograms of PLL and PDL block copolymers were shown in Figures 4.21 and 4.22, respectively. The DSC results from the 1<sup>st</sup> heating scan curves were summarized in Table 4.5 including melting temperature of homo-crystallites ( $T_{m, hc}$ ), the heat of melting of homo-crystallite ( $\Delta H_{m, hc}$ ).

From Table 4.5, it was observed that all the block copolymers showed  $T_{m, hc}$  similar to the range of 169-174°C. This value consistent to the homo-PL melting temperature, as same as several reports (Tsuji, 2005; Xiao *et al.*, 2009; Qi *et al.*, 2015). It is demonstrates that the PL melting point do not change although the PPG attached as the block copolymer structures.

To study the effect of molecular weight of PL blocks on the  $\Delta H_{m, hc}$  value was evaluated. It can be seen that the  $\Delta H_{m, hc}$  values of block copolymers increased as the PL end-block lengths were increased from 20K to 40K g/mol for both the diblock and triblock copolymers. This can be explained that the longer PL chains of the block copolymers enhanced PL crystallization (Liu *et al.*, 2014). Moreover, the diblock and triblock structures did not affect the  $\Delta H_{m, hc}$  of PL end-blocks in significant for the same type and length of PL end-block.

To investigate the effect of PPG block length on the  $\Delta H_{m, hc}$  of PL end-blocks, the block copolymers contained the same PL block length were compared; 20K-*b*-2K-*b*-20K and 20K-*b*-4K-*b*-20K. From Table 4.5, the triblock copolymers consisted the longer PPG block lengths show the lower  $\Delta H_{m, hc}$  than that of the shorter one. These results correspond with Li and Vert (2003) that the longer PEG block of PLL-*b*-PEG-*b*-PLL showed lower  $\Delta H_{m, hc}$  than the shorter PEG block. This due to the crystallization of PLL blocks was more depressed by the longer PEG middle-block.



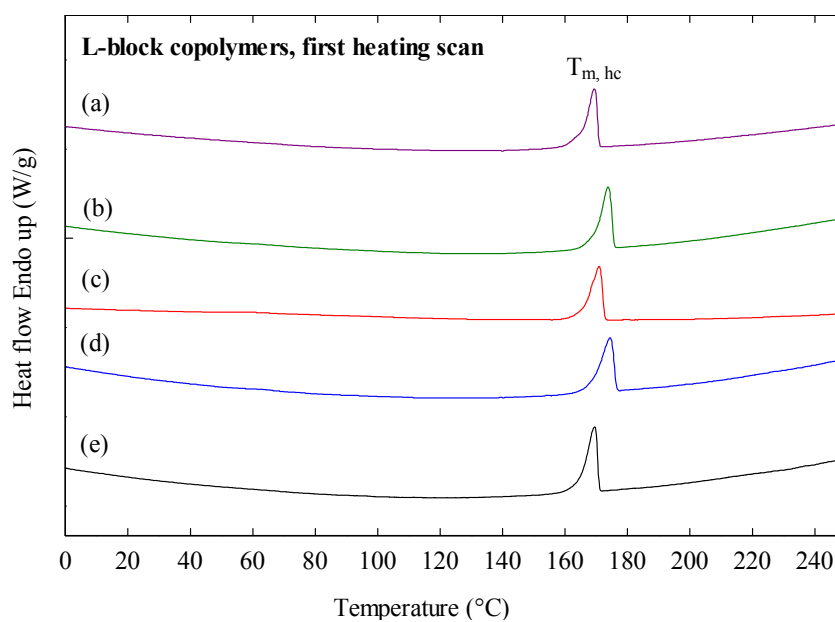


**Figure 4.21** First heating scan DSC thermograms of (a) 2.5K-*b*-L20K, (b) 2.5K-*b*-L40K, (c) L20K-*b*-2K-*b*-L20K, (d) L40K-*b*-2K-*b*-L40K and (e) L20K-*b*-4K-*b*-L20K.

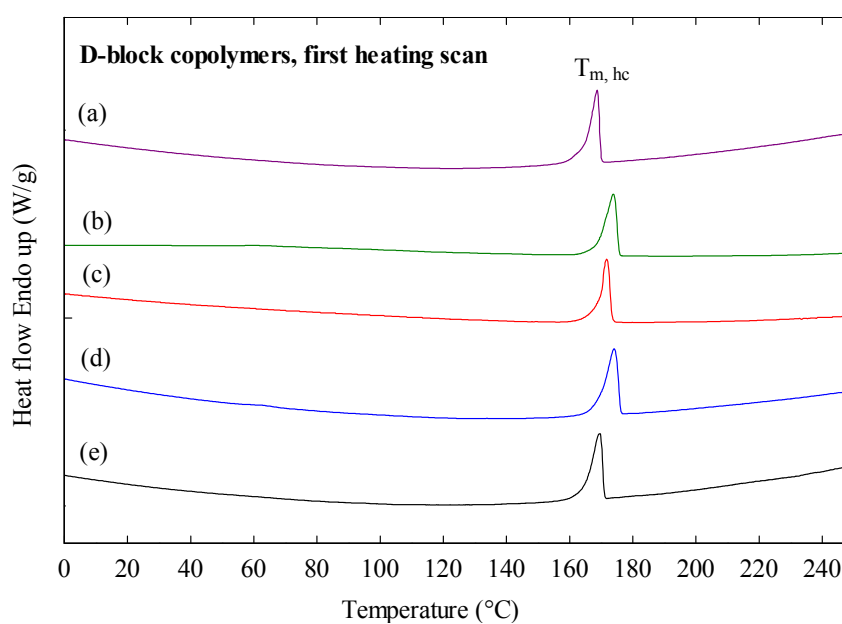


**Figure 4.22** First heating scan DSC thermograms of (a) 2.5K-*b*-D20K, (b) 2.5K-*b*-D40K, (c) D20K-*b*-2K-*b*-D20K, (d) D40K-*b*-2K-*b*-D40K and (e) D20K-*b*-4K-*b*-D20K.



**Table 4.5** DSC results of block copolymers obtained from the 1<sup>st</sup> heating scan curves.

<b>Block copolymers</b>	<b>T<sub>m, hc</sub> (°C)</b>	<b>ΔH<sub>m, hc</sub> (J/g)</b>
<b>2.5K-<i>b</i>-L20K</b>	169	41.1
<b>2.5K-<i>b</i>-D20K</b>	169	42.3
<b>2.5K-<i>b</i>-L40K</b>	174	45.0
<b>2.5K-<i>b</i>-D40K</b>	173	46.2
<b>L20K-<i>b</i>-2K-<i>b</i>-L20K</b>	171	41.4
<b>D20K-<i>b</i>-2K-<i>b</i>-D20K</b>	171	38.0
<b>L40K-<i>b</i>-2K-<i>b</i>-L40K</b>	174	47.2
<b>D40K-<i>b</i>-2K-<i>b</i>-D40K</b>	174	48.4
<b>L20K-<i>b</i>-4K-<i>b</i>-L20K</b>	170	37.2
<b>D20K-<i>b</i>-4K-<i>b</i>-D20K</b>	170	36.1

After the 1<sup>st</sup> heating scan the quench cooling process was done to 0°C and finally the samples were reheated in the same condition with the first scan (0 to 250°C, 10°C/min). The T<sub>g</sub>, cold crystallization temperature (T<sub>c</sub>) and heat of crystallization (ΔH<sub>cc</sub>) were determined in this step. The 2<sup>nd</sup> heating scan DSC thermograms of block copolymers were shown in Figures 4.23 and 4.24. The T<sub>g</sub>, T<sub>c</sub> and ΔH<sub>cc</sub> values are summarized in Table 4.6.

It can be seen that the T<sub>g</sub>, T<sub>c</sub> and ΔH<sub>c</sub> values significantly increased as the PL end-block lengths increased for the same PPG block length. This may be explained that the longer PL end-blocks reduced chain mobility of PL blocks during glassy-rubbery transition and crystallization of the PL end-blocks (Li and Vert, 2003). The diblock copolymers showed lower T<sub>g</sub> than the triblock copolymers. This may be due to the free end-chains of the PPG blocks enhanced the plasticizing effect. In addition, the T<sub>g</sub> and T<sub>c</sub> also decreased as the PPG block lengths increased from the 20K to 40K g/mol.



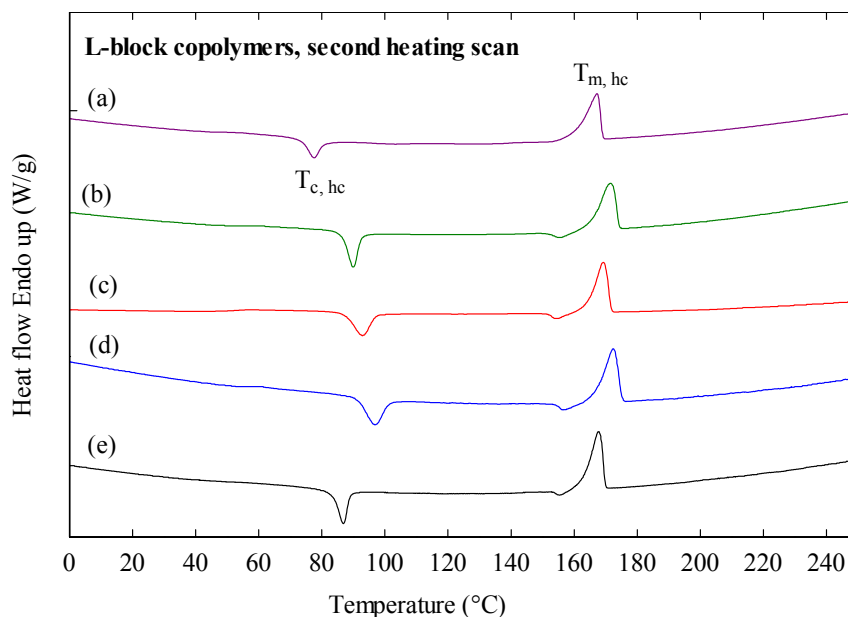


**Figure 4.23** Second heating scan DSC thermograms of (a) 2.5K-*b*-L20K, (b) 2.5K-*b*-L40K, (c) L20K-*b*-2K-*b*-L20K, (d) L40K-*b*-2K-*b*-L40K and (e) L20K-*b*-4K-*b*-L20K.

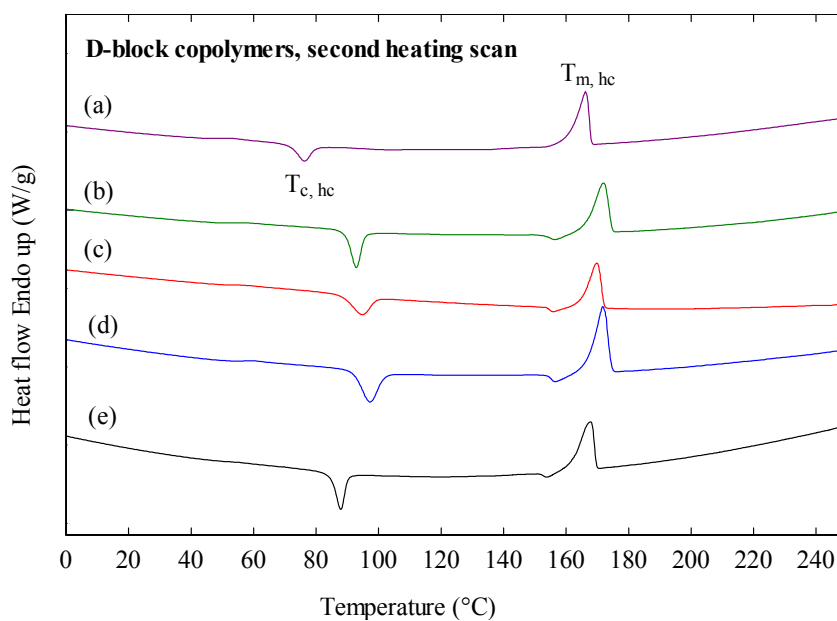


**Figure 4.24** Second heating scan DSC thermograms of (a) 2.5K-*b*-D20K, (b) 2.5K-*b*-D40K, (c) D20K-*b*-2K-*b*-D20K, (d) D40K-*b*-2K-*b*-D40K and (e) D20K-*b*-4K-*b*-D20K.



**Table 4.6** DSC results of block copolymers obtained from the 2<sup>nd</sup> heating scan curves.

Block copolymers	T <sub>g</sub> (°C)	T <sub>c, hc</sub> (°C)	ΔH <sub>c</sub> (J/g)
<b>2.5K-<i>b</i>-L20K</b>	49	78	14.0
<b>2.5K-<i>b</i>-D20K</b>	49	77	14.2
<b>2.5K-<i>b</i>-L40K</b>	54	90	23.4
<b>2.5K-<i>b</i>-D40K</b>	53	93	26.1
<b>L20K-<i>b</i>-2K-<i>b</i>-L20K</b>	52	93	25.2
<b>D20K-<i>b</i>-2K-<i>b</i>-D20K</b>	53	95	23.3
<b>L40K-<i>b</i>-2K-<i>b</i>-L40K</b>	56	96	29.1
<b>D40K-<i>b</i>-2K-<i>b</i>-D40K</b>	56	97	33.2
<b>L20K-<i>b</i>-4K-<i>b</i>-L20K</b>	50	87	21.0
<b>D20K-<i>b</i>-4K-<i>b</i>-D20K</b>	52	87	23.2

## 4.2 Characterization of stereocomplex poly lactide films

The films of mPPG-*b*-PLL/mPPG-*b*-PDL and PLL-*b*-PPG-*b*-PLL/PDL-*b*-PPG-*b*-PDL blends with different ratios of L-/D-copolymer such as 100/0, 75/25, 50/50, 25/75 and 0/100 wt% were prepared by solution blending before film casting. They were characterized about structure order to distinguish between the neat block copolymer and scPL, thermal transition properties, morphology and mechanical properties. The results are presented following:

### 4.2.1 Crystalline structure

Infrared absorption spectra of many bulk polymers are almost simple considering the large numbers of atoms incorporated into the molecular chains. In this work the Fourier Transform Infrared spectroscopy (FTIR) was applied to confirm crystal structure of the block copolymers and their blend films. The FTIR spectra in ranged 780-980 cm<sup>-1</sup> were investigated.

Figures 4.25-4.29 show FTIR spectra of the block copolymer and their blend films with different PPG block length, PL block length and blend ratios. It can be seen that the diblock and tri block copolymer films of the PLL (spectrum a) and PDL (spectrum e) presented absorbance bands at 922 cm<sup>-1</sup>, which assigned to the coupling of



C-C backbone stretching with the CH<sub>3</sub> rocking mode and is sensitive to the homo-crystalline structure of the PL blocks (Zhang, 2005; 2007; Na *et al.*, 2014). All the blend films exhibited predominant absorbance bands at 908 cm<sup>-1</sup> which attributed to the stereocomplex crystalline structure of the PL blocks (Brizzolara *et al.*, 1996). The 75/25 and 25/75 (w/w) blend films also showed shoulder bands at 922 cm<sup>-1</sup>. This suggests the 75/25 and 25/75 (w/w) blend films consisted large stereocomplex crystalline and small homo-crystalline structures. However, the shoulder bands were not detected for the 50/50 (w/w) blend films indicated that they were complete stereocomplex formation.

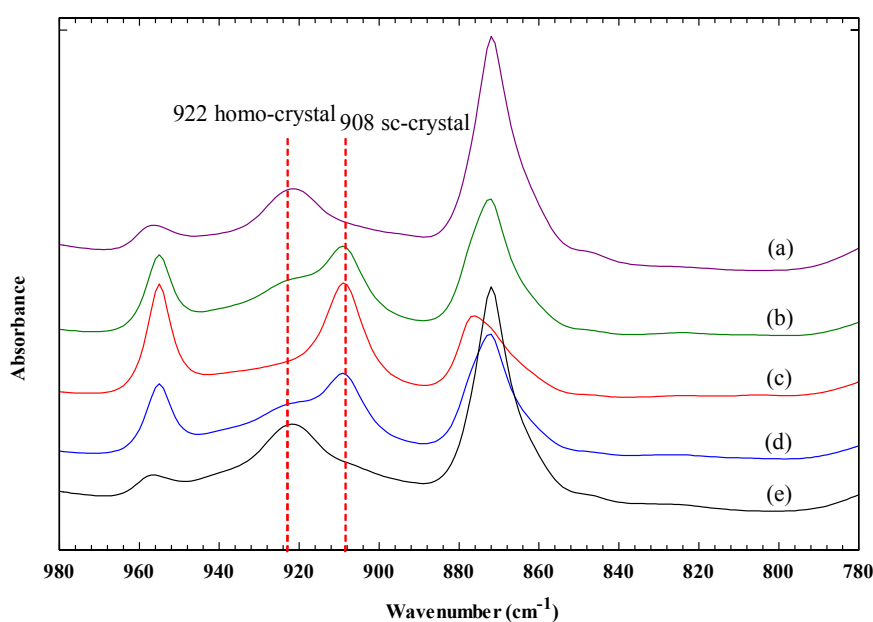


**Figure 4.25** FTIR spectra of mPPG-*b*-PL films prepared with 2.5K-*b*-L20K/2.5K-*b*-D20K blend ratios of (a) 100/0, (b) 75/25, (c) 50/50, (d) 25/75 and (e) 0/100 (w/w).



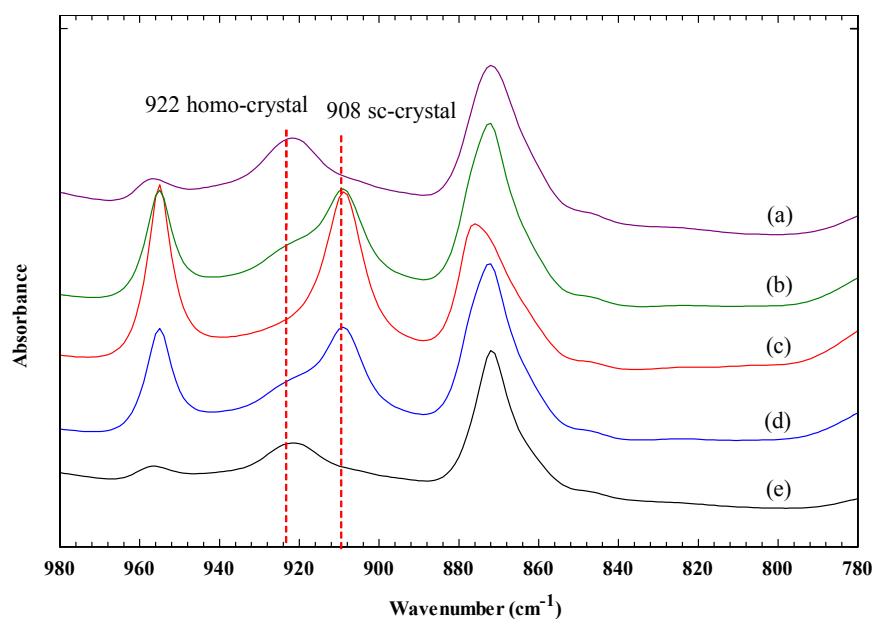


**Figure 4.26** FTIR spectra of mPPG-*b*-PL films prepared with 2.5K-*b*-L40K/2.5K-*b*-D40K blend ratios of (a) 100/0, (b) 75/25, (c) 50/50, (d) 25/75 and (e) 0/100 (w/w).

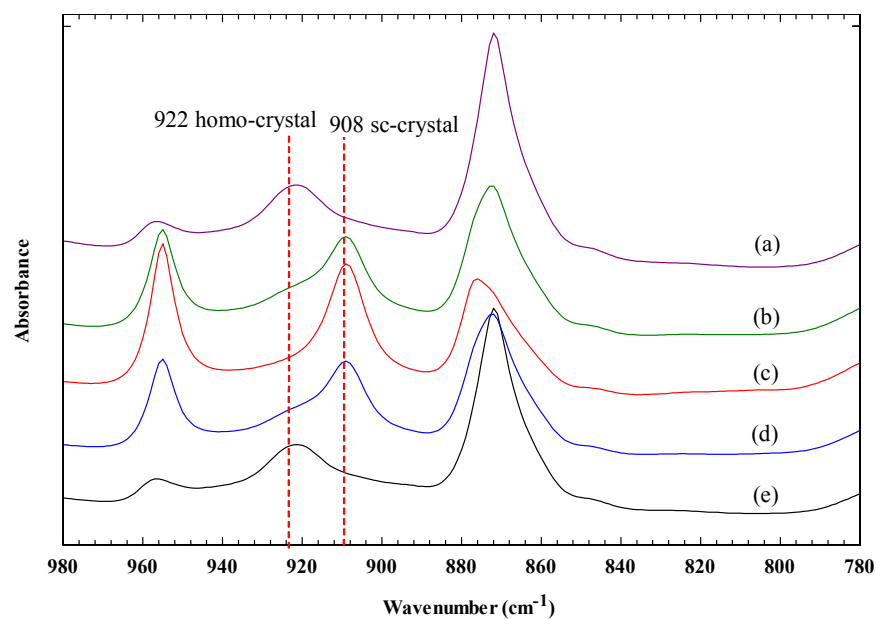


**Figure 4.27** FTIR spectra of PL-*b*-PPG-*b*-PL films prepared with L20K-*b*-2K-*b*-L20K/D20K-*b*-2K-*b*-D20K blend ratios of (a) 100/0, (b) 75/25, (c) 50/50, (d) 25/75 and (e) 0/100 (w/w).



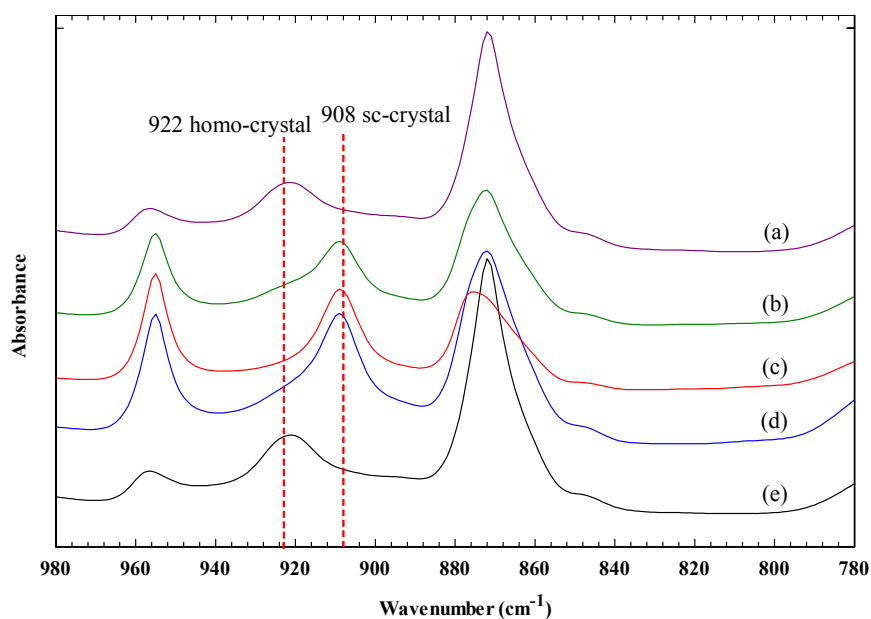


**Figure 4.28** FTIR spectra of PL-*b*-PPG-*b*-PL films prepared with L40K-*b*-2K-*b*-L40K/D40K-*b*-2K-*b*-D40K blend ratios of (a) 100/0, (b) 75/25, (c) 50/50, (d) 25/75 and (e) 0/100 (w/w).

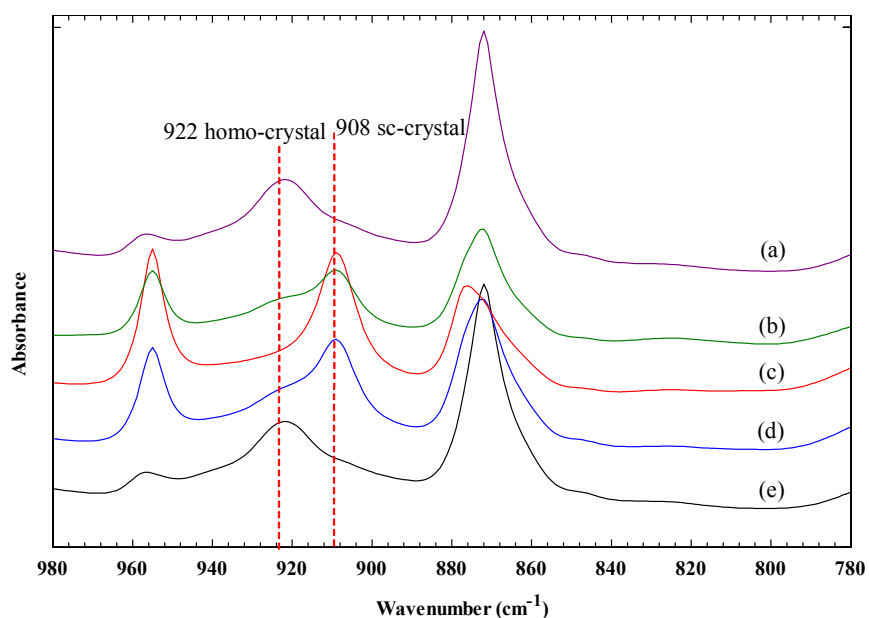


**Figure 4.29** FTIR spectra of PL-*b*-PPG-*b*-PL films prepared with L20K-*b*-4K-*b*-L20K/D20K-*b*-4K-*b*-D20K blend ratios of (a) 100/0, (b) 75/25, (c) 50/50, (d) 25/75 and (e) 0/100 (w/w).





The wide-angle scattering mode is commonly termed X-ray diffraction (XRD) and it has given valuable information on the spatial arrangement of the atoms within crystalline materials. To investigate homo- and stereocomplex crystalline structures, the XRD technique was also applied in this work. The XRD patterns of the block copolymers and their blend films with different ratios were presented in Figures 4.30-4.34.

The homo-crystalline of PL showed diffraction peaks at  $15^\circ$ ,  $16.7^\circ$ ,  $19.1^\circ$  and  $22.3^\circ$  (Qi *et al.*, 2015). Mean which the stereocomplex crystalline of PL exhibited diffraction peaks at  $11.9^\circ$ ,  $20.7^\circ$  and  $24^\circ$  (Qi *et al.*, 2015). It was found that all the diblock and triblock copolymer films of PLL and PDL showed diffraction peaks at  $15^\circ$ ,  $16.7^\circ$ ,  $19.1^\circ$  and  $22.3^\circ$  attributed to the complete homo-crystalline of PL blocks. All the 50/50 (w/w) blend films showed diffraction peaks at  $12^\circ$ ,  $20.7^\circ$  and  $24^\circ$  attributed to the complete stereocomplex crystalline structure of PL blocks. The 75/25 and 25/75 (w/w) blend films exhibited characteristic peaks of both homo and stereocomplex crystalline structures. The XRD results were accorded to the FTIR results as previously described.

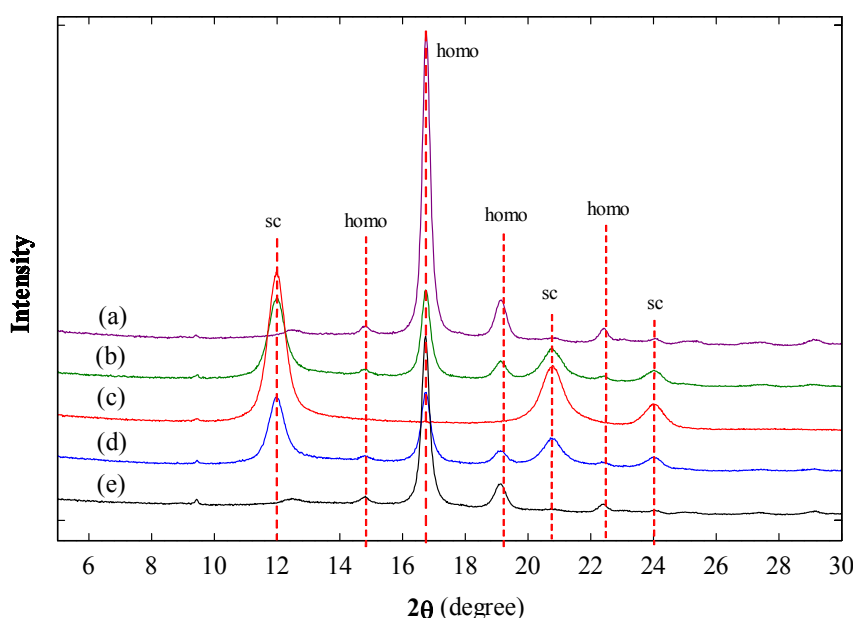


**Figure 4.30** XRD patterns of mPPG-*b*-PL films prepared with 2.5K-*b*-L20K/2.5K-*b*-D20K blend ratios of (a) 100/0, (b) 75/25, (c) 50/50, (d) 25/75 and (e) 0/100 (w/w).



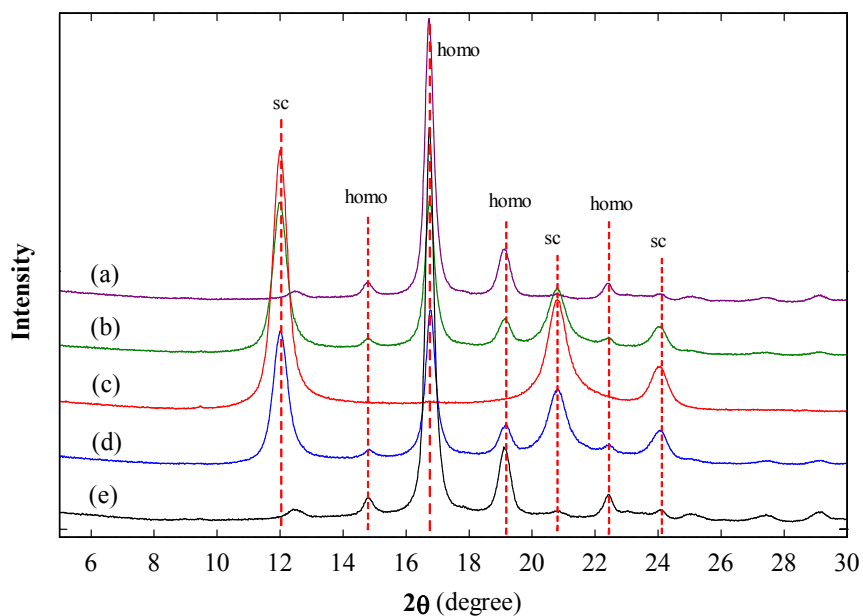


**Figure 4.31** XRD patterns of mPPG-*b*-PL films prepared with 2.5K-*b*-L40K/2.5K-*b*-D40K blend ratios of (a) 100/0, (b) 75/25, (c) 50/50, (d) 25/75 and (e) 0/100 (w/w).

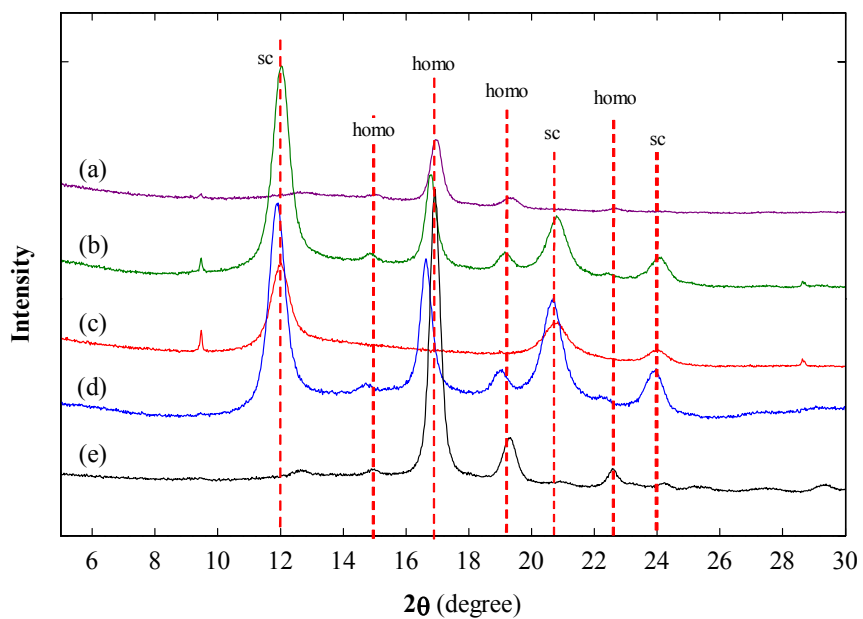


**Figure 4.32** XRD patterns of PL-*b*-PPG-*b*-PL films prepared with L20K-*b*-2K-*b*-L20K/D20K-*b*-2K-*b*-D20K blend ratios of (a) 100/0, (b) 75/25, (c) 50/50, (d) 25/75 and (e) 0/100 (w/w).



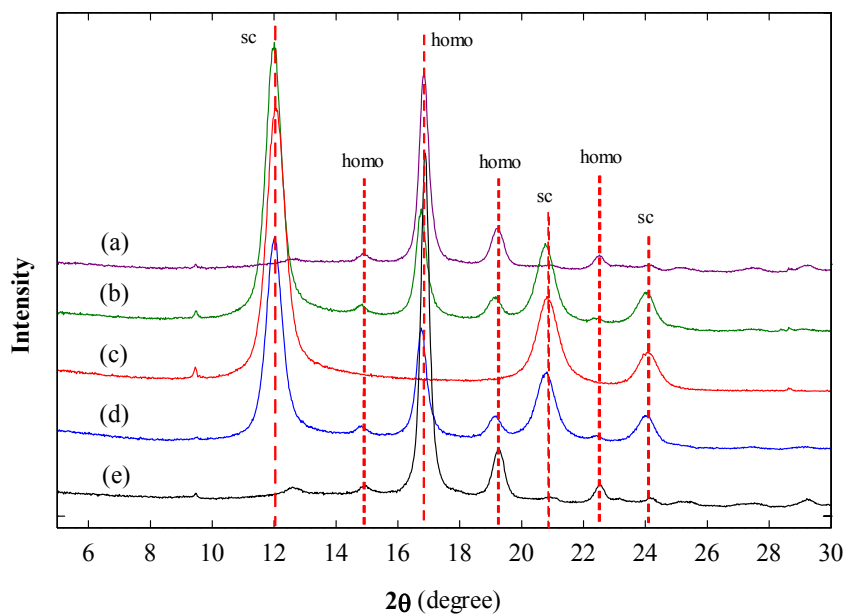


**Figure 4.33** XRD patterns of PL-*b*-PPG-*b*-PL films prepared with L40K-*b*-2K-*b*-L40K/D40K-*b*-2K-*b*-D40K blend ratios of (a) 100/0, (b) 75/25, (c) 50/50, (d) 25/75 and (e) 0/100 (w/w).

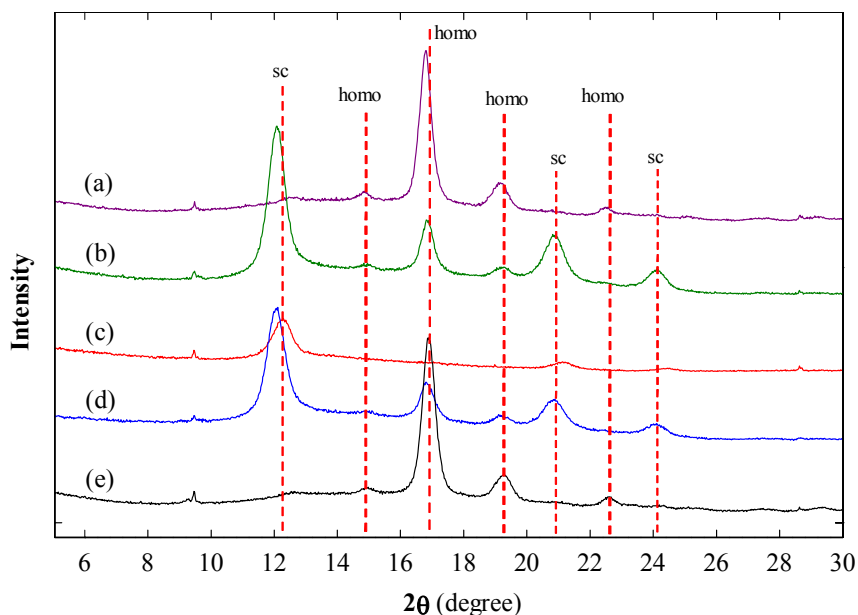


**Figure 4.34** XRD patterns of PL-*b*-PPG-*b*-PL films prepared with L20K-*b*-4K-*b*-L20K/D20K-*b*-4K-*b*-D20K blend ratios of (a) 100/0, (b) 75/25, (c) 50/50, (d) 25/75 and (e) 0/100 (w/w).



#### 4.2.2 Thermal transition properties

The blend films of mPPG-*b*-PL and PL-*b*-PPG-*b*-PL with various ratios were studied by DSC to investigate the  $T_m$  of the homo-crystallites ( $T_{m, hc}$ ) and the stereocomplex crystallites ( $T_{m, sc}$ ) from the 1<sup>st</sup> heating scan curves. The degree of crystallinity ( $\chi$ ) of the homo-crystallinities ( $\chi_{hc}$ ) and the stereocomplex crystallinities ( $\chi_{sc}$ ) were calculated from the  $\Delta H_m$  of the homo-crystallites ( $\Delta H_{m, hc}$ ) and the stereocomplex crystallites ( $\Delta H_{m, sc}$ ), respectively. Their  $T_c$  was observed during the 2<sup>nd</sup> heating scan curves. The thermal transition results by DSC were illustrated following:

The 1<sup>st</sup> heating scan DSC thermograms of the mPPG-*b*-PL and PL-*b*-PPG-*b*-PL blend films were shown in Figures 4.35-4.39. All the neat diblock and triblock copolymer films exhibited only  $T_{m, hc}$  they showed complete homo-crystallization of the PL blocks. The 50/50 (w/w) blend films showed only  $T_{m, sc}$  indicated stereocomplex crystallization of the PL blocks was complete. The  $T_{m, sc}$  is higher than the  $T_{m, hc}$  due to the stronger van der Waals forces of the stereocomplex crystallites than that of the homo-crystallites of PL (Brizzolara *et al.*, 1996; Okihara *et al.*, 1991). The 75/25 and 25/75 (w/w) blend films had both the small  $T_{m, hc}$  and large  $T_{m, sc}$  peaks. The  $\chi_{hc}$  and  $\chi_{sc}$  were calculated from the 1<sup>st</sup> heating data by equations (4.1) and (4.2), respectively.

$$\chi_{hc} (\%) = \frac{\Delta H_{hc}}{w_{PL} \times \Delta H_{hc}^{\circ}} \times 100 \dots \dots \dots (4.1)$$

$$\chi_{sc} (\%) = \frac{\Delta H_{sc}}{w_{PL} \times \Delta H_{sc}^{\circ}} \times 100 \dots \dots \dots (4.2)$$

where the  $w_{PL}$  was a weight fraction of PL including PLL and PDL that determined from <sup>1</sup>H-NMR.

The calculation example for  $w_{PL}$  of 2.5K-*b*-L20K (the PG:LL = 16:84 mol%; see Table 4.2) is illustrated as following:

$$w_{PL} = \frac{\text{weight of PL (g)}}{(\text{weight of PL (g)}) + (\text{weight of PG (g)})}$$

$$w_{PL} = \frac{84 \text{ mol} \times 144.14 \frac{\text{g}}{\text{mol}}}{\left(84 \text{ mol} \times 144.14 \frac{\text{g}}{\text{mol}}\right) + \left(16 \text{ mol} \times 58 \frac{\text{g}}{\text{mol}}\right)}$$

$$= 0.93$$



For  $w_{PL}$  of 2.5K-*b*-D20K (the PG:DL = 26:74 mol%; see Table 4.2) is illustrated as following:

$$w_{PL} = \frac{(74 \text{ mol} \times 144.14 \frac{\text{g}}{\text{mol}})}{(74 \text{ mol} \times 144.14 \frac{\text{g}}{\text{mol}}) + (26 \text{ mol} \times 58 \frac{\text{g}}{\text{mol}})}$$

$$= 0.87$$

The  $w_{PL}$  of the 75/25 (w/w) 2.5K-*b*-L20K/2.5K-*b*-D20K blend film was calculated as following:

$$\text{weight of PL on 75 wt\% 2.5K} - b - \text{L20K} = \frac{93g \times 75g}{100g} = 69.75g$$

$$\text{weight of PL on 25 wt\% 2.5K} - b - \text{D20K} = \frac{87g \times 25g}{100g} = 21.75g$$

$$w_{PL} = \frac{69.75g + 21.75g}{100g}$$

$$= 0.92$$

The weight fractions of PL in the blend films for all ratios were shown in Table 4.7. The thermal properties from the 1<sup>st</sup> heating scan DSC curves were summarized in Table 4.8.

The  $T_{m, hc}$  of 2.5K-*b*-20K blend films (164-169°C) were lower than the 2.5-*b*-40K blend films (169-174°C). This may be due to the longer PL blocks enhanced PL crystallization. The diblock copolymer blend films exhibited lower  $T_{m, hc}$  than their neat diblock copolymer films. This indicates the smaller size of homo-crystallites of the PL blocks. The  $T_{m, hc}$  peaks of 2.5K-*b*-20K blend films were broad peaks suggested the various sizes of stereocomplex crystallites were formed. The narrow  $T_{m, sc}$  peaks were observed when the PL block lengths were increased to 40K g/mol.

The  $T_{m, hc}$  of the triblock copolymer blend films increased as the PL end-block lengths increased from 20K g/mol (166-171°C) to 40K g/mol (170-174°C). However, the  $T_{m, hc}$  of the 20K-*b*-4K-*b*-20K blend films (164-170°C) were than the 20K-*b*-2K-*b*-20K blend films (170-174°C). This suggests the longer PPG middle-block length inhibited homo-crystallization of the PL end-blocks.

The  $T_{m, sc}$  peaks of the 20K-*b*-2K-*b*-20K (Figure 4.37) and 20K-*b*-4K-*b*-20K (Figure 4.39) blend films were broad peaks similar the 2.5K-*b*-20K blend films (Figure 4.35). The  $T_{m, sc}$  peaks of the 40K-*b*-2K-*b*-40K blend films (Figure 4.38) were narrow



similar the 2.5K-*b*-40K blend films (Figure 4.36). This may be proposed that the shorter PL block length (20K g/mol) enhanced chain mobility to form various sizes of stereocomplex crystallites.

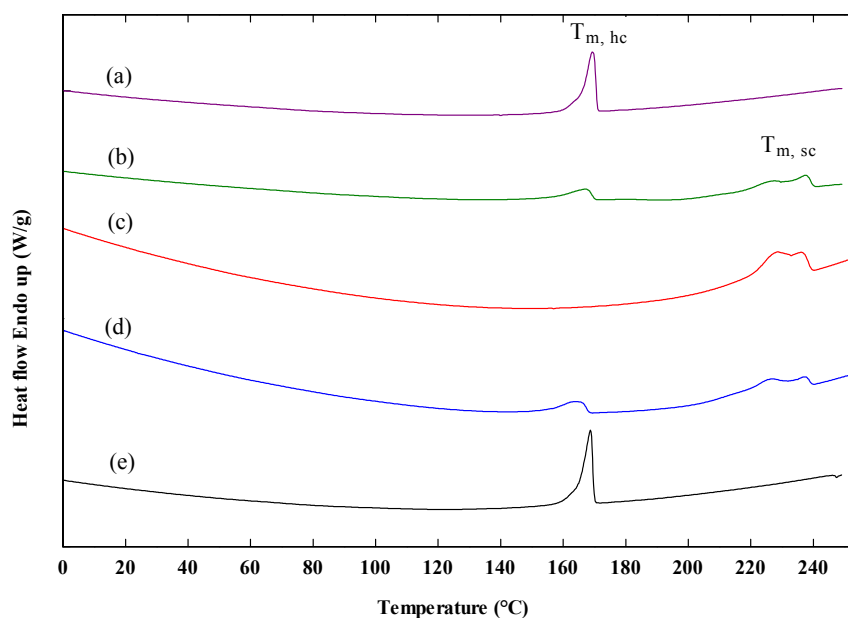


**Figure 4.35** First heating scan DSC thermograms of mPPG-*b*-PL films prepared with 2.5K-*b*-L20K/2.5K-*b*-D20K blend ratios of (a) 100/0, (b) 75/25, (c) 50/50, (d) 25/75 and (e) 0/100 (w/w).

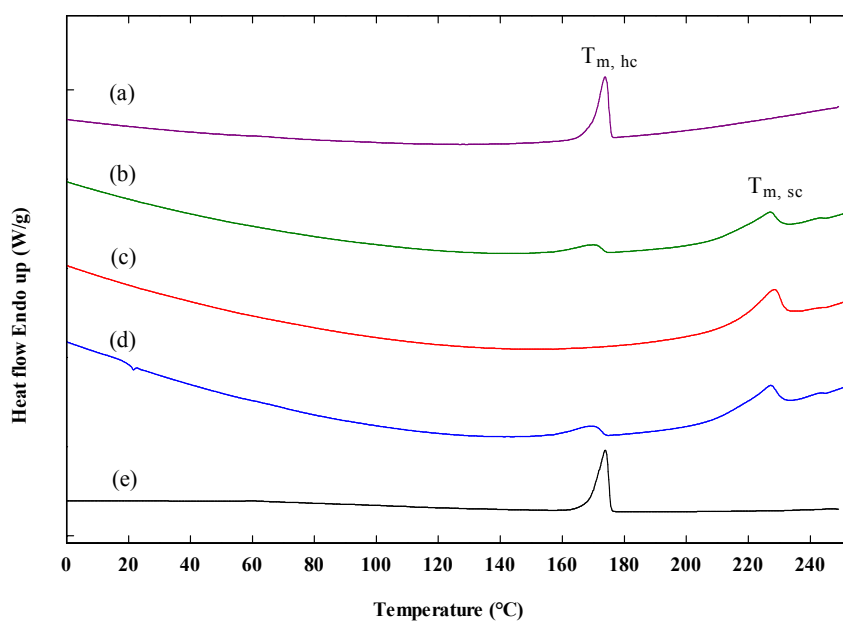


**Figure 4.36** First heating scan DSC thermograms of mPPG-*b*-PL films prepared with 2.5K-*b*-L40K/2.5K-*b*-D40K blend ratios of (a) 100/0, (b) 75/25, (c) 50/50, (d) 25/75 and (e) 0/100 (w/w).



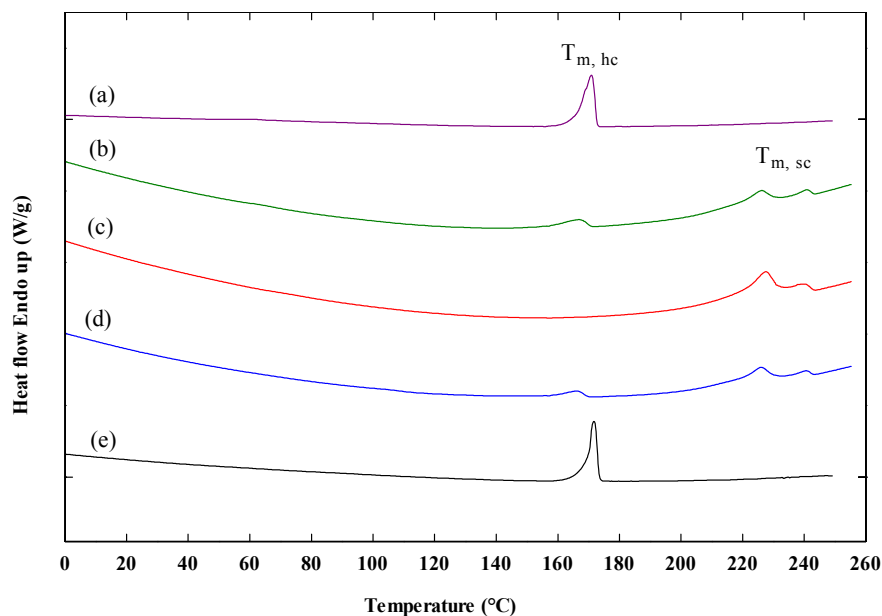


**Figure 4.37** First heating scan DSC thermograms of PL-*b*-PPG-*b*-PL films prepared with L20K-*b*-2K-*b*-L20K/ D20K-*b*-2K-*b*-D20K blend ratios of (a) 100/0, (b) 75/25, (c) 50/50, (d) 25/75 and (e) 0/100 (w/w).

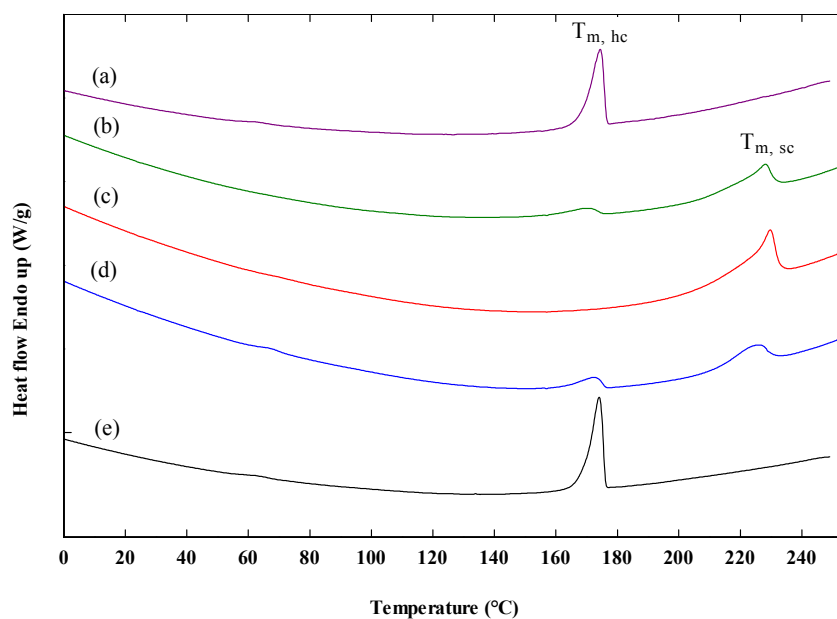


**Figure 4.38** First heating scan DSC thermograms of PL-*b*-PPG-*b*-PL films prepared with L40K-*b*-2K-*b*-L40K/ D40K-*b*-2K-*b*-D40K blend ratios of (a) 100/0, (b) 75/25, (c) 50/50, (d) 25/75 and (e) 0/100 (w/w).



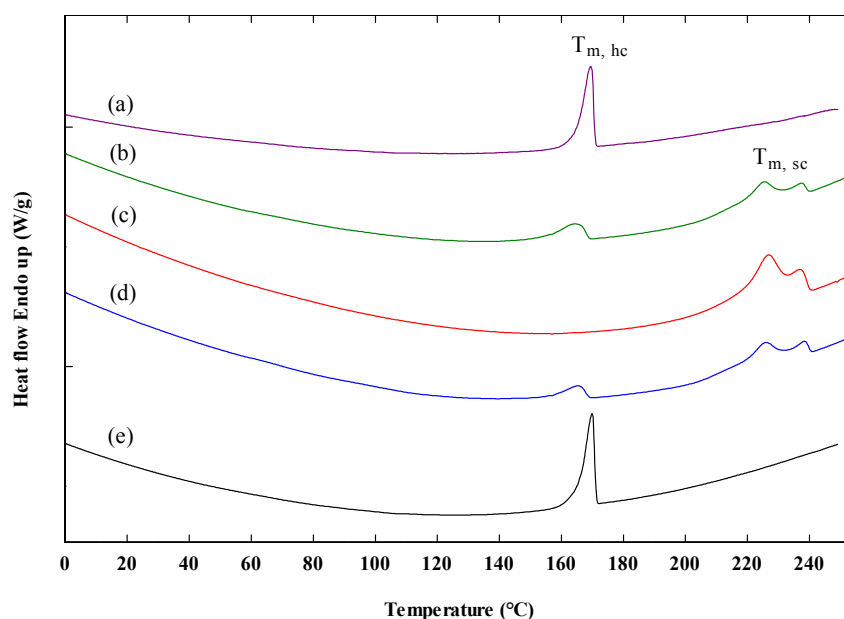


**Figure 4.39** First heating scan DSC thermograms of PL-*b*-PPG-*b*-PL films prepared with L20K-*b*-4K-*b*-L20K/ D20K-*b*-4K-*b*-D20K blend ratios of (a) 100/0, (b) 75/25, (c) 50/50, (d) 25/75 and (e) 0/100 (w/w).

**Table 4.7** The weight fraction of PL ( $w_{PL}$ ) of block copolymer blend films obtained from calculation with mole ratio of PG:PL.

Block copolymer blend films	Blend ratio (w/w)	$w_{PL}$
<b>2.5K-<i>b</i>-L20K/2.5K-<i>b</i>-D20K</b>	100/0	0.93
	75/25	0.92
	50/50	0.90
	25/75	0.89
	0/100	0.87
<b>2.5K-<i>b</i>-L40K/2.5K-<i>b</i>-D40K</b>	100/0	0.95
	75/25	0.95
	50/50	0.95
	25/75	0.95
	0/100	0.95





**Table 4.7** The weight fraction of PL ( $w_{PL}$ ) of block copolymer blend films obtained from calculation with mole ratio of PG:PL. (continue)

<b>Block copolymer blend films</b>	<b>Blend ratio (w/w)</b>	<b><math>w_{PL}</math></b>
<b>L20K-<i>b</i>-2K-<i>b</i>-L20K/D20K-<i>b</i>-2K-<i>b</i>-D20K</b>	100/0	0.95
	75/25	0.95
	50/50	0.95
	25/75	0.95
	0/100	0.95
<b>L40K-<i>b</i>-2K-<i>b</i>-L40K/D40K-<i>b</i>-2K-<i>b</i>-D40K</b>	100/0	0.97
	75/25	0.97
	50/50	0.97
	25/75	0.97
	0/100	0.97
<b>L20K-<i>b</i>-4K-<i>b</i>-L20K/D20K-<i>b</i>-4K-<i>b</i>-D20K</b>	100/0	0.92
	75/25	0.92
	50/50	0.91
	25/75	0.91
	0/100	0.90



**Table 4.8** DSC results of block copolymer blend films obtained from the 1<sup>st</sup> heating scan curves.

<b>Block copolymer blend films</b>	<b>Blend ratio (w/w)</b>	<b>T<sub>m, hc</sub> (°C)</b>	<b>T<sub>m, sc</sub> (°C)</b>	<b>ΔH<sub>m, hc</sub> (J/g)</b>	<b>ΔH<sub>m, sc</sub> (J/g)</b>	<b>χ<sub>hc</sub> (%)</b>	<b>χ<sub>sc</sub> (%)</b>
<b>2.5K-<i>b</i>-L20K/ 2.5K-<i>b</i>-D20K</b>	100/0	169	-	41	-	47	-
	75/25	167	237	13	27	15	21
	50/50	-	228	-	36	-	28
	25/75	164	226	17	25	21	20
	0/100	169	-	39	-	48	-
<b>2.5K-<i>b</i>-L40K/ 2.5K-<i>b</i>-D40K</b>	100/0	174	-	45	-	51	-
	75/25	170	-	13	27	15	20
	50/50	-	227	-	41	-	30
	25/75	169	227	16	39	18	29
	0/100	173	-	46	-	52	-
<b>L20K-<i>b</i>-2K-<i>b</i>-L20K/ D20K-<i>b</i>-2K-<i>b</i>-D20K</b>	100/0	171	-	41	-	46	-
	75/25	167	226	10	18.5	11	14
	50/50	-	227	-	40	-	30
	25/75	166	226	6	13	7	10
	0/100	171	-	38	-	43	-
<b>L40K-<i>b</i>-2K-<i>b</i>-L40K/ D40K-<i>b</i>-2K-<i>b</i>-D40K</b>	100/0	174	-	47	-	52	-
	75/25	170	227	7	24	8	17
	50/50	-	230	-	49	-	36
	25/75	172	224	11	23	12	17
	0/100	174	-	48	-	53	-
<b>L20K-<i>b</i>-4K-<i>b</i>-L20K/ D20K-<i>b</i>-4K-<i>b</i>-D20K</b>	100/0	170	-	35	-	41	-
	75/25	164	225	17	14	20	11
	50/50	-	226	-	24	-	19
	25/75	165	225	7	12	8	9
	0/100	170	-	34	-	41	-



The  $\chi_{hc}$  and  $\chi_{sc}$  values were clearly compared as bar graphs in Figures 4.40 and 4.41 for the diblock and triblock copolymer blend films, respectively.

It was found that the  $\chi_{hc}$  decreased and the  $\chi_{sc}$  increased as the blend ratios of blend films changed from 100/0 or 0/100 to 50/50 (w/w) for all the block copolymer blend films. The 50/50 (w/w) blend films showed the highest  $\chi_{sc}$  without the  $\chi_{hc}$ . This suggests the stereocomplexation of PL blocks was complete similar the 50/50 (w/w) PLL/PDL blend films (Tsuji and Ikada, 1999). Therefore, the PPG block of copolymers did not induced homo-crystallization of the PL blocks.

The  $\chi_{sc}$  values of the 50/50 (w/w) blend films slightly increased as the PL block lengths increased from 20K to 40K g/mol for both diblock and triblock copolymer blend films with the same PPG block length according to the crystallinity results of PLL-*b*-PEG/PDL-*b*-PEG blend films (Kang *et al.*, 2005). The  $\chi_{sc}$  values decreased from 35% to 17% as the PPG middle block length increased from 2K to 4K g/mol as shown in Figure 4.41. This result suggests the longer PPG block length reduced stereocomplex crystallization of the PL blocks.

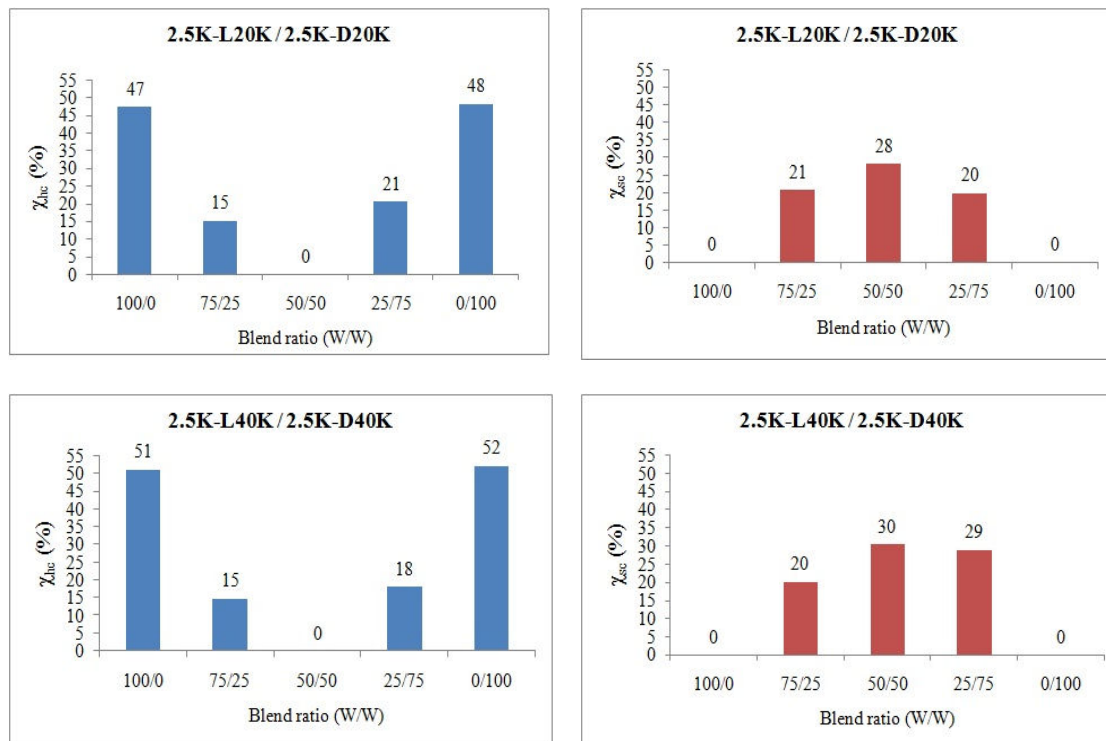


**Figure 4.40**  $\chi_{hc}$  (left row) and  $\chi_{sc}$  (right row) of mPPG-*b*-PL blend films.



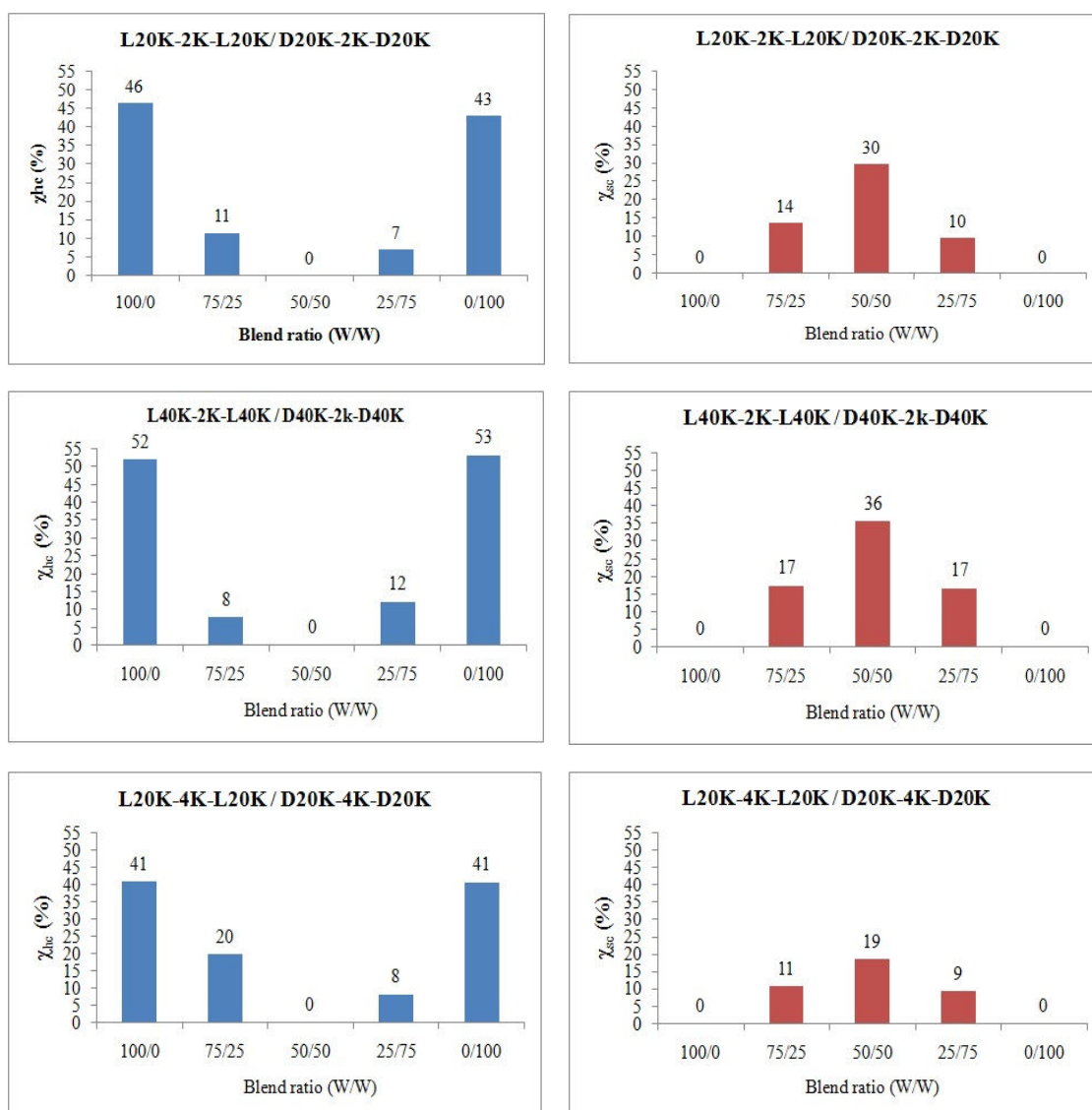


**Figure 4.41**  $\chi_{hc}$  (left row) and  $\chi_{sc}$  (right row) of PL-*b*-PPG-PL blend films.

The  $T_g$  and  $T_c$  of homo-crystallites ( $T_{c, hc}$ ) and of stereocomplex crystallites ( $T_{c, sc}$ ) were determined from the 2<sup>nd</sup> heating scan DSC thermograms as shown in Figures 4.42-4.46. The  $T_{c, hc}$  was lower than that of the  $T_{c, sc}$  due to its lower intermolecular forces. The DSC results from the 2<sup>nd</sup> heating scan curves were summarized in Table 4.9.

The  $T_g$  values of the blend films were nearly with their neat block copolymer films. The stereocomplexation did not affect the  $T_g$  of blend films. The  $T_g$  values of the 2.5K-*b*-20K and 2.5K-*b*-40K diblock copolymer blend films were similar to the range 47-49°C and 53-55°C, respectively. The  $T_g$  values of the 20K-*b*-2K-*b*-20K



and 40K-*b*-2K-*b*-40K triblock copolymer blend films were similar to the range 52-53°C and 56-57°C, respectively. The  $T_g$  values of the blend films increased with the PL block length. The triblock copolymer blend films showed higher  $T_g$  than the diblock copolymer blend films. This may be explained that the PPG block of diblock copolymers had free PPG end-chains to induce more plasticizing effect than the triblock copolymers. The 20K-*b*-4K-*b*-20K triblock copolymer blend films had  $T_g$  to the range 49-52°C that were lower than the 20K-*b*-2K-*b*-20K blend films (52-53°C). The longer PPG block length enhanced chain mobility of the PL blocks.

The  $T_{c, hc}$  of block copolymer blend films increased with the PL block lengths. The  $T_{c, hc}$  of the 2.5K-*b*-40K blend films (80-93°C) were higher than the 2.5K-*b*-20K blend films (68-78°C). The  $T_{c, hc}$  of the 40K-*b*-2K-*b*-40K blend films were to the range 96-101°C that higher than the 20K-*b*-2K-*b*-20K blend films (83-95°C). This may be explained by the longer PL blocks reduced chain mobility for PL homo-crystallization.

The  $T_{c, hc}$  of block copolymer blend films were lower than the neat block copolymer films excepted the 40K-*b*-2K-*b*-40K blend films. This may be due to the stereocomplex crystallites can act as a nucleating agent for PL homo-crystallization (Srithep *et al.*, 2016; Li and Huneault, 2007). This was supported by decreasing of the  $\Delta H_{c, hc}$  of the blend films. The 50/50 (w/w) blend films showed the lowest  $T_{c, hc}$  and excepted the 40K-*b*-2K-*b*-40K blend films.

The longer PL block length (40K g/mol) of the triblock copolymer blend films may inhibit the PL homo-crystallization. The longer PPG block length (4K g/mol) enhanced chain mobility to improve the PL homo-crystallization. Then the  $T_{c, hc}$  of the 20K-*b*-4K-*b*-20K blend films were not detected.

The  $T_{c, sc}$  of the 20K-*b*-4K-*b*-20K blend films were only observed at 134°C. In addition, the 50/50 (w/w) 20K-*b*-4K-*b*-20K and 2.5K-*b*-20K blend films had no the  $T_c$ . This demonstrates that the longer PPG blocks and the shorter PL blocks induced complete stereocomplexation.



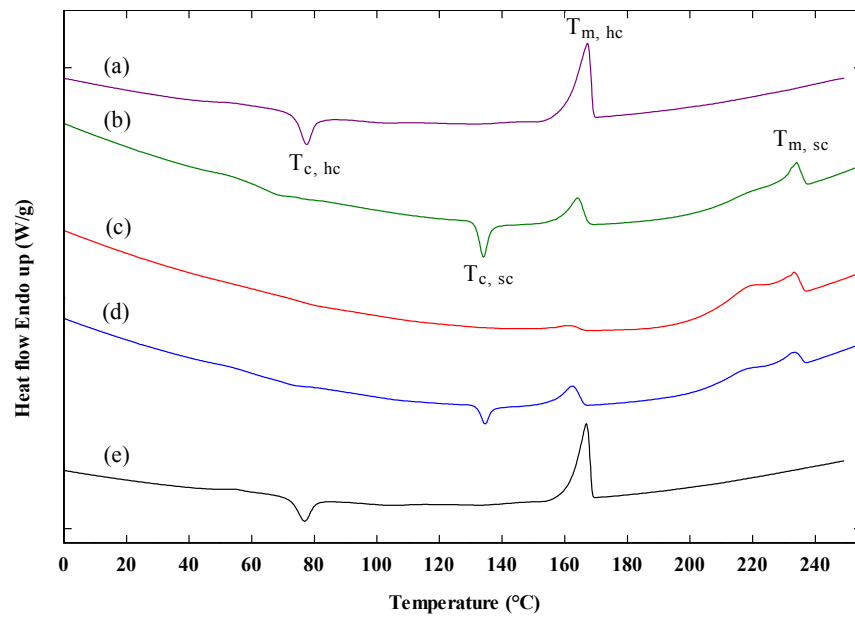


**Figure 4.42** Second heating scan DSC thermograms of mPPG-*b*-PL films prepared with 2.5K-*b*-L20K/2.5K-*b*-D20K blend ratios of (a) 100/0, (b) 75/25, (c) 50/50, (d) 25/75 and (e) 0/100 (w/w).

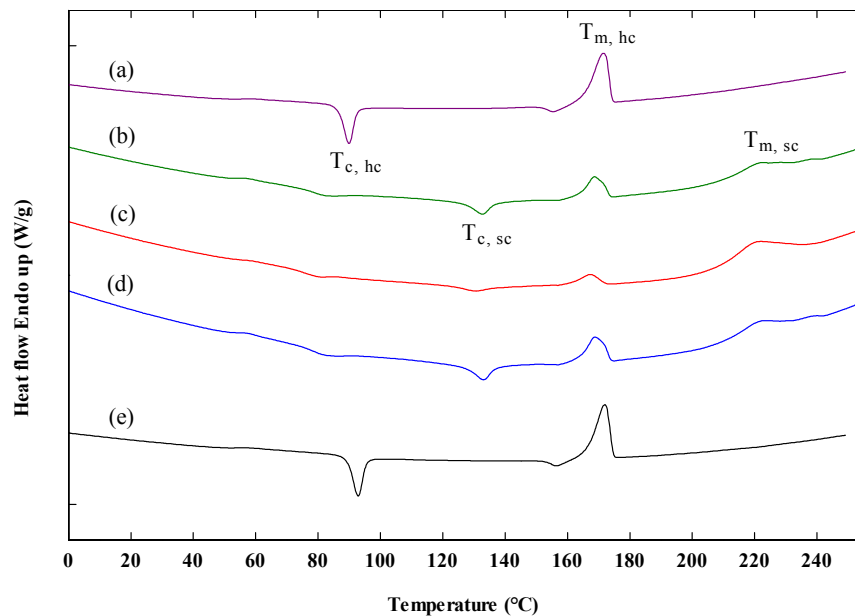


**Figure 4.43** Second heating scan DSC thermograms of mPPG-*b*-PL films prepared with 2.5K-*b*-L40K/2.5K-*b*-D40K blend ratios of (a) 100/0, (b) 75/25, (c) 50/50, (d) 25/75 and (e) 0/100 (w/w).



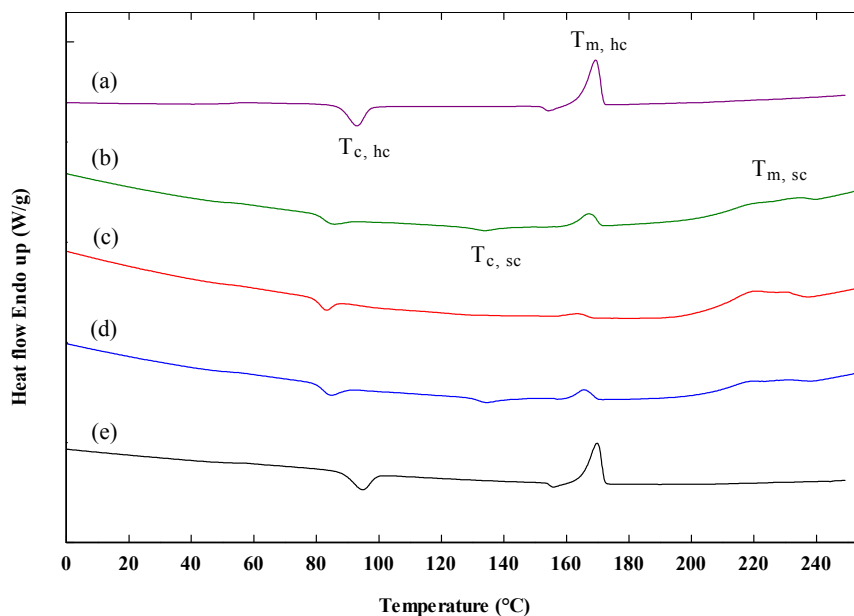


**Figure 4.44** Second heating scan DSC thermograms of PL-*b*-PPG-*b*-PL films prepared with L20K-*b*-2K-*b*-L20K/ D20K-*b*-2K-*b*-D20K blend ratios of (a) 100/0, (b) 75/25, (c) 50/50, (d) 25/75 and (e) 0/100 (w/w).

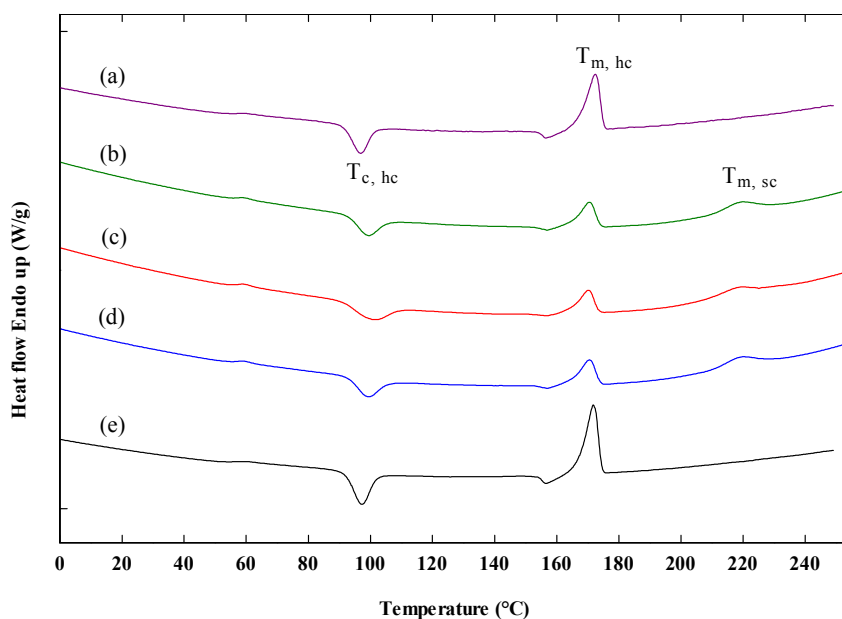


**Figure 4.45** Second heating scan DSC thermograms of PL-*b*-PPG-*b*-PL films prepared with L40K-*b*-2K-*b*-L40K/ D40K-*b*-2K-*b*-D40K blend ratios of (a) 100/0, (b) 75/25, (c) 50/50, (d) 25/75 and (e) 0/100 (w/w).



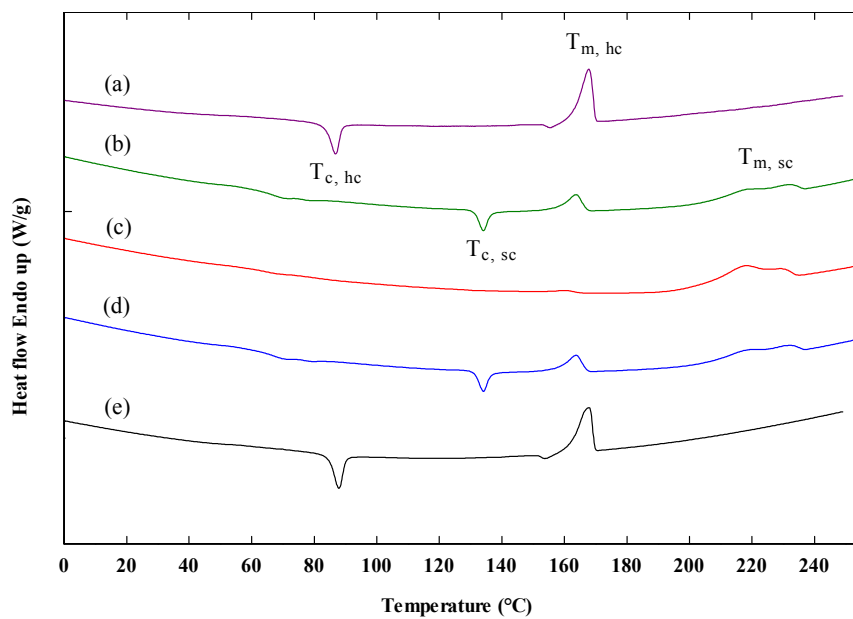


**Figure 4.46** Second heating scan DSC thermograms of PL-*b*-PPG-*b*-PL films prepared with L20K-*b*-4K-*b*-L20K/ D20K-*b*-4K-*b*-D20K blend ratios of (a) 100/0, (b) 75/25, (c) 50/50, (d) 25/75 and (e) 0/100 (w/w).





**Table 4.9** DSC results of block copolymer blend films obtained from the 2<sup>nd</sup> heating scan curves.

Block copolymer blend film	L/D	T <sub>g</sub> (°C)	T <sub>c, hc</sub> (°C)	T <sub>c, sc</sub> (°C)	ΔH <sub>c, hc</sub> (J/g)	ΔH <sub>c, sc</sub> (J/g)
<b>2.5K-<i>b</i>-L20K/ 2.5K-<i>b</i>-D20K</b>	100/0	49	78	-	14	-
	75/25	47	68	134	2	13
	50/50	49	-	-	-	-
	25/75	48	-	135	-	7
	0/100	49	77	-	14	-
<b>2.5K-<i>b</i>-L40K/ 2.5K-<i>b</i>-D40K</b>	100/0	54	90	-	23	-
	75/25	54	83	133	7	14
	50/50	55	80	131	5	6
	25/75	53	82	133	13	17
	0/100	53	93	-	26	-
<b>L20K-<i>b</i>-2K-<i>b</i>-L20K/ D20K-<i>b</i>-2K-<i>b</i>-D20K</b>	100/0	52	93	-	25	-
	75/25	53	85	134	9.3	3.2
	50/50	52	83	-	10	-
	25/75	53	84	134	13	6
	0/100	53	95	-	23	-
<b>L40K-<i>b</i>-2K-<i>b</i>-L40K/ D40K-<i>b</i>-2K-<i>b</i>-D40K</b>	100/0	56	96	-	29	-
	75/25	57	99	-	23	-
	50/50	56	101	-	26	-
	25/75	57	99	-	23	-
	0/100	56	97	-	33	-
<b>L20K-<i>b</i>-4K-<i>b</i>-L20K/ D20K-<i>b</i>-4K-<i>b</i>-D20K</b>	100/0	50	87	-	20.5	-
	75/25	49	-	134	-	13
	50/50	51	-	-	-	-
	25/75	49	-	134	-	13
	0/100	52	87	-	23	-



### 4.2.3 Film morphology

As mentioned previously, the drawbacks of PLL are rigid and brittle. Kulinski *et al.* (2006) have been aimed to improve the elongation at break of PLL by blending with the PPG. They found that the phase separation between PPG and PLL had occurred when used high molecular weight PPG (1,000 g/mol) at 12.5%wt. The separation of plasticizer reduced efficiency of plasticizeable. Thus, in this work we tried to verify that the producing of block copolymer of PL and PPG would absent the phase separation of PPG.

The phase morphology of the block copolymers and their blend films were observed by Scanning Electron Microscopy (SEM). The SEM images of cross-section of diblock and triblock copolymer blend films were showed in Figures 4.47 and 4.48, respectively.

The phase separation of all the block copolymer and their blend films were not occurred. The SEM results indicated that the block copolymer structures can improved phase compatibility between the PL and PPG phase. It can be concluded that the PL end-block length, PPG block length and di-/triblock types did not affect phase morphology of the films.



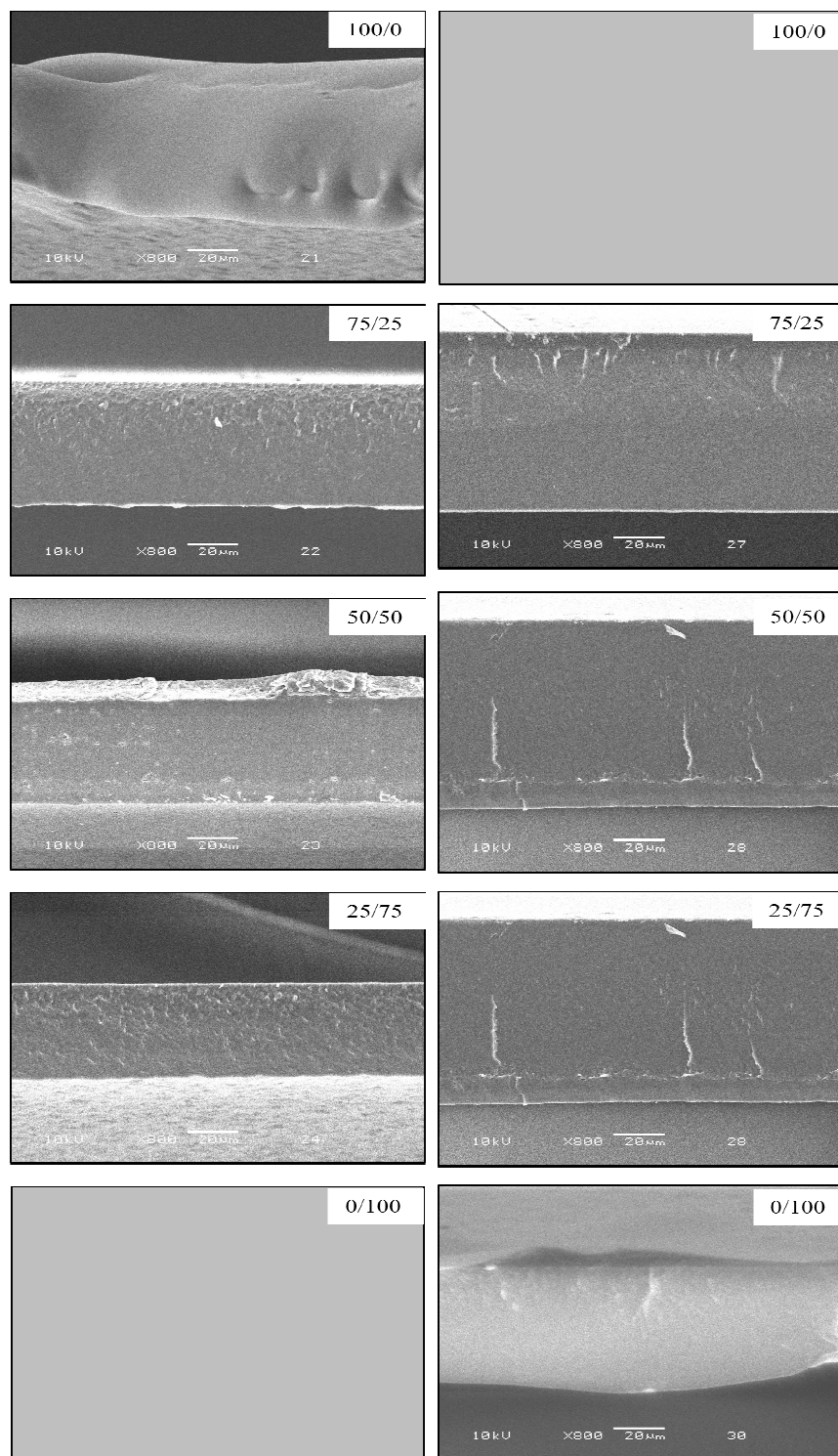


**Figure 4.47** SEM images of cross-section of 2.5K-*b*-L20K/2.5K-*b*-D20K (left row) and 2.5K-*b*-L40K/2.5K-*b*-D40K (right row) blend films.

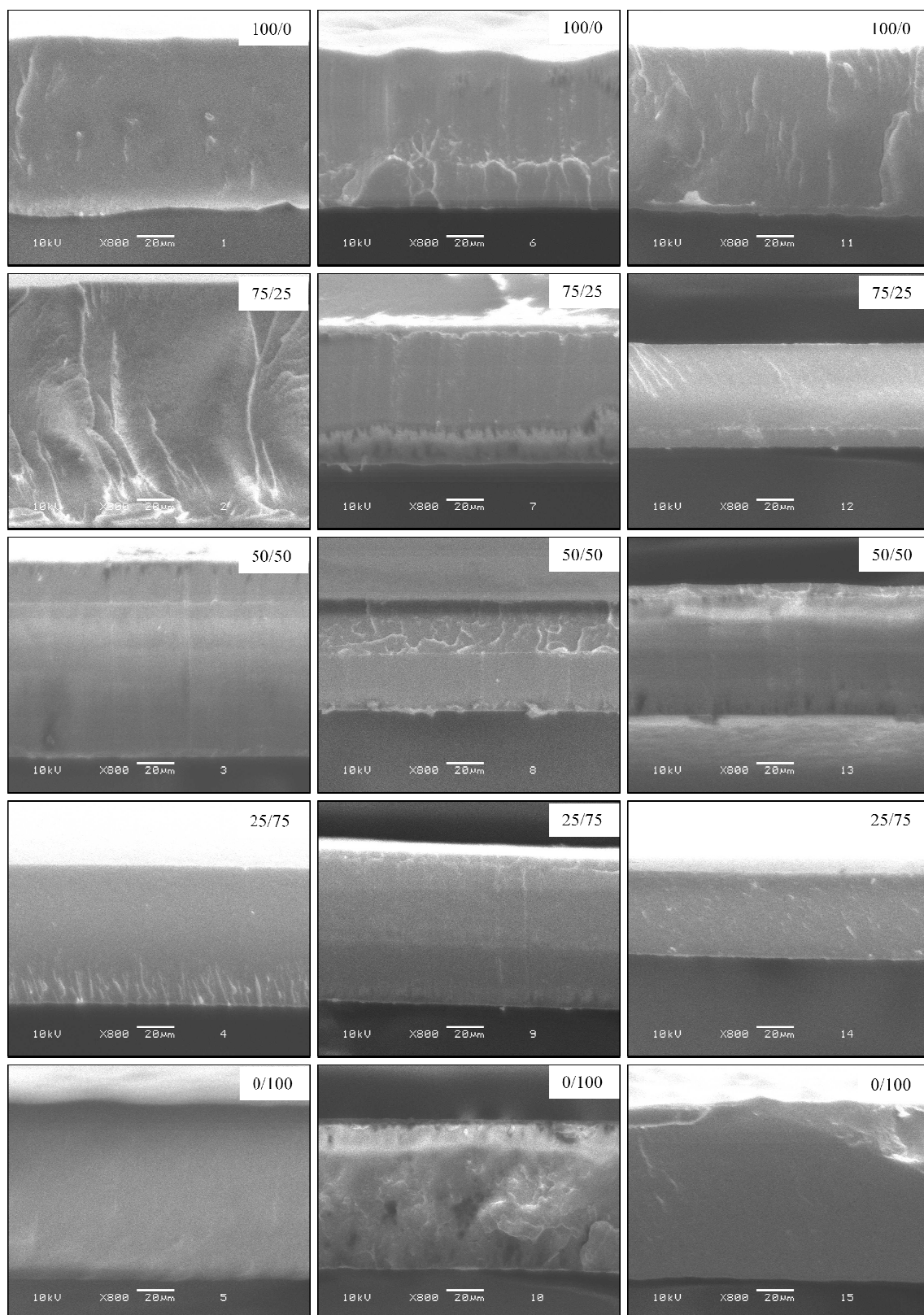


**Figure 4.48** SEM images of cross-section of L20K-*b*-2K-*b*-L20K/ D20K-*b*-2K-*b*-D20K (left row), L40K-*b*-2K-*b*-L40K/ D40K-*b*-2K-*b*-D40K (middle row) and L20K-*b*-4K-*b*-L20K/ D20K-*b*-4K-*b*-D20K (right row) blend films.

#### 4.2.4 Mechanical properties

The mechanical properties including stress at break, elongation at break and initial Young's modulus of the blend films were investigated by tensile testing. The tensile curves of the blend films were illustrated in Figures 4.49-4.52. The tensile testing of 2.5K-*b*-L20K/2.5K-*b*-D20K blend films were not measured because these films were too brittle. The continuous films cannot be prepared.

From the tensile curves, it can be seen that the mechanical properties of the blend films were better than the neat block copolymer films. The 50/50 (w/w) blend films showed the best mechanical properties. The results suggested that the stereocomplexation improved the mechanical properties of the blend films. This may be explained by the stereocomplex crystallites had stronger van der Waals force than the homo-crystallites (Brizzolara *et al.*, 1996; Okihara *et al.*, 1991). The average value of stress at break, elongation at break and Young's modulus were clearly compared in Figures 4.53-4.55, respectively. The 50/50 (w/w) blend films had the highest stress and elongation at break. This may be due to the  $\chi_{sc}$  or stereocomplexation were the highest on the 50/50 (w/w) blend ratio. The Young's modulus did not significantly change with the blend ratio.

The stress at break of the blend films increased when the PL end-block lengths were increased from 20K to 40K g/mol for the triblock copolymer blend films prepared with the same PPG block length (2K g/mol) and blend ratio. The stress at break decreased as the PPG block length increased from 2K to 4K g/mol for the triblock copolymer blend films prepared with the same PL end-block length (20K g/mol).

The elongation at break of the 40K-*b*-2K-*b*-40K and 20K-*b*-4K-*b*-20K blend films were slightly higher than the 20K-*b*-2K-*b*-20K blend films excepted the 50/50 (w/w) 40K-*b*-2K-*b*-40K blend films. The results indicated that the mechanical properties of the blend films depended up on the block length of PPG and PL.



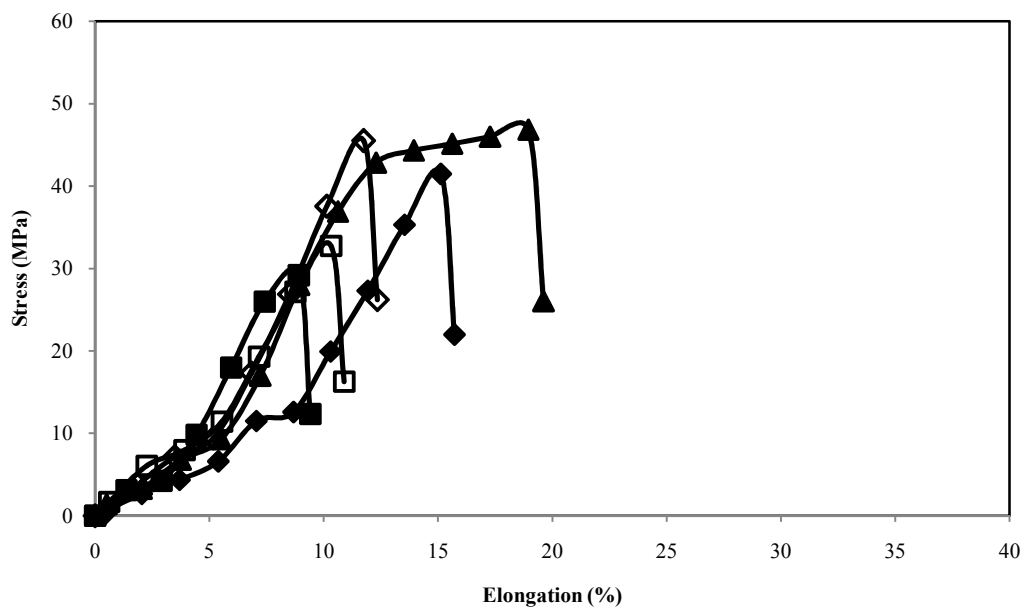


**Figure 4.49** Tensile curves of diblock copolymer films prepared with 2.5K-*b*-L40K/2.5K-*b*-D40K blend ratios of (□) 100/0, (◇) 75/25, (▲) 50/50, (◆) 25/75 and (■) 0/100 (w/w).

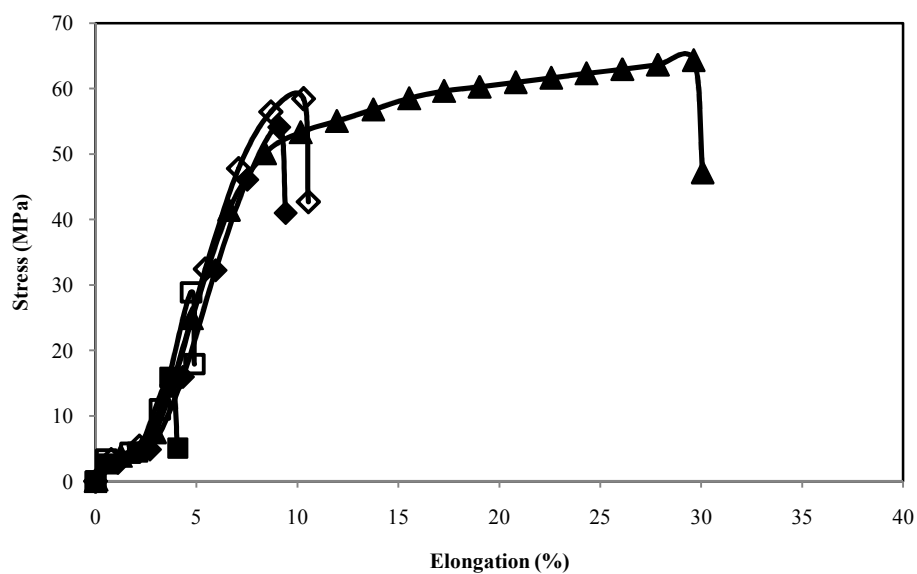


**Figure 4.50** Tensile curves of triblock copolymer films prepared with L20K-*b*-2K-*b*-L20K/D20K-*b*-2K-*b*-D20K blend ratios of (□) 100/0, (◇) 75/25, (▲) 50/50, (◆) 25/75 and (■) 0/100 (w/w).



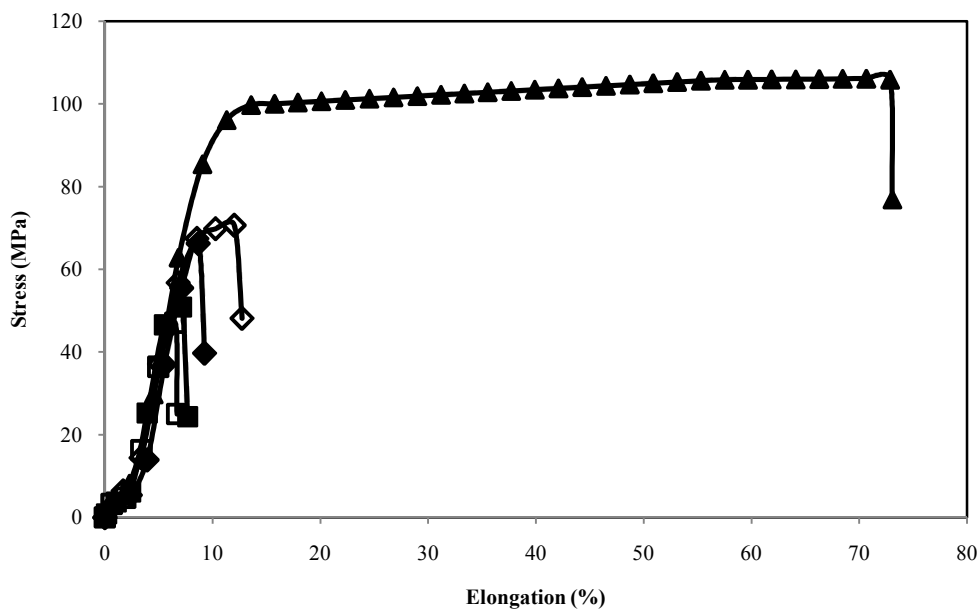


**Figure 4.51** Tensile curves of triblock copolymer films prepared with L40K-*b*-2K-*b*-L40K/D40K-*b*-2K-*b*-D40K blend ratios of (□) 100/0, (◇) 75/25, (▲) 50/50, (◆) 25/75 and (■) 0/100 (w/w).

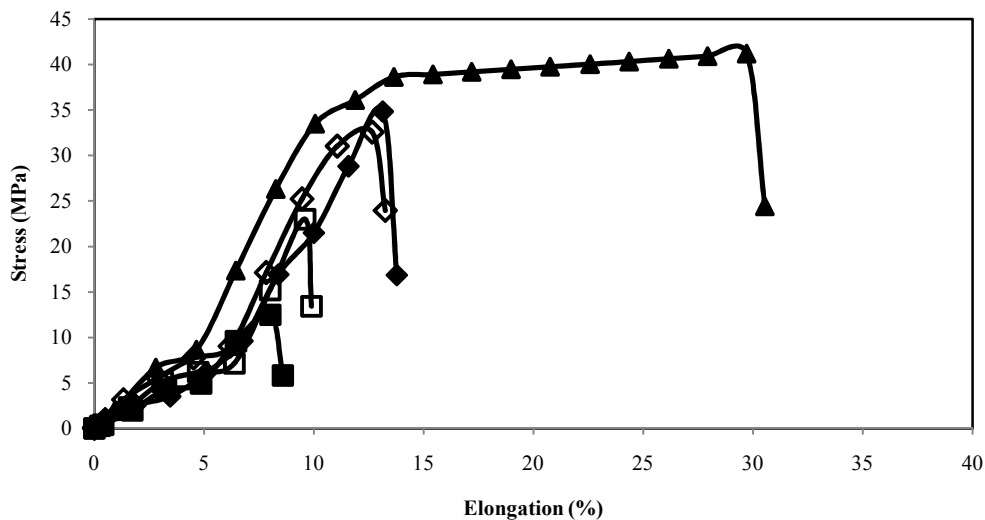


**Figure 4.52** Tensile curves of triblock copolymer films prepared with L20K-*b*-4K-*b*-L20K/D20K-*b*-4K-*b*-D20K blend ratios of (□) 100/0, (◇) 75/25, (▲) 50/50, (◆) 25/75 and (■) 0/100 (w/w).



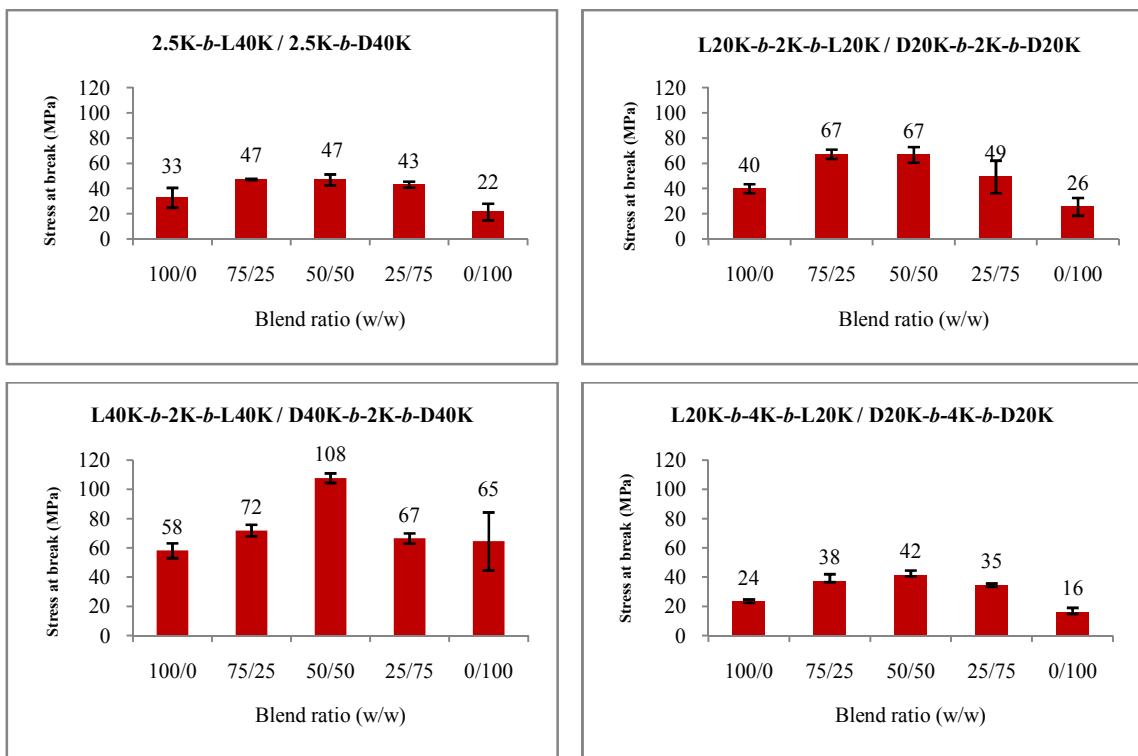


Figure 4.53 Stress at break of diblock and triblock copolymer films.

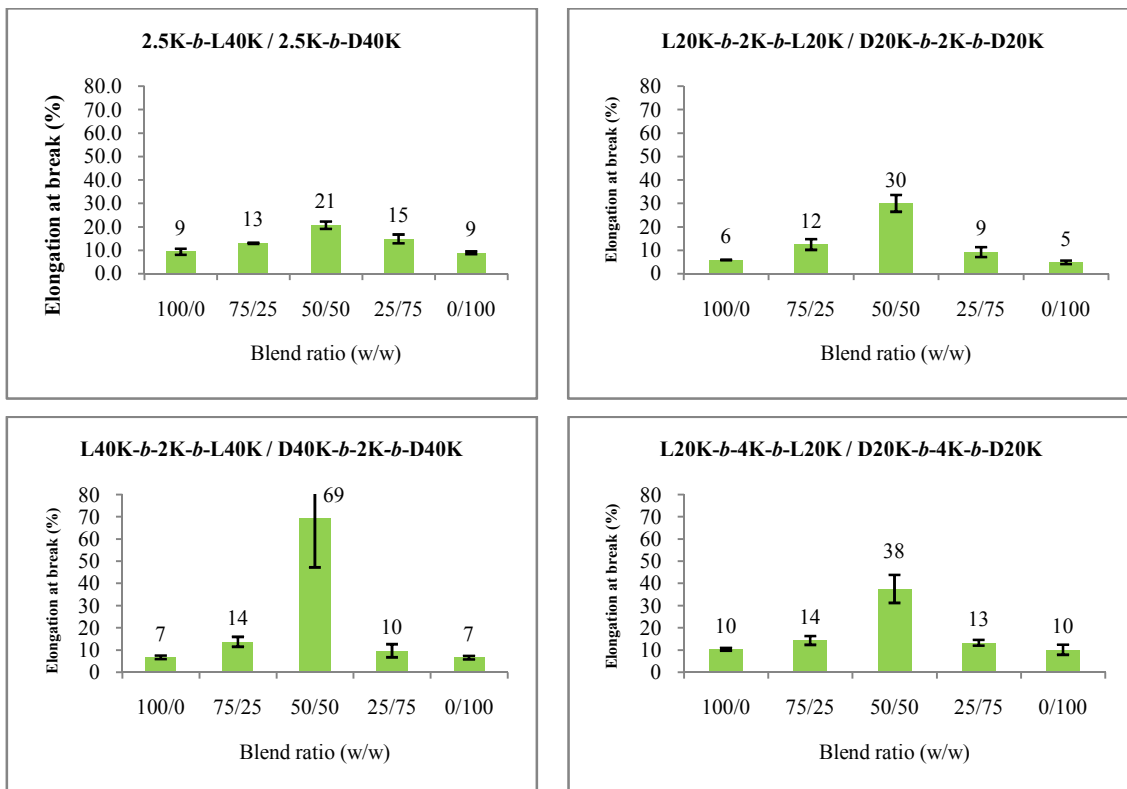
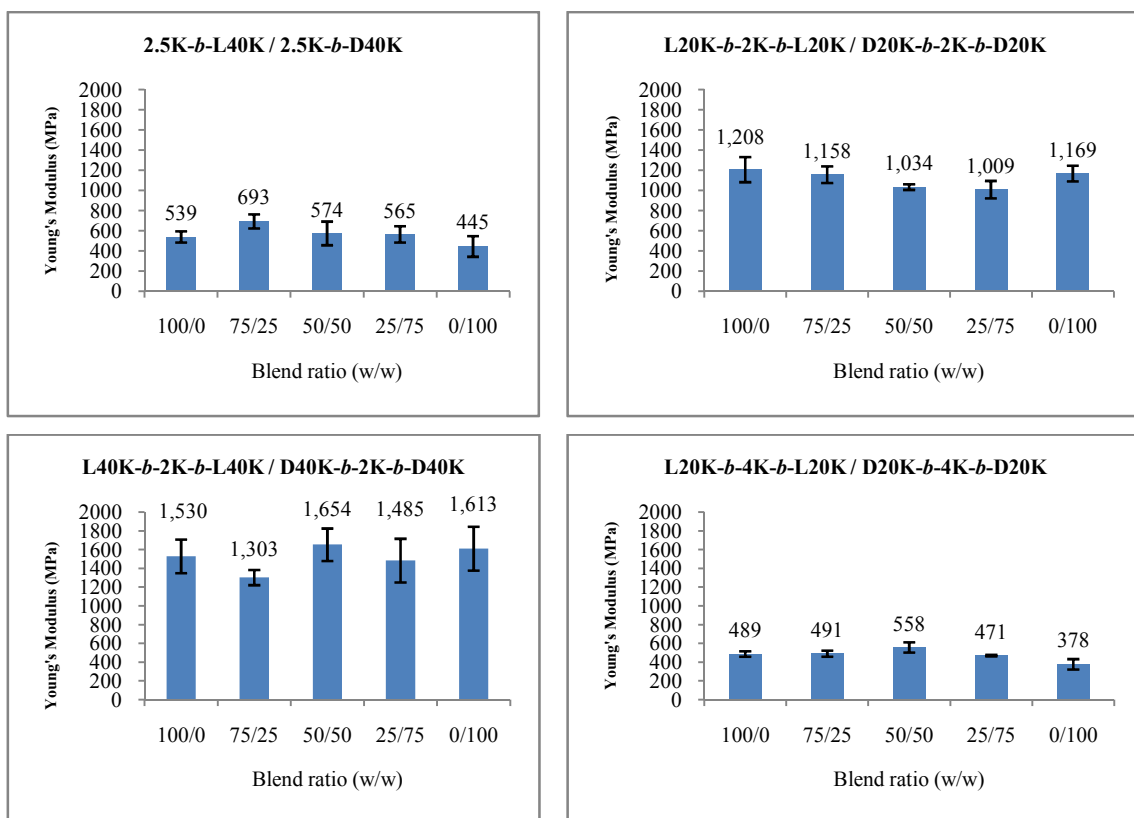


Figure 4.54 Elongation at break of diblock and triblock copolymer films.





**Figure 4.55** Young's modulus of diblock and triblock copolymer films.



## CHAPTER 5

### CONCLUSIONS

This chapter brings together the conclusions drawn from all the findings in this research, which can be divided into two main topics as follows:

5.1 Synthesis and characterization of block copolymers

5.2 Preparation and characterization of stereocomplex block copolymer films

#### 5.1 Synthesis and characterization of block copolymers

In this work diblock and triblock copolymers of poly(lactide)s [poly(L-lactide) and poly(D-lactide)] were synthesized by ring-opening polymerization of lactide monomers using mPPG and PPG as the initiators, respectively. The stannous octoate was used as a catalyst. The molecular weight of polylactide blocks was controlled by varying the initiator:monomer ratio.

Polymer characterization in this work was carried out by a combination of analytical techniques, namely: optical property (polarimetry), copolymer composition analysis ( $^1\text{H-NMR}$ ), molecular weight measurements ( $^1\text{H-NMR}$  and GPC) and thermal analysis (DSC). The main conclusions can be summarized as following:

(1) From optical rotation measurement, the negative and positive specific optical rotation ( $[\alpha]_{25}$ ) values of the L-type and D-type block copolymers indicated that they consisted on predominant L-form and D-form, respectively.

(2) The copolymer compositions (mol%) from their  $^1\text{H-NMR}$  spectra corresponded closely to their feed comonomer ratios, as would be expected if the copolymerisations were taken to near-quantitative conversion. This result shows that the reaction conditions employed were appropriate for the attainment of near-quantitative conversion.

(3) The molecular weights of the block copolymers from both  $^1\text{H-NMR}$  and GPC were nearly to the theoretical values. The PPG/lactide ratio can effectively control the molecular weight of block copolymers.



(4) From DSC the  $T_g$ ,  $T_c$ ,  $\Delta H_c$ ,  $T_{m, hc}$  and  $\Delta H_{m, hc}$  values of block copolymers slightly increased as the PL block lengths was increased. These thermal properties decreased when the PPG block length was increased from 2K to 4K.

## 5.2 Preparation and characterization of stereocomplex block copolymer films

In this work, neat block copolymers and blend films were prepared by solution blending before film casting. Chloroform was used as the blending solvent. The film samples were characterized by a combination of analytical techniques, namely: crystalline structure study (FTIR and XRD), thermal properties (DSC), morphology determination (SEM) and mechanical properties (tensile testing). The main conclusions can be summarized as follows:

(1) From FTIR and XRD, the neat block copolymer films consisted of only homo-crystalline of PL blocks. The 75/25 and 25/75 (w/w) blend films exhibited both homo- and stereocomplex crystalline characters. Meanwhile the 50/50 (w/w) blend films consisted of only stereocomplex crystalline for all the block copolymer types.

(2) From the 1<sup>st</sup> heating scan DSC curves, the  $T_{m, hc}$  and  $T_{m, sc}$  peaks were detected for the 75/25 and 25/75 (w/w) blend films. The 50/50 (w/w) blend films exhibited only  $T_{m, sc}$ . It can be concluded that the stereocomplexation of the blend films was complete with 50/50 (w/w) blend ratio according to the FTIR and XRD results. The  $\chi_{sc}$  values of 50/50 (w/w) blend films increased with the PL block length but decreased as the PPG block length was increased. From the 2<sup>nd</sup> heating scan DSC curves, the  $T_g$  of PL blocks increased with the PL block length but decreased as the PPG block length increased.

(3) From SEM, the diblock and triblock copolymer structure improved phase compatibility between PPG and PL phase of both the neat and blend films.

(4) From tensile test, the triblock structure and increasing of PL block length improved stress at break of the blend films. The stress at break of the blend films decreased as the PPG block length was increased. The elongation at break of the blend films increased as the PL and PPG block lengths were increased. The blend films with 50/50 (w/w) ratio exhibited the highest stress and elongation at break. The Young's modulus values of the blend films increased as the PL block length increased. The



longer PPG block reduced Young's modulus of the films. The blend ratio were not affect the Young's modulus in significant.



## REFERENCES



## REFERENCES

- Abe H, Kikkawa Y, Inoue Y and Doi Y (2001) Morphological and kinetic analyses of regime transition for poly[(S)-lactide] crystal growth. *Biomacromolecules*, 2, 1007-1014.
- Baiardo M, Frisoni G, Scandola M, Rimelen M, Lips D and Ruffieux K (2003) Thermal and mechanical properties of plasticized poly(l-lactic acid). *Journal of Applied Polymer Science*, 90, 1731–1738.
- Brizzolara D, Cantow HJ, Diederichs K, Keller E and Domb AJ (1996) Mechanism of the stereocomplex formation between enantiomeric poly(lactide)s. *Macromolecules*, 29, 191–197.
- Cicero JA, Dorgan JR, Dec SF and Knauss DM (2002) Phosphite stabilization effects on two-step melt-spun fibers of polylactide, *Polymer Degradation and Stability*, 78, 95-105.
- Chhaya E, Jigisha P and Ankur R (2011) Review on Hydrolytic Degradation Behavior of Biodegradable Polymers from Controlled Drug Delivery System. *Trends in Biomaterials and Artificial Organs*, 25, 79-85.
- Dorgan JR, Lehermeier H and Mang M (2000) Thermal and rheological properties of commercial-grade poly(lactic acid)s. *Journal Polymers and the Environment*, 8, 1-9.
- Fan Y, Nishida H, Shirai Y, Tokiwa Y and Endo T (2004) Thermal degradation behaviour of poly(lactic acid) stereocomplex. *Polymer Degradation and Stability*, 86, 197-208.
- Feng Q and Hanna MA (1999) Rheological properties of amorphous and semicrystalline polylactic acid polymers. *Industrial Crops and Products*, 10, 47-53.
- Fischer EW, Sterzel HJ and Wegner G (1973) Investigation of the structure of solution grown crystals of lactide copolymers by means of chemical reactions. *Kolloid Z.u.Z Polymers*, 251, 980-990.



- Fukuzaki H, Aiba Y, Yoshida M, Asano M and Kumakura M (1989) Low molecular-weight copolymers composed of l-lactic acid and various m-hydroxy acids as biodegradable carriers. *Macromolecular Chemistry and Physics*, 190, 2571–2577.
- Fukuzaki H, Yoshida M, Asano M, Kumakura M, Mashimo T and Yuasa H (1990) Synthesis of low-molecular-weight copoly(l-lactic acid/ $\epsilon$ -caprolactone) by direct copolycondensation in the absence of catalysts, and enzymatic degradation of the polymers. *Polymer*, 31, 2006–2014.
- Fundador NGV, Takemura A and Iwata T (2010) Structural properties and enzymatic degradation behavior of PLLA and stereocomplexed PLA nanofibers. *Macromolecular Materials and Engineering*, 295, 865–871.
- Garlotta D (2001) A Literature Review of Poly(Lactic Acid). *Journal of Polymers and the Environment*, 9, 63-84.
- Grijpma DW and Pennings AJ (1994) (Co)polymers of l-lactide. 1. Synthesis, thermal properties and hydrolytic degradation. *Macromolecular Chemistry and Physics*, 195, 1633–1647.
- Grijpma DW and Pennings AJ (1994) (Co)polymers of l-lactide. 2. Mechanical properties. *Macromolecular Chemistry and Physics*, 195, 1649–1663.
- Gruber PR, Kolstad JJ, Hall ES, Eichen-Conn RS and Ryan CM (1999) Melt stable lactide polymer compositions and their manufacture. *Patent Cooperation Treaty International Application*. Patent No. US 08/966,111.
- Han L, Yu Ch, Zhou J, Shan G, Bao Y, Yun X, Dong T and Pan P (2016) Enantiomeric blends of high-molecular-weight poly(lactic acid)/poly(ethylene glycol) triblock copolymers: Enhanced stereocomplexation and thermomechanical properties. *Polymer*, 103, 376-386.
- Haynes D, Abayasinghe NK, Harrison GM, Burg KJ and Smith Jr DW (2007) In situ copolyesters containing poly(l-lactide) and poly(hydroxyalkanoate) units. *Biomacromolecule*, 8, 1131–1137.
- Hirata M and Kimura Y (2008) Thermomechanical properties of stereoblock poly(lactic acid)s with different PLLA/PDLA block compositions. *Polymer*, 49, 2656–2661.
- Henton ED, Gruber P, Lunt J and Randall J (2005) Polylactic Acid Technology. *Natural Fibers, Biopolymers and Biocomposites*, 16, 527-578.



- Ho SM and Young AM (2006) Synthesis, polymerization and degradation of poly(lactide-co-propylene glycol) dimethacrylate adhesives. *European Polymer Journal*, 42, 1775-1785.
- Ikada Y, Jamshidi K, Tsuji H and Hyon SH (1987) Stereocomplex formation between enantiomeric poly(lactides). *Macromolecules*, 20, 904–906.
- Izunobi JI and Higginbotham CL (2011) Polymer Molecular Weight Analysis by <sup>1</sup>H NMR Spectroscopy. *Journal of Chemical Education*, 88, 1098–1104.
- Kaitian X, Kozluca A, Denkbaz EB, Piskin E (1996) Poly(D,L-lactic acid) homopolymers: synthesis and characterization. *Journal of Chemistry*, 20, 43-53.
- Kang N, Perron M E, Prud'homme R E, Zhang Y, Gaucher G V and Leroux J Ch (2005) Stereocomplex Block Copolymer Micelles: Core–Shell Nanostructures with Enhanced Stability. *Nano Letters*, 5, 315-319.
- Kolstad JJ (1996) Crystallization kinetics of poly(L-lactide-co-meso-lactide). *Journal of Applied Polymer Science*, 62, 1079-1091.
- Kulinski Z, Piorkowska E, Gadzinowska K and Stasiak M (2006) Plasticization of Poly(L-lactide) with Poly(propylene glycol). *Biomacromolecules*, 7, 2128-2135.
- Kumar KS, Ghosh AK and Bhatnagar N (2007) Mechanical properties of injection molded long fiber polypropylene composites, Part 1: Tensile and flexural properties. *Polymer Composites*, 28, 259-266.
- Lai WC, Liao WB and Lin TT (2004) The effect of end groups of PEG on the crystallization behaviors of binary crystalline polymer blends PEG/PLLA. *Polymer*, 45, 3073–3080.
- Lakshmi S Nair and Cato T Laurencin (2007) Biodegradable polymers as biomaterials. *Progress in Polymer Science*, 32, 762–798.
- Lanfranche E, Frawczak P, Ciolczyk JP and Maugey P (2005) Injection molding of long glass fiber reinforced polyamide 66: processing condition /microstructure / flexural properties relationship. *Advance in Polymer Technology*, 24, 114-131.
- Lehermeier HJ and Dorgan JR (2001) Melt rheology of poly(lactic acid): consequences of blending chain architectures. *Polymer Engineering and Science*, 41, 2172-2184.
- Li H and Huneault M A (2007) Effect of nucleation and plasticization on the crystallization of poly(lactic acid). *Polymer*, 48, 6855-6866.





- Li S and Vert M (2003) Synthesis, Characterization, and Stereocomplex-Induced elation of Block Copolymers Prepared by Ring-Opening Polymerization of L(D)-Lactide in the Presence of Poly(ethylene glycol). *Macromolecules*, 36, 8008-8014
- Ljungberg N and Wesslén B (2002) The effects of plasticizers on the dynamic mechanical and thermal properties of poly(lactic acid). *Journal of Applied Polymer Science*, 86, 1227–1234.
- Lloyd AW (2002) Interfacial bioengineering to enhance surface biocompatibility. *Medical Device Technologies*, 13, 18–21.
- Liu Y, Jun S, Jingru S, Xinchao B, Lidong F, Sheng X, Bin S, Zhiming C, Gao L and Xuesi C (2014) Improved mechanical and thermal properties of PLLA by solvent blending with PDLA-*b*-PEG-*b*-PDLA. *Polymer Degradation and Stability*, 101, 10-17.
- Martin O and Avėrous L (2001) Poly(lactic acid): plasticization and properties of biodegradable multiphase system. *Polymer*, 42, 6209–6219.
- Na B., Zhu J, Lv R, Ju Y, Tian R, and Chen B (2014) Stereocomplex Formation in Enantiomeric Polylactides by Melting Recrystallization of Homocrystals: Crystallization Kinetics and Crystal Morphology. *Macromolecules*, 47, 347-352.
- Nair L S and Luarencin C T (2007) Biodegradable polymers as biomaterials. *Progress in Polymer Science*, 32, 762-798.
- Okihara T, Tsuji M and Katayama K (1991) Crystal structure of stereocomplex of poly(L-lactide) and poly(D-lactide). *Journal of Macromolecular Science: Physics*, 30, 119-140.
- Pakkethati K and Baimark Y (2017) Plasticization of Biodegradable Stereocomplex Polylactides with Poly(propylene glycol). *Polymer Science, Series A*, 59, 124–132.
- Paulsen K and Frasco D [2016] *Determination of Polymer Molecular Weight and Composition Using PicoSpin NMR Spectroscop.* [Online]. Available from: <https://tools.thermofisher.com/content/sfs/brochures/Case-Western-Polymer-App-Note-r16-11-22.pdf> [Cited 10 March 2017].
- Pilla S (2011) *Handbook of Bioplastics and Biocomposites Engineering Applications.* USA, Scrivener Publishing LLC.



- Pillin I, Montrelay N and Grohens Y (2006) Thermo-mechanical characterization of plasticized PLA: is the miscibility the only significant factor. *Polymer*, 47, 4676–2682.
- Piorowska E, Kulinski Z, Galeski A and Masirek R (2006) Plasticization of semicrystalline poly(L-lactide) with poly(propylene glycol). *Polymer*, 47, 7178-7188.
- Premraj R and Mukesh D (2004) Biodegradation of Polymers. *Indian Journal of Biotechnology*, 4, 186-193.
- Qi F, Tang M, Chen X, Chen M, Guo G and Zhang Z (2015) Morphological structure, thermal and mechanical properties of tough poly(lactic acid) upon stereocomplexes. *European Polymer Journal*, 71, 314-324.
- Quynh T M, Mai Hoang H and Lan P N (2013) Stereocomplexation of low molecular weight poly(L-lactic acid) and high molecular weight poly(D-lactic acid), radiation crosslinking PLLA/PDLA stereocomplexes and their characterization. *Radiation Physics and Chemistry*, 83, 105-110.
- Rahul MR, Amol VJ and Douglas EH (2010) Poly(lactic acid) modifications. *Progress in Polymer Science*, 35, 338-356.
- Ramkumar DHS and Bhattacharya M (1998) Steady shear and dynamic properties of biodegradable polyesters. *Polymer Engineering and Science*, 38, 1426-1435.
- Rasal RM and Hirt DE (2008) Toughness decrease of PLA–PHBHHx blend films upon surface-confined photopolymerization. *Journal of Biomedical Materials Research Part A*, 88A, 1079–1086.
- Rodriguez NL, Arenaza IM, Meaurio E and Sarasua JR (2014) Improvement of toughness by stereocomplex crystal formation in optically pure polylactides of high molecular weight. *Journal of the Mechanical Behavior of Biomedical Materials*, 37, 219-225.
- Sheth M, Kumar RA, Davé V, Gross RA and McCarthy SP (1997) Biodegradable polymer blends of poly(lactic acid) and poly(ethylene glycol). *Journal of Applied Polymer Science*, 66, 1495–1505.
- Srithep Y, Pholharn D, Turng L Sh, Veang-in O and Morris J (2016) Effects of nucleation and stereocomplex formation of poly(lactic acid). *Journal of Polymer Engineering*, 7, 673-680.



- Tasaka F, Ohya Y and Ouchi T (2002) One-pot synthesis of novel branched polylactide through the copolymerization of lactide with mevalonolactone. *Macromolecular Rapid Communications*, 22, 820-824.
- Tsuji H and Ikada Y (1992) Stereocomplex formation between enantiomeric poly(lactic acid)s VI: Binary blends from copolymers. *Macromolecules*, 25, 5719-5723.
- Tsuji H and Ikada Y (1999) Stereocomplex formation between enantiomeric poly(lactic acid)s. XI. Mechanical properties and morphology of solution-cast films. *Polymer*, 40, 6699-6708.
- Tsuji H and Miyauchi S (2000) Poly(L-lactide): VI effects of crystallinity on enzymatic hydrolysis of poly(L-lactide) without free amorphous region. *Polymer Degradation and Stability*, 71, 415-424.
- Tsuji H and Miyauchi S (2001) Poly(L-lactide): 7. enzymatic hydrolysis of free and restricted amorphous regions in poly(L-lactide) films with different crystallinities and a fixed crystalline thickness. *Polymer*, 42, 4463-4467.
- Tsuji H (2005) Poly(lactide) stereocomplexes: formation, structure, properties, degradation, and applications. *Macromolecular Bioscience*, 5, 569-597.
- Witzke DR (1997) *Introduction to Properties, Engineering, and Prospects of Polylactide Polymer*. Ph.D. thesis, Michigan State University.
- Xiao H, Lu W and Yeh JT (2009) Effect of Plasticizer on the Crystallization Behavior of Poly(lactic acid). *Journal of Applied Polymer Science*, 113, 112-121.
- Zhang J, Sato H, Tsuji H, Noda I and Ozaki Y (2005) Infrared spectroscopic study of interaction during poly(L-lactide)/poly(D-lactide) stereocomplex formation. *Macromolecules*, 38, 1822-1828.
- Zhang J, Duan Y, Sato H, Tsuji H, Noda I, Yan S and Ozaki Y (2005) Crystal Modifications and Thermal Behavior of Poly(L-lactic acid) Revealed by Infrared Spectroscopy. *Macromolecules*, 38, 8012-8021.
- Zhang J, Tashiro K, Tsuji H, and Domb A J (2007) Investigation of Phase Transitional Behavior of Poly(L-lactide)/Poly(D-lactide) Blend Used to Prepare the Highly-Oriented Stereocomplex. *Macromolecules*, 40, 1049-1054.



## **BIOGRAPHY**



## BIOGRAPHY

<b>Name</b>	Miss Dutchanee Pholharn
<b>Date of birth</b>	November 19, 1984
<b>Place of birth</b>	Maharakham Province, Thailand.
<b>Institution attended</b>	
2006	Bachelor of Science in Chemistry, Faculty of Science, King Mongkut's University of Technology Thonburi, Thailand
2009	Master of Science in Polymer Science and Technology, Faculty of Science, Mahidol University, Thailand.
2017	Doctoral of Philosophy Program in Chemistry, Faculty of Science, Maharakham University, Thailand.
<b>Position and Work Place</b>	Department of Chemistry, Faculty of Science and Technology, Rajabhat Maha Sarakham University, Thailand.
<b>Contact address</b>	Department of Chemistry, Faculty of Science and Technology, Rajabhat Maha Sarakham University, Thailand. 80 Nakhonsawan Road, Muang Maha Sarakham, 44000, Thailand.

### Research output

- [1] Pholharn D, Baimark Y, "Effects of Blend Ratio and Block Length on Crystallinity and Mechanical Properties of Biodegradable Stereocomplex Polylactide-*b*-Poly(Propylene Glycol)-*b*-Polylactide". Proceeding of the Pure and Applied Chemistry International Conference (PACCON). 21<sup>st</sup> -23<sup>rd</sup> January 2015, Amari Watergate Hotel, Bangkok, Thailand. (Oral presentation)

